Hydration, Ion Binding and Self-Aggregation of Choline and Choline-based Surfactants

Dissertation
zur Erlangung des
Doktorgrades der Naturwissenschaften
(Dr. rer. nat.)
der Naturwissenschaftlichen Fakultät IV
Chemie und Pharmazie
der Universität Regensburg

vorgelegt von
Saadia Shaukat
aus Rawalpindi / Pakistan

Regensburg 2012

Promotionsgesuch eingereicht am:	30.10.2012
Tag des Kolloquiums:	20.12.2012
Die Arbeit wurde angeleitet von:	Apl. Prof. Dr. R. Buchner
Prüfungsausschuss:	Apl. Prof. Dr. R. Buchner Prof. Dr. W. Kunz Prof. Dr. A. Pfitzner Prof. Dr. D. Horinek (Vorsitzender)

Dedicated to
My Parents, Abd Ur Rahman, Huzaifa
and
Hamza

Contents

Preface

This dissertation is based on research carried out between February 2009 and October 2012 at Institute of Physical and Theoretical Chemistry (Faculty of Natural Sciences IV) of the University of Regensburg.

I would like to express my sincere thanks to my supervisor Prof. Dr. Richard Buchner for providing me the opportunity to work in his group. His continuous guidance and encouragement throughout the whole period of my PhD studies helped me to successfully complete the designed project work.

I would like to express my gratitude to the head of the institute Prof. Dr. Werner Kunz for providing the laboratory facilities. Furthermore, his support in terms of providing required annual referee's report is highly acknowledged.

I am also thankful to the Higher Education Commission of Pakistan (HEC) for a PhD grant and German Academic Exchange Service (DAAD) for guidance and support.

I would like to express my gratitude to my current and former colleagues in the microwave group, Dr. Johannes Hunger, Dr. Alexander Stoppa, Dr. Hafiz Muhammad Abd Ur Rahman, Thomas Sonnleitner, Andreas Eiberweiser, and Bernd Muehldorf, for their support and valuable discussions.

Thanks to all members of workshops for completing my orders reliably and quickly. Furthermore, I would like to thank all staff members of the Institute of Physical and Theoretical Chemistry for their cooperativeness.

Finally, I wish to express my profound gratitude to my beloved parents, husband and brothers for their love and continuous support.

Constants, symbols and acronyms

Constants

elementary charge	e_0	$= 1.60217739 \cdot 10^{-19}\,\mathrm{C}$
permittivity of free space	ε_0	$= 8.854187816 \cdot 10^{-12}\,\mathrm{C^2(Jm)^{-1}}$
Avogadro's constant	N_A	$= 6.0221367 \cdot 10^{23}\,\mathrm{mol^{-1}}$
speed of light	c_0	$= 2.99792458 \cdot 10^{8}\,\mathrm{m\,s^{-1}}$
Boltzmann's constant	k_B	$= 1.380658 \cdot 10^{-23}\,\mathrm{J\,K^{-1}}$
permeability of free space	μ_0	$= 4\pi \cdot 10^{-7}\,\mathrm{(Js)^2(C^2m)^{-1}}$
Planck's constant	h	$= 6.6260755 \cdot 10^{-34}\,\mathrm{Js}$

Symbols

$\vec{B}$	magnetic induction $[\mathrm{Vs\,m^{-2}}]$	$\vec{D}$	electric induction $[\mathrm{C\,m^{-2}}]$
$\vec{E}$	electric field strength $[\mathrm{V\,m^{-1}}]$	$\vec{H}$	magnetic field strength $[\mathrm{A\,m^{-1}}]$
ν	frequency $[\mathrm{s^{-1}}]$	ω	angular frequency $[\mathrm{s^{-1}}]$
$\vec{P}$	polarization $[\mathrm{C\,m^{-2}}]$	μ	dipole moment $[\mathrm{C\,m}]$
$\hat{\varepsilon}$	complex dielectric permittivity	ε'	real part of $\hat{\varepsilon}$
ε''	imaginary part of $\hat{\varepsilon}$	ε	$\lim_{\nu\to 0}(\varepsilon')$
ε_∞	$\lim_{\nu\to\infty}(\varepsilon')$	τ	relaxation time [s]
T	thermodynamic temperature [K]	c	molarity $\left[\mathrm{mol\,dm^{-3}}\right]$
κ	conductivity $[\mathrm{S\,m^{-1}}]$	ρ	density $[\mathrm{kg\,m^{-3}}]$

Acronyms

DRS	dielectric relaxation spectroscopy	NMR	nuclear magnetic resonance
IFM	interferometer	VNA	vector network analyzer
TDR	time domain reflectometry	MD	molecular dynamics
DMA	*N*,*N*-dimethylacetamide	PC	propylene carbonate
SED	Stokes-Einstein-Debye	HN	Havriliak-Negami
D	Debye	CC	Cole-Cole
CD	Cole-Davidson	DHO	damped harmonic oscillator

Introduction

Basic aspects

Since long, the study of structure and dynamics of electrolyte solutions has been a topic of profound interest. Several theories and experimental techniques have been evolved to understand the behavior of so called "simple" electrolytes and a vast body of data has been generated for these systems. However, the level of agreement between the results obtained from different methods/techniques puts a questionmark on our claimed understanding of these systems. For electrolyte solutions, in order to grip the knowledge of fundamental molecular level mechanisms behind various phenomena, a thorough understanding of ion-association and ion-hydration is necessary. In case of aqueous solutions the co-operative dynamics of hydrogen bonded network of water could be probed to study solute effects on water in terms of its hydration and/or aggregation pattern. It is known that hydration of small and large particles differs qualitatively, with a crossover on nanometer length scale,[1] hence, the study of salts having both hydrophilic and hydrophobic moieties is of great focus. In this regard, tetraalkylammonium (TAA) salts proved to be model substances to study both "hydrophilic" and "hydrophobic" hydration. These salts, especially the symmetric TAA compounds have got history of investigations via different theoretical as well as experimental techniques. In the present study a special type of asymmetric tetraalkylammonium ion, namely choline (2-hydroxyethyl trimethyl ammonium ion, Ch^+) and generally known as vitamin B4, has been chosen to study. Being a biogenic ion choline is abundantly found in nature[2–4] hence, data pertaining to its dielectric properties is potentially very important and relevant to the nature. Furthermore, considering ammonium (NH_4^+) as parent ion of all TAA compounds, aqueous solutions of ammonium chloride (NH_4Cl) were also studied.

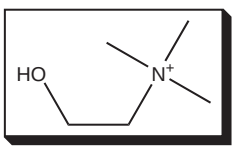

Figure 1: Molecular structure of choline ion.

In addition to simple electrolytes, surfactants, a special class of amphiphilic compounds, are a significant part of our every day life. Surfactants are frequently used in detergents, shampoos, washing gels, washing powders, textile, paper industry and food etc.[5] Their

presence in such vast variety of fields make them inevitable for us. Most commonly known surfactants are soaps, which are used since thousands of years.[6] Due to their usage in such versatile fields, surfactants are synthesized in enormous amounts and thus large concerns about their "eco-friendliness" and biodegradability arise. As already mentioned, choline is an ion of biological origin, surfactants having choline as counterions have been successfully synthesized and patented by the University of Regensburg.[7] Details of their cytotoxic and biodegradability analysis are available in literature.[8] Furthermore, room temperature ionic liquids (RTIL) having choline as cations are also a field of growing interest.[8,9] So using choline as a bio-relevant ion, opens a horizon to design a wide range of "green" materials. Present study includes investigations of two types of systems, i.e., choline-based electrolytes and choline-based surfactants. Special emphasis is given on hydration, ion-binding and self-association of these compounds. Aqueous solutions of choline containing compounds have been studied through dielectric relaxation spectroscopy (DRS). Principally, DRS probes the fluctuations of permanent dipoles in response to an oscillating electromagnetic field in the microwave (GHz) region and is sensitive to reorientational and cooperative motions of dipolar species in pico- to nanosecond timescale.[10] Furthermore, DRS has unique sensitivity towards different types of ion pairs which many other experimental methods lack.[10,11]
The dissertation includes as well, a set of supplementary measurements for conductivities and densities for each of the studied system. Moreover, viscosity data is also reported for few systems only.

Systems investigated and motivation

The main aim of present study is the application of DRS to aqueous solutions of choline-based electrolytes and surfactants. For this purpose, choline chloride (ChCl), chlorocholine chloride (Cl-ChCl) and ammonium chloride (NH_4Cl) have been chosen as examples of electrolytes. Comparison is made between the DRS results of tetra-*n*-alkylammonium ions[12] and our findings for choline salts. Reasonable concentration range have been studied for each of these systems. Special features like ion pairing and ion hydration have been studied in detail for these solutions.
For the investigations of micellar systems two bio-compatible surfactants, namely choline dodecanoate (ChC12) and choline dodecylsulfate (ChDS), and sodium dodecanoate (NaC12) have been studied. Despite the fact that natural soaps are easy to prepare and are at the same time ecofriendly, neverthless, long chain derivatives of theses soaps are most desired due to better detergency and related properties. This however, has to be done at the cost of decreased water solubility. As, for example, under ambient conditions, sodium and potassium soaps can be prepared upto a maximum chain length of twelve carbons.[13] This arose the demand of having such surfactants which have better solubility and at least similar biodegradability as do the natural soaps possess. In this regard surfactants with choline as counterions (synthesized in the University of Regensburg) are claimed to have pronouncedly lower krafft points compared to their corresponding alkali counterparts and are non-toxic and biologically degradable.[14] Being "new", the literature data pertaining to ChC12 and ChDS is scarce, hence, the presented work aimed to investigate dielectrically aqueous solutions of ChC12 and ChDS. It was also aimed to compare the results of choline-

based surfactants with corresponding surfactants having sodium (Na^+) as counterion. For this purpose literature data of sodium dodeylsulfate (SDS)[15] was used and the experimental work was extended to study aqueous solutions of NaC12 as well. For the micellar solutions DRS has proved to be a promising tool to investigate various micelle-related processes and distinct dynamics of water in bound state (as a part of hydration shell) and in free state (bulk water). Features like micelle-specific relaxations, micellar hydration and counterion-headgroup binding have been studied in detail. The potential of the presented work using DRS should through some light on various micelle-related properties. Based on specific ion effects[16] and Collins's "law of matching water affinities",[17,18] it is expected that counterion-headgroup binding is preferable for soft-soft and hard-hard couple compared to soft-hard binding. This is cross checked for the studied surfactants having two types of headgroups, RCO_2^- and $ROSO_3^-$, and counterions, Na^+ and Ch^+. The hydration pattern of these surfactants is used to explain difference in the preferential binding of choline and sodium ions to carboxylate or sulfate headgroups. In order to validate the claimed low salt sensitivity of choline dodecylsulfate,[8] aqueous solutions of ChDS with added NaCl and ChCl are additionally measured and the obtained spectra are analyzed qualitatively. Dielectric spectra have been recorded over a sufficiently broad frequency range, 0.01 or 0.2 $\leq \nu/\mathrm{GHz} \leq 89$.

It should be noted that, for the measurements of micellar systems, low frequency data (down to few tens of MHz) was indeed necessary. This however, offered major difficulties regarding the optimization of proper cells to reduce "electrode polarization" and related unwanted features. An empirical methodology is adopted to overcome this undesired feature from the DR spectra of micellar solutions, wherever necessary.

Chapter 1

Theoretical background

1.1 Fundamental equations of electromagnetism

1.1.1 Maxwell equations

All electro-magnetic phenomena are governed by the Maxwell's equations[19,20] which are based on four laws as

$$\vec{\mathrm{rot}}\,\vec{H} = \vec{j} + \frac{\partial}{\partial t}\vec{D} \tag{1.1}$$

$$\vec{\mathrm{rot}}\,\vec{E} = -\frac{\partial}{\partial t}\vec{B} \tag{1.2}$$

$$\mathrm{div}\,\vec{D} = \rho_{\mathrm{el}} \tag{1.3}$$

$$\mathrm{div}\,\vec{B} = 0 \tag{1.4}$$

Where $\vec{H}$ is magnetic and $\vec{E}$ is electric field strength, $\vec{j}$ represents the current density and $\vec{B}$ and $\vec{D}$ account for the magnetic and electric induction, also called magnetic flux density or electric displacement field, respectively whereas ρ_{el}, is electric charge density. Eq. 1.1 (Ampère-Maxwell's law) gives a quantitative description of production of magnetic fields by the electric current. Faraday's law of electro-magnetic induction (Eq. 1.2) describes the generation of electric field if the magnetic flux going across a closed circuit changes. Gauss's law of electric field (Eq. 1.3) states that, on a closed surface, the number of lines of electric flux going through that surface equals the total quantity of electric charge contained within it. Eq. 1.4 (Gauss's law of magnetic field) is nothing but an expression for the fact that magnetic flux does not have origins.
The above mentioned laws along with the Newton equation

$$m\frac{\partial^2}{\partial t^2}\vec{r} = q(\vec{E} + \vec{v} \times \vec{B}) \tag{1.5}$$

are sufficient to explain all electro-magnetic phenomena. In the above equation q denotes a moving charge and $\vec{v}$ is its velocity.

1.1.2 Constitutive equations for static or low fields

The relation between the dielectric displacement ($\vec{D}$) and electric field strength ($\vec{E}$) can be written as[21]

$$\vec{D} = \varepsilon\varepsilon_0\vec{E} \tag{1.6}$$

which is applicable only for homogenous, non-dispersive, isotropic materials at static (time-independent) and low fields (linear response regime). In the above relation ε is the relative permittivity and ε_0 is the the dielectric permittivity of vacuum. Similarly a linear relationship between $\vec{H}$ and $\vec{B}$ can be defined as

$$\vec{H} = \frac{\vec{B}}{\mu\mu_0} \tag{1.7}$$

where μ is the relative magnetic permittivity and μ_0 is the magnetic permittivity of vacuum. The relation between μ_0 and ε_0 is given by, $\mu_0 = 1/\varepsilon_0 c^2$, where c is the velocity of light in vacuum.
Similar to Eq. 1.6 Ohms law

$$\vec{j} = \kappa\vec{E} \tag{1.8}$$

gives the relationship between $\vec{j}$ and $\vec{E}$ where κ is the electric conductivity.
The constitutive equations (Eqs. 1.6 - 1.8), which relate $\vec{D}$ and $\vec{H}$ to $\vec{E}$ and $\vec{B}$ by time- and field strength-independent scalars (material properties) like ε, κ and μ, are valid only for the special case of a time-independent field response.

1.1.3 Equations for dynamic field

The simplest description of dynamic fields can be done with the help of sinusoidally varying (harmonic) electric fields. The time dependence of electric field strength is given by[21]

$$\vec{E}(t) = \vec{E}_0 \cos(\omega t) \tag{1.9}$$

In the above equation $\vec{E}_0$ is the amplitude and $\omega = 2\pi\nu$ the angular frequency of the sinusoidally varying electric field. When the frequency of the sinusoidal variation is sufficiently high (typically in the region of 1 MHz to 1 GHz for the condensed phase), the motion of the microscopic particles does not follow the changes in the field due to interaction or inertia within the system, hence both polarization and dielectric displacement can no longer be described by the quasi-static relations. For a linear and isotropic system a frequency-dependent phase delay, $\delta(\omega)$, is observed between the electric field and the electric displacement as

$$\vec{D}(t) = \vec{D}_0 \cos(\omega t - \delta(\omega)) \tag{1.10}$$

where $\vec{D}_0$ is the amplitude of the sinusoidal variation. Splitting Eq. 1.10 according to the addition theorem of the cosine function into two sinusoidally varying parts, one in phase and the other having a phase difference of $\pi/2$ with the electric field yields

$$\vec{D}(t) = \vec{D}_0 \cos(\delta(\omega)) \cos(\omega t) + \vec{D}_0 \sin(\delta(\omega)) \sin(\omega t) \tag{1.11}$$

Accordingly a new notation can be introduced as

$$\vec{D}_0 \cos(\delta(\omega)) = \varepsilon'(\omega)\varepsilon_0 \vec{E}_0 \tag{1.12}$$

$$\vec{D}_0 \sin(\delta(\omega)) = \varepsilon''(\omega)\varepsilon_0 \vec{E}_0 \tag{1.13}$$

so that the electric displacement field can be expressed as

$$\vec{D}(t) = \varepsilon'(\omega)\varepsilon_0 \vec{E}_0 \cos(\omega t) + \varepsilon''(\omega)\varepsilon_0 \vec{E}_0 \sin(\omega t) \tag{1.14}$$

and the phase delay as

$$\tan(\delta(\omega)) = \frac{\varepsilon''(\omega)}{\varepsilon'(\omega)} \tag{1.15}$$

In case of static field ($\omega = 0$), the Eq. 1.14 reduces to:

$$\vec{D}(t) = \varepsilon'(0)\varepsilon_0 \vec{E}_0 \tag{1.16}$$

In Eq. 1.14, $\vec{D}(t)$ has contributions from the frequency dependent relative permittivity (or the frequency dependent dielectric constant), $\varepsilon'(\omega)$, and the loss factor, $\varepsilon''(\omega)$, which determines the loss of energy in the dielectric. By using complex notation, the complex field vectors ($\hat{\vec{E}}(t)$ and $\hat{\vec{D}}(t)$) and related constitutive equations can be rewritten for the dynamic fields as[21]

$$\hat{\vec{E}}(t) = \vec{E}_0 \cos(\omega t) + \mathrm{i}\vec{E}_0 \sin(\omega t) = \vec{E}_0 \exp(\mathrm{i}\omega t) \tag{1.17}$$

$$\hat{\vec{D}}(t) = \vec{D}_0 \cos(\omega t - \delta) + \mathrm{i}\vec{D}_0 \sin(\omega t - \delta) = \vec{D}_0 \exp[\mathrm{i}(\omega t - \delta)] \tag{1.18}$$

and thus

$$\hat{\varepsilon}(\omega) = \varepsilon'(\omega) - \mathrm{i}\varepsilon''(\omega) \tag{1.19}$$

For zero frequency, however the complex dielectric constant changes into the static dielectric constant, i.e. $\varepsilon = \varepsilon'(0)$.
Hence

$$\hat{\vec{D}}(t) = \hat{\varepsilon}(\omega)\varepsilon_0 \hat{\vec{E}}(t) \tag{1.20}$$

$$\hat{\vec{j}}(t) = \hat{\kappa}(\omega)\hat{\vec{E}}(t) \tag{1.21}$$

$$\hat{\vec{B}}(t) = \hat{\mu}(\omega)\mu_0 \hat{\vec{H}}(t) \tag{1.22}$$

Where $\hat{\mu}(\omega)$ is the complex relative magnetic permeability and $\hat{\kappa}(\omega)$ is the complex conductivity of the dielectric.

1.1.4 Reduced wave equations for electric and magnetic fields

As already mentioned, the harmonic field can be represented in a compact way by using a complex notation as

$$\hat{\vec{E}}(t) = \vec{E}_0 \exp(\mathrm{i}\omega t) \tag{1.23}$$

$$\hat{\vec{H}}(t) = \vec{H}_0 \exp(\mathrm{i}\omega t) \tag{1.24}$$

Comparison of complex constitutive equations (1.20 - 1.22) with the Maxwell equations (1.1 and 1.2) results in

$$\vec{\mathrm{rot}}\, \vec{H}_0 = (\hat{\kappa}(\omega) + \mathrm{i}\omega\hat{\varepsilon}(\omega)\varepsilon_0)\vec{E}_0 \tag{1.25}$$

and

$$\vec{\mathrm{rot}}\, \vec{E}_0 = -\mathrm{i}\omega\hat{\mu}(\omega)\mu_0\vec{H}_0 \tag{1.26}$$

Subsequent application of the rotation operator to Eq. 1.25 in combination with Eq. 1.26 and the Legendre vectorial identity yields

$$\vec{\mathrm{rot}}\, \vec{\mathrm{rot}}\, \vec{H}_0 = \vec{\mathrm{grad}}\, \mathrm{div}\, \vec{H}_0 - \triangle\vec{H}_0 = \vec{\mathrm{grad}}\, (0) - \triangle\vec{H}_0 = -\triangle\, \vec{H}_0 \tag{1.27}$$

the reduced wave equation of the magnetic field

$$\triangle\vec{H}_0 + \hat{k}^2\vec{H}_0 = 0 \tag{1.28}$$

Where $\hat{k}$, in the above equation is defined as propagation constant

$$\hat{k}^2 = k_0^2 \left(\hat{\mu}(\omega)\hat{\varepsilon}(\omega) + \frac{\hat{\mu}(\omega)\hat{\kappa}(\omega)}{\mathrm{i}\omega\varepsilon_0} \right) \tag{1.29}$$

The propagation constant of free space, k_0, is given by

$$k_0 = \omega\sqrt{\varepsilon_0\mu_0} = \frac{2\pi}{\lambda_0} \tag{1.30}$$

with

$$c_0 = \frac{1}{\sqrt{\varepsilon_0\mu_0}} \tag{1.31}$$

where c_0 and λ_0 are the speed of light and the wavelength of a monochromatic wave in vacuum, respectively. For a source-free medium ($\mathrm{div}\, \vec{E} = 0$) a reduced wave equation for $\vec{E}$ can be obtained

$$\triangle\hat{\vec{E}}_0 + \hat{k}^2\hat{\vec{E}}_0 = 0 \tag{1.32}$$

Since for non-magnetizable materials, $\hat{\mu} = 1$, hence Eq. 1.29 can be written as

$$\hat{k}^2 = k_0^2 \left(\hat{\varepsilon}(\omega) + \frac{\hat{\kappa}(\omega)}{\mathrm{i}\omega\varepsilon_0} \right) \equiv k_0^2 \hat{\eta}(\omega) \tag{1.33}$$

and the generalized complex permittivity, $\hat{\eta}(\omega) = \eta'(\omega) - \mathrm{i}\eta''(\omega)$, is defined with its real and imaginary parts as

$$\eta'(\omega) = \varepsilon'(\omega) - \frac{\kappa''(\omega)}{\omega\varepsilon_0} \tag{1.34}$$

$$\eta''(\omega) = \varepsilon''(\omega) + \frac{\kappa'(\omega)}{\omega\varepsilon_0} \tag{1.35}$$

Note that $\hat{\eta}(\omega)$ is the only experimentally accessible quantity in a dielectric experiment. Applying the limits of $\hat{\kappa}(\omega)$, i.e., $\lim_{\nu\to 0} \kappa' = \kappa$ and $\lim_{\nu\to 0} \kappa'' = 0$, where κ is the dc conductivity, helps to separate the conductivity contribution from the $\hat{\eta}(\omega)$ as

$$\varepsilon'(\omega) = \eta'(\omega) \tag{1.36}$$

and

$$\varepsilon''(\omega) = \eta''(\omega) - \frac{\kappa}{\omega\varepsilon_0} \tag{1.37}$$

The complex relative permittivity, $\hat{\varepsilon}(\omega)$ encapsulates all contributions to the time dependent polarization, $\vec{P}(t)$, that depend on frequency, irrespective of their rotational, vibrational, or translational character, hence reflects the dynamics of the investigated system. This includes the dispersion of conductivity due to ion-cloud relaxation[22] as well.

1.2 Dielectric relaxation

1.2.1 Polarization response

For a non-conducting system the polarization $\hat{\vec{P}}$ is related to the dielectric displacement field $\hat{\vec{D}}$ which originates from the response of a material to an external field only, hence

$$\hat{\vec{P}} = \hat{\vec{D}} - \vec{D_0} = \hat{\varepsilon}\varepsilon_0\hat{\vec{E}} - \varepsilon_0\hat{\vec{E}} \tag{1.38}$$

thus

$$\hat{\vec{P}} = (\hat{\varepsilon} - 1)\varepsilon_0\hat{\vec{E}} \tag{1.39}$$

Where $\hat{\chi} = (\hat{\varepsilon} - 1)$, is the dielectric susceptibility of the material under the influence of an outer electric field and $\varepsilon_0\hat{\vec{E}}$ is independent of medium.
The macroscopic polarization $\hat{\vec{P}}$ can be related to its microscopic constituents which describe the microscopic dipole moments of the particles as[21,23]

$$\hat{\vec{P}} = \hat{\vec{P}}_\mu + \hat{\vec{P}}_\alpha \tag{1.40}$$

where $\hat{\vec{P}}_\mu$ denotes orientational polarization (originating due to presence of permanent dipoles which are oriented by an electric field) and $\hat{\vec{P}}_\alpha$ is induced polarization (could be of electronic or atomic in nature).

$$\hat{\vec{P}}_\mu = \sum_k \rho_k \langle \vec{\mu}_k \rangle \tag{1.41}$$

$$\hat{\vec{P}}_\alpha = \sum_k \rho_k \alpha_k (\hat{\vec{E}}_\mathrm{i})_k \tag{1.42}$$

Eq. 1.41 describes the orientation of molecular dipoles of species k with permanent dipole moment, $\vec{\mu}_k$, and number density, ρ_k, in the external field against their thermal motion. However, Eq. 1.42 describes the induced polarization for species with molecular polarizability, α_k, in the medium caused by the inner field, $(\hat{\vec{E}}_\mathrm{i})_k$, (which distorts the neutral distribution of charges) acting at the position of the molecule.
Orientational polarization in liquids occurs at pico- to nanosecond time scales, corresponding to an approximate frequency scale of 1 MHz to 10 THz. Due to the coupling of the reorienting dipoles with the surrounding medium rather broad bands are observed. In this regard, determination of the frequency dependent complex permittivity can provide valuable insight into the dynamics of liquids.
The value of $\hat{\vec{P}}_\alpha$ is rather constant in the microwave range and its frequency dependence leads to information about the intramolecular dynamics of the system. It consists of two contributions, one in the infrared (atomic polarization) and the other in the ultraviolet range (electron polarization). The absorption peaks are in most cases sharper compared to those at microwave frequencies.[24]
Due to the different time scales of $\hat{\vec{P}}_\mu$ and $\hat{\vec{P}}_\alpha$, both effects are generally well separated and can be regarded as linearly independent.[25] Thus the induced polarization can be incorporated into the infinite frequency permittivity, ε_∞, as

$$\hat{\vec{P}}_\mu = \varepsilon_0(\hat{\varepsilon} - \varepsilon_\infty)\hat{\vec{E}} \tag{1.43}$$

$$\hat{\vec{P}}_\alpha = \varepsilon_0(\varepsilon_\infty - 1)\hat{\vec{E}} \tag{1.44}$$

Situated in the far-infrared, ε_∞ denotes the permittivity after the decay of orientational polarization, whereas the contribution arising from induced polarization still remains unchanged. In practice, the limiting value of the permittivity for infinite frequencies as extrapolated from the microwave range is taken for ε_∞.[24]

1.2.2 Response functions of the orientational polarization

In the time scale ranging from mega-hertz to the giga-hertz frequencies, $\hat{\vec{P}}_\mu$ lags behind the changes in the applied field $\hat{\vec{E}}$ as the molecular dipoles cannot align parallel to the

alternating field due to inertia and friction. On the other hand, the induced polarization $\hat{\vec{P}}_\alpha$ always remains in equilibrium with the applied field.
In case of an isotropic linear dielectric (linearity holds if a field $\vec{E}_1$ generates a polarization $\vec{P}_1$ and field $\vec{E}_2$ a polarization $\vec{P}_2$, then the field $\vec{E}_1 + \vec{E}_2$ results in a polarization $\vec{P}_1 + \vec{P}_2$) exposed to a jump in the applied field strength at $t = 0$, the time-dependent polarization $\hat{\vec{P}}_\mu(t)$ can be represented by the equilibrium values corresponding to the field at $t \leq t_o$, $\hat{\vec{P}}_\mu(0)$, and at $t > t_o$, $\hat{\vec{P}}_\mu(\infty)$. The corresponding polarization can be written as[21]

$$\hat{\vec{P}}_\mu(t) = \hat{\vec{P}}_\mu(0) \cdot F_P^{\mathrm{or}}(t) \tag{1.45}$$

where $F_P^{\mathrm{or}}(t)$ is the step response function of the polarization. It is defined as

$$F_P^{\mathrm{or}}(t) = \frac{\langle \vec{P}_\mu(0) \cdot \vec{P}_\mu(t) \rangle}{\langle \vec{P}_\mu(0) \cdot \vec{P}_\mu(0) \rangle} \tag{1.46}$$

For $t = 0$ it follows that $F_P^{\mathrm{or}}(0) = 1$; for high values of t, $\hat{\vec{P}}$ will reach the equilibrium value and consequently $F_P^{\mathrm{or}}(\infty) = 0$. The time domain reflectometry (TDR), one of the experimental technique used in the presented work, is based on this principle.[26]
For a monochromatic harmonic electric field, $\hat{\vec{E}}(t) = \hat{\vec{E}}_0 \exp(-\mathrm{i}\omega t)$ of angular frequency, ω, the orientational polarization at any time t can be expressed as

$$\hat{\vec{P}}(\omega, t) = \varepsilon_0(\varepsilon - \varepsilon_\infty)\hat{\vec{E}}(t)\mathcal{L}_{\mathrm{i}\omega}[f_P^{\mathrm{or}}(t')] \tag{1.47}$$

with

$$\mathcal{L}_{\mathrm{i}\omega}[f_P^{\mathrm{or}}(t')] = \int_0^\infty \exp(-\mathrm{i}\omega t') f_P^{\mathrm{or}}(t') \mathrm{d}t' \tag{1.48}$$

Where $\mathcal{L}_{iw}[f_P^{\mathrm{or}}(t')]$ is the Laplace-transformed pulse response function of the orientational polarization. The pulse response function is related to the step response function as

$$f_P^{\mathrm{or}}(t') = -\frac{\partial F_P^{\mathrm{or}}(t - t')}{\partial(t - t')} \quad \text{normalized with} \quad \int_0^\infty f_P^{\mathrm{or}}(t')\mathrm{d}t' = 1 \tag{1.49}$$

The complex permittivity, $\hat{\varepsilon}(\omega)$, can then be calculated as[21]

$$\hat{\varepsilon}(\omega) = \varepsilon'(\omega) - \mathrm{i}\varepsilon''(\omega) = \varepsilon_\infty + (\varepsilon - \varepsilon_\infty) \cdot \mathcal{L}_{\mathrm{i}\omega}[f_P^{\mathrm{or}}(t')] \tag{1.50}$$

1.3 Empirical description of dielectric relaxation

For the macroscopic description of the complex dielectric permittivity, several mathematical models have been used in literature. For a practical view point, however, a single relaxation model is most often not sufficient hence, useful information is extracted via combination of several models.

1.3.1 Debye equation

For the simplest description of dielectric spectra, the Debye (D) equation[27] (in which the dispersion curve is point-symmetric, $\varepsilon' = \varepsilon'(\ln(\omega))$, and the absorption curve, $\varepsilon'' = \varepsilon''(\ln(\omega))$ reaches maximum value at $\omega = 1/\tau$) is very useful. It is assumed that the decrease of the orientational polarization in the absence of an external electric field is directly proportional to the polarization itself.[28], and the decay of orientational polarization follows the first order as

$$\frac{\partial}{\partial t}\vec{P}_\mu(t) = -\frac{1}{\tau}\vec{P}_\mu(t) \tag{1.51}$$

The relaxation time, τ describes the dynamics of the process. The solution of above equation gives

$$\vec{P}_\mu(t) = \vec{P}_\mu(0)\exp\left(-\frac{t}{\tau}\right) \tag{1.52}$$

and the step response function, $F_P^{\mathrm{or}}(t) = \exp\left(-\frac{t}{\tau}\right)$, can be obtained. While the pulse response function can be calculated by using Eq. 1.49.

$$f_P^{\mathrm{or}}(t) = \frac{1}{\tau}\exp\left(-\frac{t}{\tau}\right) \tag{1.53}$$

Fourier transformation of the pulse response function (see Eq. 1.50) generates the complex dielectric permittivity as

$$\hat{\varepsilon}(\omega) = \varepsilon_\infty + (\varepsilon - \varepsilon_\infty)\cdot\mathcal{L}_{\mathrm{i}\omega}\left[\frac{1}{\tau}\exp\left(-\frac{t}{\tau}\right)\right] \tag{1.54}$$

So the Debye equation can be written as

$$\hat{\varepsilon}(\omega) = \varepsilon_\infty + \frac{\varepsilon - \varepsilon_\infty}{1 + \mathrm{i}\omega\tau} \tag{1.55}$$

which can be split into the real part (proportional to the reversible storage of energy in the system per cycle)

$$\varepsilon'(\omega) = \varepsilon_\infty + \frac{\varepsilon - \varepsilon_\infty}{1 + \omega^2\tau^2} \tag{1.56}$$

and imaginary part[23](proportional to the energy dissipated per cycle).

$$\varepsilon''(\omega) = \omega\tau\frac{\varepsilon - \varepsilon_\infty}{1 + \omega^2\tau^2} \tag{1.57}$$

1.3.2 Non-Debye type relaxations

With an increase in the experimental frequency range (also increased accuracy of the measurements), deviations from the Debye equation occur, hence a single relaxation time can not provide a satisfying description of the spectra. This can be improved by using

an empirical relaxation time distribution, $g(\tau)$.[21] Due to practical reasons, the logarithmic representation, $G(\ln\tau)$, is usually preferred. The complex permittivity will be then

$$\hat{\varepsilon}(\omega) = \varepsilon_\infty + (\varepsilon - \varepsilon_\infty)\int_0^\infty \frac{G(\ln\tau)}{(1+\mathrm{i}\omega\tau)}\mathrm{d}\ln\tau \quad \text{with} \quad \int_0^\infty G(\ln\tau)\mathrm{d}\ln\tau = 1. \tag{1.58}$$

Since $G(\ln\tau)$ can not be obtained directly from the experimental data, therefore empirical parameters are used which account for the broadness and shape of the relaxation time distribution function.

Cole-Cole equation. By introducing an empirical parameter $0 \leq \alpha < 1$ into the Debye equation, the Cole-Cole (CC) equation[29,30] (with a symmetric relaxation time distribution around a principal relaxation time τ_0, describing symmetric dispersion and absorption curves) is obtained

$$\hat{\varepsilon}(\omega) = \varepsilon_\infty + \frac{\varepsilon - \varepsilon_\infty}{1 + (\mathrm{i}\omega\tau_0)^{1-\alpha}} \tag{1.59}$$

Cole-Cole distribution results in flatter dispersion curves and broadened absorption spectra. For $\alpha = 0$, Eq. 1.59 turns into Debye equation.

Cole-Davidson equation. The Cole-Davidson (CD) equation,[31,32] uses another empirical parameter $0 < \beta \leq 1$ and it describes an asymmetrical relaxation time distribution around the center of gravity τ_0

$$\hat{\varepsilon}(\omega) = \varepsilon_\infty + \frac{\varepsilon - \varepsilon_\infty}{(1 + \mathrm{i}\omega\tau_0)^{\beta}} \tag{1.60}$$

For CD equation both dispersions and absorption curves are asymmetric. For $\beta = 1$ CD equation turns into the Debye equation.

Havriliak-Negami equation. For the description of broad asymmetric relaxation time distribution, Havriliak-Negami (HN) equation[33] (uses both $0 \leq \alpha < 1$ and $0 < \beta \leq 1$) is used as

$$\hat{\varepsilon}(\omega) = \varepsilon_\infty + \frac{\varepsilon - \varepsilon_\infty}{[1 + (\mathrm{i}\omega\tau_0)^{1-\alpha}]^{\beta}} \tag{1.61}$$

In this case both dispersion and absorption curves are asymmetric. When $\alpha = 0$ and $\beta = 1$, Eq. 1.61 is converted to the Debye equation.

1.3.3 Damped harmonic oscillator

The time dependent dielectric response of the sample may not arise only due to the relaxation phenomenon but the resonance processes (due to atomic or molecular vibrations and liberations) may contribute as well. Resonance processes may appear in the THz or far-infrared regions and damped harmonic oscillator (DHO) model is used to describe them. Considering a harmonic oscillator subjected to a damping force and driven by a

harmonically oscillating field $E(t) = E_0 e^{i\omega t}$, the frequency dependent response function of the system can be obtained from the solution of the differential equation (given below) describing the

$$\hat{\varepsilon}(\omega) = \varepsilon_\infty + \frac{(\varepsilon - \varepsilon_\infty)\,\omega_0^2}{(\omega_0^2 - \omega^2) + i\omega\tau_D^{-1}} = \varepsilon_\infty + \frac{(\varepsilon - \varepsilon_\infty)\,\nu_0^2}{\nu_0^2 - (\frac{\omega}{2\pi})^2 + i\frac{\omega}{2\pi}\gamma} \tag{1.62}$$

time-dependent motion, $x(t)$, of an effective charge, q.[34] In Eq. 1.62, $\omega_0 = \sqrt{k/m} = 2\pi\nu_0$ and $\gamma = 1/(2\pi\tau_D)$ are the angular resonance frequency and damping constant of the oscillator, respectively. For $\tau_D \ll \omega_0^{-1}$, Eq. 1.62 reduces to the Debye equation.

1.3.4 Combination of models

Most often a single mathematical model is insufficient to describe the complex permittivity spectrum (as it may consists of more than one relaxations), thus several models can be combined together and tested for a given system. Therefore, Eq. 1.58 can be written as a superposition of n single relaxation processes

$$\hat{\varepsilon}(\omega) = \varepsilon_\infty + \sum_{j=1}^{n}(\varepsilon_j - \varepsilon_{\infty,j}) \int_0^\infty \frac{G_j(\ln\tau_j)}{1 + i\omega\tau_j} d\ln\tau_j \tag{1.63}$$

Each of the processes is characterized by its own relaxation time, τ_j, and dispersion amplitude, S_j, that can be defined as

$$\varepsilon - \varepsilon_\infty = \sum_{j=1}^{n}(\varepsilon_j - \varepsilon_{\infty,j}) = \sum_{j=1}^{n} S_j \tag{1.64}$$

$$\varepsilon_{\infty,j} = \varepsilon_{j+1} \tag{1.65}$$

So the HN and DHO equations can be rewritten in summation form as

$$\begin{aligned} \hat{\varepsilon}(\omega) = \varepsilon_\infty \quad &+ \quad \sum_j \frac{S_j}{[1 + (i\omega\tau_j)^{1-\alpha_j}]^{\beta_j}} \\ &+ \quad \sum_l \frac{S_l\,\omega_{0,l}^2}{(\omega_{0,l}^2 - \omega^2) + i\omega\tau_{D,l}^{-1}} \end{aligned} \tag{1.66}$$

1.4 Microscopic models of dielectric relaxation

1.4.1 Onsager equation

The Onsager model[21,35] describes the response of a single dipole embedded in a continuum medium (characterized by its macroscopic properties). Specific interactions (short range) and the anisotropy of the field are neglected by this model, the model generally does not hold for the liquids where the associations are known to occur.

Onsager deduced following equation to relate macroscopic (ε) and microscopic (the polarizability, α_j, and the dipole moment, μ_j, of molecular-level species j) properties of a dielectric

$$\varepsilon_0(\varepsilon - 1)\vec{E} = \vec{E}_h \cdot \sum_j \frac{\rho_j}{1 - \alpha_j f_j}\left(\alpha_j + \frac{1}{3k_\mathrm{B}T} \cdot \frac{\mu_j^2}{1 - \alpha_j f_j}\right) \tag{1.67}$$

where ρ_j represents the dipole density and f_j the reaction field factor describing a spherical cavity of finite radius, in which the particle is embedded. Note, that the Onsager equation is only valid for systems with a single dispersion step.
For a spherical cavity (space where the surroundings can adapt to new environment) in a dielectric material, the homogeneous cavity field, $\vec{E}_h$, is given by[21]

$$\vec{E}_h = \frac{3\varepsilon}{2\varepsilon + 1}\vec{E} \tag{1.68}$$

so the Onsager equation can be written in a general form as

$$\frac{(\varepsilon - 1)(2\varepsilon + 1)\varepsilon_0}{3\varepsilon} = \sum_j \frac{\rho_j}{1 - \alpha_j f_j}\left(\alpha_j + \frac{1}{3k_\mathrm{B}T} \cdot \frac{\mu_j^2}{1 - \alpha_j f_j}\right) \tag{1.69}$$

In the case of a pure dipole liquid with non-polarizable molecules ($\alpha = 0$) Eq. 1.69 reduces to

$$\frac{(\varepsilon - \varepsilon_\infty)(2\varepsilon + \varepsilon_\infty)}{\varepsilon(\varepsilon_\infty + 2)^2} = \frac{\rho\mu^2}{9\varepsilon_0 k_\mathrm{B}T} \tag{1.70}$$

From the above equations it is plausible to find the permanent dipole moment of a species from its dielectric constant, provided that the density and ε_∞ are already known.

1.4.2 Kirkwood-Fröhlich equation

The Kirkwood and Fröhlich equation is based on a continuum medium with dielectric constant ε_∞ in which the permanent dipoles are embedded (correlations between positions and induced moments of the molecules are neglected)[21]. For the associating liquids the Kirkwood and Fröhlich equation incorporates the factor responsible for the deviations from the Onsager equation. This theory[36,37] is based on a model of a dipole whose orientation correlates with its neighboring dipoles resulting in

$$\frac{(\varepsilon - \varepsilon_\infty)(2\varepsilon + \varepsilon_\infty)}{\varepsilon(\varepsilon_\infty + 2)^2} = \frac{\rho\mu^2}{9\varepsilon_0 k_\mathrm{B}T} \cdot g_\mathrm{K} \tag{1.71}$$

where g_K is the Kirkwood correlation factor (accounts for the correlation between molecular orientations). For $g_\mathrm{K} = 1$, molecular orientations has no correlation or in other words the dipoles are randomly located. While $g_\mathrm{K} > 1$ corresponds to preferentially parallel orientations and $g_\mathrm{K} < 1$ to antiparallel orientations.

1.4.3 Cavell equation

Onsager's equation (Eq. 1.69) can be extended for systems with more than one dispersion steps due to different dipolar species as

$$\frac{\varepsilon + A_j(1-\varepsilon)}{\varepsilon} \cdot S_j = \frac{N_\mathrm{A} c_j}{3 k_\mathrm{B} T \varepsilon_0} \cdot \mu_{\mathrm{eff},j}^2 \tag{1.72}$$

The above equation is known as Cavell equation[38] which relates the dispersion amplitude, $S_j = \varepsilon_j - \varepsilon_{j+1}$, of relaxation process j to the molar concentration of the species, c_j, and their effective dipole moments, $\mu_{\mathrm{eff},j}$. The shape factor A_j accounts for the shape of the relaxing particle; for spheres, $A_j = 1/3$, but it can be calculated for ellipsoids of any shape (half-axes $a_j > b_j > c_j$) through the equation[21,24]

$$A_j = \frac{a_j b_j c_j}{2} \int_0^\infty \frac{\mathrm{d}s}{(s + a_j^2)^{3/2}(s + b_j^2)^{1/2}(s + c_j^2)^{1/2}} \tag{1.73}$$

For prolate ellipsoids ($b_j = c_j$), Scholte,[39] derived an expression as

$$A_j = -\frac{1}{p_j^2 - 1} + \frac{p_j}{(p_j^2 - 1)^{1.5}} \ln\left(p_j + \sqrt{p_j^2 - 1}\right) \qquad \text{with} \qquad p_j = \frac{a_j}{b_j} \tag{1.74}$$

Where $\mu_{\mathrm{eff},j}$ (which can be calculated using Eq. 1.72 if c_j is known) is related to $\mu_{\mathrm{ap},j}$, the apparent dipole moment of the species in solutions in the absence of orientational correlations, as

$$\mu_{\mathrm{eff},j} = \sqrt{g_j}\mu_{\mathrm{ap},j} \tag{1.75}$$

and

$$\mu_{\mathrm{ap},j} = \frac{\mu_j}{1 - f_j \alpha_j} \tag{1.76}$$

includes cavity- and reaction-field effects on μ_j, the dipole moment of the isolated (gas phase) species. The (empirical) factor g_j is a measure for the strength of the correlations whose values are interpreted as for the Kirkwood factor g_K (Eq. 1.71), and the reaction field factor f_j can be defined for a spherical cavity of radius a_j via[21]

$$f_j = \frac{1}{4\pi\varepsilon_0 a_j^3} \cdot \frac{2\varepsilon - 2}{2\varepsilon + 1} \tag{1.77}$$

or, more generally, for ellipsoidal particles via[40]

$$f_j = \frac{3}{4\pi\varepsilon_0 a_j b_j c_j} \cdot \frac{A_j(1 - A_j)(\varepsilon - 1)}{\varepsilon + (1 - \varepsilon)A_j} \tag{1.78}$$

1.4.4 Microscopic and macroscopic relaxation times

It is very meaningful to relate the experimentally accessible (macroscopic) dielectric relaxation time, τ, and the microscopic relaxation time (rotational correlation time), τ_rot, as

far as the interpretation of dielectric spectra and a number of theoretical approaches are concerned. Debye suggested the expression[27]

$$\tau = \frac{\varepsilon + 2}{\varepsilon_\infty + 2} \cdot \tau_{\mathrm{rot}} \tag{1.79}$$

derived under the assumption of a Lorentz field as inner field (to which particle is exposed to). However, this approach is not accurate enough for polar dielectrics and applies only to non-polar systems. For the case of pure rotational diffusion, Powles and Glarum,[41,42] proposed following expression

$$\tau = \frac{3\varepsilon}{2\varepsilon + \varepsilon_\infty} \cdot \tau_{\mathrm{rot}} \tag{1.80}$$

for relating microscopic and macroscopic relaxation times. A more generalized equation, accounting for dipole-dipole correlation, is given by Madden and Kivelson[43]

$$\tau = \frac{3\varepsilon}{2\varepsilon + \varepsilon_\infty} \cdot \frac{g_{\mathrm{K}}}{\dot{g}} \cdot \tau_{\mathrm{rot}} \tag{1.81}$$

where g_{K} is the Kirkwood correlation factor and $\dot{g}$ is the dynamic correlation factor. For the limit $g_{\mathrm{K}}/\dot{g} = 1$ Eq. 1.81 reduces to the Powles-Glarum equation (Eq. 1.80) and the microscopic relaxation time obtained from above equations can be compared with one as mentioned in section 1.4.5.

1.4.5 Debye model of rotational diffusion

Debye predicted the relaxation time of a simple system consisting of an aggregation of spherical inelastic dipoles which do not interact with each other. Microscopically, uncorrelated collisions of the dipolar particles cause a reorientation of the dipoles, resulting in angular Brownian motion through very small angular steps, this mechanism is called diffusion of dipole orientation or rotational diffusion.[27]
However, Debye's theory is only valid for non-associating systems and particles that are large compared to their surrounding ones[44] because of involved assumptions: (1) for the reorientation of spherical particles, inertial effects and dipole-dipole interactions are neglected; (2) the hydrodynamic laws of rotation of macroscopic particles in a liquid can be applied on the microscopic level.[27]
Having these limitations and by using Lorentz field as the inner field, Debye obtained the dipole correlation function[21]

$$\gamma(t) = \exp\left(-\frac{t}{\tau_{\mathrm{rot}}}\right) \tag{1.82}$$

The microscopic relaxation time, τ_{rot}, is related to the friction factor, ζ, as

$$\tau_{\mathrm{rot}} = \frac{\zeta}{2k_{\mathrm{B}}T} \tag{1.83}$$

Assuming a hydrodynamically controlled rotation of the sphere in a viscous media, the Stokes-Einstein-Debye (SED) equation

$$\tau_{\mathrm{rot}} = \tau' = \frac{3V_{\mathrm{m}}\eta'}{k_{\mathrm{B}}T} \tag{1.84}$$

is obtained, where, V_{m} is the molecular volume of the rotating sphere and η' represents the microscopic viscosity (i.e., the dynamic viscosity of the environment of the sphere). However, the application of this theory is limited as the relation between microscopic and macroscopic (measured), η, viscosities is not clear. To overcome this problem, Dote et al.[45] derived a more general expression for the microscopic relaxation time

$$\tau_{\mathrm{rot}} = \tau' = \frac{3V_{\mathrm{eff}}\eta}{k_{\mathrm{B}}T} + \tau^0_{\mathrm{rot}} \tag{1.85}$$

where τ^0_{rot} (the empirical axis intercept) can be interpreted as the correlation time of the freely rotating particle. The effective volume of rotation, V_{eff}, can be defined as

$$V_{\mathrm{eff}} = fCV_{\mathrm{m}} \tag{1.86}$$

For a prolate ellipsoid with major half-axis a and minor half-axis b, the shape factor, f, that accounts for deviations of the rotating particle from that of spherical shape can be calculated from the geometry of the molecule as[46]

$$f = \frac{\frac{2}{3}[1-(\alpha^{\perp})^4]}{\frac{[2-(\alpha^{\perp})^2](\alpha^{\perp})^2}{[1-(\alpha^{\perp})^2]^{1/2}} \ln\left[\frac{1+[1-(\alpha^{\perp})^2]^{1/2}}{\alpha^{\perp}}\right] - (\alpha^{\perp})^2} \tag{1.87}$$

where $\alpha^{\perp}$ is the ratio between the volume of particle and the volume swept out as the particle rotates about an axis perpendicular to the symmetry axis through the center of hydrodynamic stress ($\alpha^{\perp} = b/a$ for a prolate ellipsoid).[47] The hydrodynamic friction factor, C, (an empirical parameter) couples macroscopic to microscopic viscosity, its limiting values are $C = 1$ for stick (appropriate for macroscopic molecules) and $C = 1 - f^{-2/3}$ for slip boundary conditions (preferably used for small molecules in non-polar and noninteracting solvents). However, under special conditions, for example the rotation of very small molecules, values of $C < C_{\mathrm{slip}}$ are possible[48] and this accounts for the "subslip" boundary conditions that can be interpreted as evidence of the molecularity of the system[45]. For the solvated ions (moving along with their hydration shells), the slip boundary conditions are taken as to be physically more appropriate[10,49].

1.4.6 Molecular jump model

Despite the usefulness of the Debye rotational diffusion model for simple systems, its validity to be the actual mechanism underlying the dipolar dynamics is sporadically questioned.[50–52] In principle several experimental techniques can be employed to study the the reorientation mechanism in different systems, in this regard infrared (IR) pump-probe spectroscopy[53], nuclear magnetic resonance (NMR)[54], quasi-elastic neutron scattering (QENS)[55], optical kerr-effect spectroscopy[50] and DRS[56] can be very promising. In addition molecular dynamics (MD) simulations[57,58] provide insight into the reorientation dynamics in aqueous systems.
On the basis of time-correlation function (TCF) of the molecular orientation the dipolar dynamics in liquids can be imagined as consisting of two different mechanisms as recently

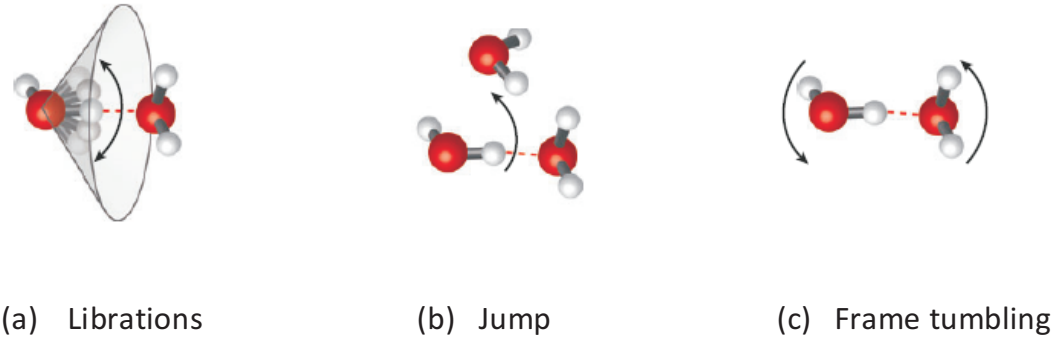

Figure 1.1: Pictorial representation of water reorientation dynamics.[59]

suggested by Laage et al for the aqueous systems[59]. The first one being the faster occuring at $\lesssim$ 200 fs depicts the librational motions leading only to limited reorientation. The second step is a relatively slow process, picosecond reorientation, which results from the large-amplitude angular jumps of a water molecule between two available acceptor sites (Figure 1.1)[59]. According to Ivanov[60], the nth order reorientation time of TCF can be written as

$$\tau_n^{\text{jump}} = \tau_{\text{jump}} \left\{ 1 - \frac{1}{2n+1} \frac{\sin[(n+1/2) \triangle \theta]}{\sin(\triangle\theta/2)} \right\}^{-1} \tag{1.88}$$

where $\triangle\theta$ is the jump amplitude. It should be noted that for $\triangle\theta \to 0$ the jump model is reduced to rotational diffusion. The Eq. 1.88 is however, incomplete and it can be modified using the extended jump model (EJM)[61] where the frame contributions are also taken into account hence the actual reorientation time of TCF would be

$$\frac{1}{\tau_n^{\text{EJM}}} = \frac{1}{\tau_n^{\text{jump}}} + \frac{1}{\tau_n^{\text{frame}}} \tag{1.89}$$

The Eq. 1.89 implies that between the jumps the molecular orientation is not fixed.

1.5 Temperature dependence of relaxation times

1.5.1 Arrhenius equation

Temperature effects on reaction rates can be successfully described by the Arrhenius equation[62] which is based on the idea that reaction occurs as a result of thermal excitation of reactants, via the formation of an excited state called *activated complex*, this is accompanied by the energy requirement (provided by the thermal fluctuations) known as the activation energy, E_{a} (see sections 1.4.5 and 1.4.6). The Arrhenius equation can be

modified for relaxation times as

$$\ln \tau = \ln \tau_0 + \frac{E_\mathrm{a}}{RT} \tag{1.90}$$

Where E_a can be obtained through the slope and τ_0, the pre-exponential factor represents the intercept of the above straight line relation. Since increase in temperature results in decrease in observed relaxation times (due to increased dynamics of the related relaxation process) the τ_0 value represents the minimum of τ for a relaxation process.

1.5.2 Eyring equation

A trivial equivalence to the Arrhenius equation is the transition state or Eyring equation[63] which results from a theoretical model, based on transition state theory. Eyring equation can be can be applied to study the temperature dependence of experimental relaxation time, τ as

$$\ln \tau = \ln \frac{h}{k_\mathrm{B} T} - \frac{\Delta S^{\neq}}{R} + \frac{\Delta H^{\neq}}{RT} \tag{1.91}$$

where h is Planck's constant, R is the universal gas constant and $\Delta S^{\neq}$ and $\Delta H^{\neq}$ are respectively the activation entropy and activation enthalpy. Equation 1.91 neglects the temperature dependencies of $\Delta H^{\neq}$ and $\Delta S^{\neq}$ but extensions are possible, see reference[64]. The Gibbs energy of activation, $\Delta G^{\neq}$, can be calculated as

$$\Delta G^{\neq} = \Delta H^{\neq} - T\Delta S^{\neq} \tag{1.92}$$

The quantities $\Delta H^{\neq}$ and E_a can be interconverted via the thermodynamic relation

$$E_\mathrm{a} = \Delta H^{\neq} + RT \tag{1.93}$$

1.6 Solute-related relaxations

1.6.1 Ion-pair relaxation

The steady accretion of experimental data providing direct indication of ion-pairing has put more stress to have a keen look into this phenomenon as its presence leaves visible effects in many experimental techniques such as conductivity, potentiometry as well as on various thermodynamic parameters as osmotic coefficient and activity coefficient. Among various spectroscopic techniques (UV-vis, IR, Raman and NMR), DRS has unique sensitivity towards various types of ion pairs and DRS studies have been able to show ion pairing *to some extent* in virtually all classical strong electrolytes.[10]

Two Charged species, separated by a distance, d could be described as ion pairs if $a < d < r$, where a is the distance of closest approach and r is certain cutoff distance, provided that the residence time of such pair at distance d is greater than the diffusion time.[65] This is essentially equivalent to the notion that, in order to detect ion pairs as distinct species in solution, their life time ($\tau_L = \frac{\ln 2}{k_d}$, k_d is the decay constant of ion pairs) should be atleast

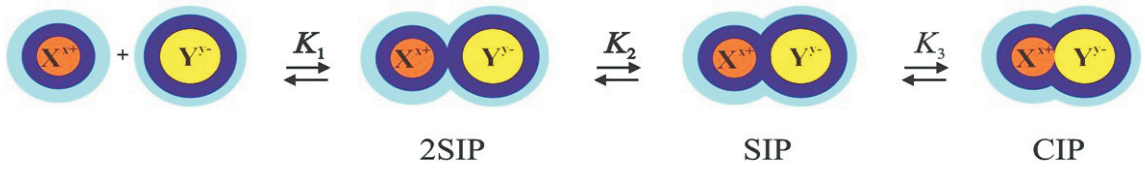

Figure 1.2: Eigen's scheme of stepwise ion association.[67]

comparable to the rotational correlation time. Literature reports values of ion-pair life times of ~ 1 ns.[66] Ion association is mainly dependent on the ionic charges of the partners and the solvent permittivity.

$$\underset{\text{hydrated free ions}}{\mathrm{C}^{c+}(\mathrm{aq}) + \mathrm{A}^{a-}(\mathrm{aq})} \overset{K_A}{\rightleftharpoons} \underset{\text{2SIP}}{\mathrm{CA}^{0}(\mathrm{aq})} \tag{1.94}$$

Where K_A is the equilibrium constant for the overall ion association. DRS detects ion-pairing even if its very weak i.e. for $K_\mathrm{A} \leq 1\ \mathrm{M}^{-1}$.[10]
On the basis of ultrasonic absorption data Eigen and Tamm suggested a multistep mechanism (Figure 1.2) for the formation of ion pairs in aqueous solutions.[67] This mechanism proceeds with the successive formation of different kinds of ion pairs as a result of competition between ion-solvent and ion-ion interactions. First stage of Eigen and Tamm mechanism is essentially a diffusion controlled reaction (very fast) and is associated with the formation of double-solvent-separated ion pair (2SIP) or an outer-outer-sphere complex (both the ionic partners keep their solvation shells hence a double layer of solvent molecules intervene between the centers of cation and anion).

$$\underset{\text{hydrated free ions}}{\mathrm{C}^{c+}(\mathrm{aq}) + \mathrm{A}^{a-}(\mathrm{aq})} \overset{K_1}{\rightleftharpoons} \underset{\text{2SIP}}{[\mathrm{C}^{c+}(\mathrm{OH_2})(\mathrm{OH_2})\mathrm{A}^{a-}](\mathrm{aq})} \tag{1.95}$$

Successive ejection of water molecules from 2SIP leads to the formation of a solvent-shared ion pair (SIP) or outer sphere complex (with single layer of solvent molecules between centers of two ionic partners, formation of SIP is slower than the 2SIP)

$$\underset{\text{2SIP}}{[\mathrm{C}^{c+}(\mathrm{OH_2})(\mathrm{OH_2})\mathrm{A}^{a-}](\mathrm{aq})} \overset{K_2}{\rightleftharpoons} \underset{\text{SIP}}{[\mathrm{C}^{c+}(\mathrm{OH_2})\mathrm{A}^{a-}](\mathrm{aq})} \tag{1.96}$$

finally in the last slowest step, total elimination of solvent molecules from SIP results into a contact ion pair (CIP) or inner-sphere complex (cation and anion are in direct contact)

$$\underset{\text{SIP}}{[\mathrm{C}^{c+}(\mathrm{OH_2})\mathrm{A}^{a-}](\mathrm{aq})} \overset{K_3}{\rightleftharpoons} \underset{\text{CIP}}{[\mathrm{CA}]^{(c-a)+}(\mathrm{aq})} \tag{1.97}$$

Each of these three steps is characterized by its equilibrium constant, $K_i, i = 1, 2, 3$, and the association constant $K_\mathrm{A} = K_1 + K_1K_2 + K_1K_2K_3$. Limited number of techniques are available to find K_1, K_2 and K_3, however conventional thermodynamic and conductivity measurements are able to find K_A.[68,69] Depending on the solute concentration and relative

strength of ion-ion-, ion-solvent- and solvent solvent interactions, it is possible that the above mentioned sequence of reactions stops at first or second stage.[11] Being dependent on the dipole moment of the species the sensitivity of DRS towards various ion-pair types varies in the order: 2SIP > SIP > CIP.[11,65]
DRS measurements allow the calculation of K_A as

$$K_A = c_{IP}/(c - c_{IP})^2 \tag{1.98}$$

where c_{IP}, in solution can be determined via Eqs. 1.72-1.78 (with $j = IP$). For the calculation of A_{IP} and μ_{IP}, geometrical parameters, the polarizability and the gas phase dipole moment of the corresponding species should be known (which for the presented study are calculated from the MOPAC). The obtained $K_A(I)$ can be fitted in a Guggenheim-type equation[11] using I ($\equiv c$ for 1:1 electrolytes), the stoichiometric ionic strength as independent variable of the equation as

$$\log K_A = \log K_A^o - \frac{2A_{DH}|z_+z_-|\sqrt{I}}{1 + A_K\sqrt{I}} + B_K I + C_K I^{3/2} \tag{1.99}$$

where A_{DH} is the Debye-Hückel coefficient (0.5115 $L^{1/2}mol^{-1/2}$ for water at 25 °C), and Y_K ($Y = A$, B, C) are adjustable parameters (A_K is fixed at 1.00 $M^{-1/2}$ throughout for present studies).[70]

1.6.2 Ion-cloud relaxation

In solutions of electrolytes or charged colloids, any single ion can be viewed as charged species surrounded by the ions of opposite charge (forming an oppositely charged ionic atmosphere) due to long-range Coulombic interactions. Under the influence of an electric field ions move in certain direction while the ionic atmosphere renews its position accordingly in a finite time (ion-cloud relaxation), this effect was depicted by Debye and Falkenhagen in 1928[71]. The presence of this ion-cloud has remarkable effects on the conductivities of electrolyte solutions mainly due to *electrophoretic effect* and *time-of-relaxation effect*.[72]
The relaxation time of ion-cloud relaxation mode is related to the molar conductivity of electrolyte at infinite dilution, Λ_∞, as[22]

$$\tau_{ic} = \frac{\varepsilon\varepsilon_o}{c\Lambda_\infty} \tag{1.100}$$

Eq. 1.100 predicts a pronounced decrease of τ_{ic} with increasing concentration of solute.
Until recently, ion-cloud relaxation was neglected in the analysis of DRS spectra of electrolytes as its amplitude was thought to be small[73–75]. Features in the 10 MHz to 1 GHz region were commonly assigned to ion pairing only[10]. Via his theoretical model, Yamaguchi et al[76,77] found a low frequency composite mode (jointly arising from ion-cloud relaxation and ion-pair reorientation) whose amplitude is very similar to the relaxation strengths of the low-frequency modes, very often observed for 1:1 electrolytes. Thus this process should be detectable by DRS as is observed for the aqueous solutions of NaCl[78]. However, up to date neither the theoretical approaches nor the experimental techniques

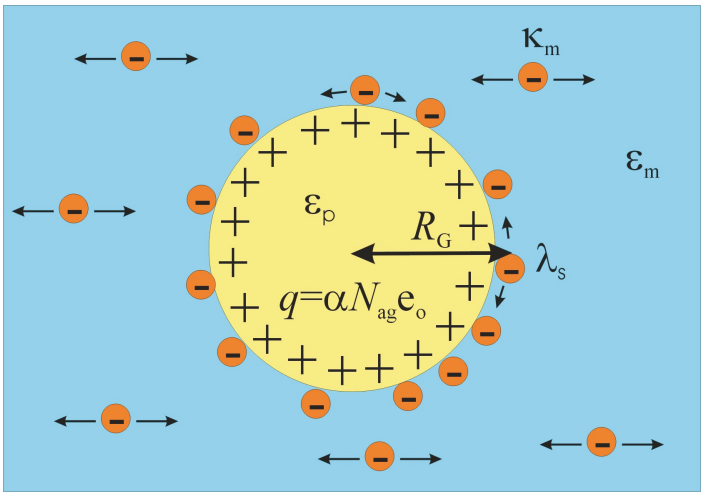

Figure 1.3: Grosse's model for solutions of charged colloids (cationic as example). Arrows show the directions of motion of the counterions either in the diffused ion-cloud or adsorbed to the micellar surface, as a result of an applied horizontal ac field.[79]

are able to completely distinguish these two solute-related relaxations from each other. For colloids, however, including charged micelles, ion-cloud relaxation contributes significantly to the dielectric spectra. The theory presented in the following section for DRS of colloids incorporates this ion-cloud relaxation.

1.6.3 Grosse's model

Dielectric properties of colloidal systems can be described by the theory of Grosse[79]. The model considers a suspension of colloidal particles with a volume fraction, ϕ_{mic},

$$\phi_{\mathrm{mic}} = \frac{4\pi N_{\mathrm{A}} R_{\mathrm{G}}^3}{3N_{\mathrm{ag}}} \times (c - c_{\mathrm{f}}) \tag{1.101}$$

charge, q, conductivity, $\kappa_{\mathrm{p}} = 0$, and permittivity, ε_{p}, embedded in a medium of conductivity, κ_{m}, and permittivity, ε_{m} (Figure 1.3). In Eq. 1.101, c_{f} is the concentration of free monomers and N_{ag} is the aggregation number of the micelle. The theory predicts two dispersion steps. The process occurring at lower frequencies is assigned to the ion-cloud relaxation in the colloids. DRS spectra of micellar solutions reveal that, in the frequency regime this process occupies the range ~ 100 MHz to 1 GHz[15,80] The model yields for the amplitude and relaxation time of the ion-cloud relaxation process the expressions as

$$\tau_1 \approx \frac{R_{\mathrm{G}}^2}{D} \tag{1.102}$$

where R_G and D are the effective Grosses's radius and diffusion coefficient of the counterions respectively.

$$S_1 = \frac{9\phi_{mic}\varepsilon_m(2\chi\lambda_s/\kappa_m)^4}{16[\frac{2\chi\lambda_s}{\kappa_m}(\frac{2\lambda_s}{R_G\kappa_m}+1)+2]^2} \tag{1.103}$$

In Eq. 1.103, λ_s denotes surface conductance whereas the parameter χ is related to Debye length, χ^{-1} (characterizes the size of ion cloud) which can be written as

$$\chi^{-1} = \sqrt{\frac{\varepsilon_o\varepsilon_m D}{\kappa_m}} \tag{1.104}$$

The process occurring at relatively higher frequencies reflects the interfacial polarization at the micelle/solvent boundary and it results from the tangential motion of the bound counterions. The relaxation time of this process can be written as

$$\tau_2 = \frac{\varepsilon_o\varepsilon_m(\frac{\varepsilon_p}{\varepsilon_m}+2)}{\kappa_m(\frac{2\lambda_s}{R_G\kappa_m}+2)} \tag{1.105}$$

whereas its amplitude can be defined as

$$S_2 = \frac{9\phi_{mic}\varepsilon_m(\frac{2\lambda_s}{R_G\kappa_m}-\frac{\varepsilon_p}{\varepsilon_m})^2}{(\frac{\varepsilon_p}{\varepsilon_m}+2)(\frac{2\lambda_s}{R_G\kappa_m}+2)^2} \tag{1.106}$$

The relaxation times (τ_1 and τ_2) and amplitudes (S_1 and S_2) are derived by assuming that ϕ_{mic} is small and $R_G \gg \chi^{-1}$.

Chapter 2

Experimental

2.1 Sample preparation

Choline chloride, chlorocholine chloride, ammonium chloride and sodium dodecanoate used in the present study were analytical reagents of commercial grade. Choline dodecylsulfate and choline dodecanoate were prepared by R. Klein at our Institute. The details of the synthesis procedure and characterization can be found in her Ph.D thesis.[8]

Prior to use, the studied salts were dried in vacuum for about 72 hours (see Table 2.1 for details) using P_2O_5 (Sicapent, Merck) as a desiccant. Dried salts were stored under dry N_2 atmosphere and solutions were prepared by weight without buoyancy corrections (thus a relative uncertainty in solute molality, m, of ± 0.002) using deionized water having conductivity, $\kappa < 2 \times 10^{-5}\,\mathrm{S \cdot m^{-1}}$ (Millipore Corp.).

Table 2.1: Data regarding used salts, their Purities and drying temperatures, T.

Material (Abb.)	Source	Purity	T / K
Choline chloride (ChCl)	Sigma-Aldrich	$\geq 98\,\%$	313
Chlorocholine chloride (Cl-ChCl)	Sigma-Aldrich	$\geq 98\,\%$	313
Ammonium chloride (NH_4Cl)	Merck	$\geq 99.8\,\%$	333
Choline dodecylsulfate (ChDS)	Reference 8	-	333
Choline dodecanoate (ChC12)	Reference 8	-	333
Sodium dodecanoate (NaC12)	Sigma-Aldrich	$\geq 99\,\%$	333

2.2 Measurement of dielectric properties

2.2.1 Time-domain reflectometry

Dielectric data in the low frequency regime (down to few MHz) is of great importance to study the fundamental aspects of structure and dynamics in liquids, in this regard time domain reflectometry (TDR) is capable of determining the dielectric properties of liquids at MHz to low GHz frequencies. The measurement cell (Figure 2.1) consist of coaxial line terminated by a coaxial line of different dimensions, where the insulating material is replaced by the sample. Ideally, the outer conductor is infinitely continued, while the inner conductor has a certain length, l. At the end of the inner conductor, a coaxial to circular waveguide transition is the electromagnetic boundary condition.[81] Due to a step in the impedance at the coaxial-line sample cell transition, an electromagnetic wave is partly reflected. The complex permittivity measurements are based on the determination of the complex reflection coefficients at this impedance step.[82]

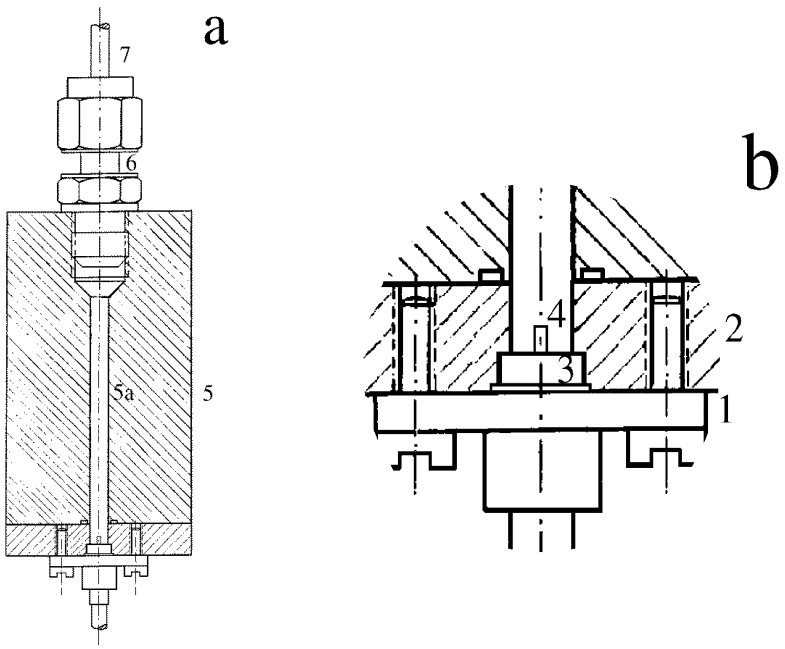

Figure 2.1: A cut-off type reflection cell:[82] **1** 0.085″ semi-rigid feeding line with flange, **2** cell base plate with **3** soldered hermetic feed through, **4** inner conductor of diameter d_1 and length l, **5** cell body with gold-plated bore **5a** as outer conductor of diameter d_2, **6** Swage-Lock® fitting, **7** fitting capillary.

Theory A fast rising voltage pulse, $V_o(t)$, is applied to the sample. The pulse propagating in the sample is deformed according to the dielectric properties of the sample, and reflected signal, $V_r(t)$, is obtained. The shape of $V_o(t)$, registered by a fast sampling scope, is then

compared to $V_r(t)$. Fourier transformation of the time-dependent intensities of the signal yields the intensities in the frequency domain, $\upsilon_o(\omega)$ and $\upsilon_r(\omega)$:

$$\upsilon_o(\omega) = \mathcal{L}_{\mathrm{i}\omega}\left[\frac{\mathrm{d}}{\mathrm{d}t}V_o(t)\right] = \int_0^\infty \frac{\mathrm{d}}{\mathrm{d}t}V_o(t)\cdot\exp(\mathrm{i}\omega t)\mathrm{d}t \tag{2.1}$$

$$\upsilon_r(\omega) = \mathcal{L}_{\mathrm{i}\omega}\left[\frac{\mathrm{d}}{\mathrm{d}t}V_r(t)\right] = \int_0^\infty \frac{\mathrm{d}}{\mathrm{d}t}V_r(t)\cdot\exp(\mathrm{i}\omega t)\mathrm{d}t \tag{2.2}$$

Eq. 2.1 and 2.2 can be used to calculate the absolute complex reflection coefficient of the cell, $\hat{\rho}(\omega)$,

$$\hat{\rho}(\omega) = \frac{c_o}{\mathrm{i}\omega g l}\cdot\frac{\upsilon_o(\omega)-\upsilon_r(\omega)}{\upsilon_o(\omega)+\upsilon_r(\omega)} \tag{2.3}$$

in the above equation l is the pin-length of the inner conductor and g is the ratio between the wave resistance of the empty cell and the feeding line. Due to fringing fields at the coaxial line to waveguide transition the effective pin length, l_{el}, slightly exceeds the mechanical pin length, l, hence in Eq. 2.3 l_{el} is used. Within some approximations, the generalized complex dielectric permittivity, $\hat{\eta}(\omega)$, can be obtained from $\hat{\rho}(\omega)$ by the numerical solution of,

$$\hat{\eta}(\omega) = \hat{\rho}(\omega)\cdot\hat{z}\cot\hat{z} \tag{2.4}$$

where

$$\hat{z} = \frac{\omega l}{c_o}\sqrt{\hat{\eta}(\omega)} \tag{2.5}$$

It should be noted that, the incident wave is not easily accessible from the measurement. Therefore, a sample of known (and preferably similar) dielectric properties is used as reference, and the relative reflection coefficient is determined as

$$\hat{\rho}_{xr}(\omega) = \frac{c}{\mathrm{i}\omega g l}\cdot\frac{\mathcal{L}_{\mathrm{i}\omega}\left[\frac{\mathrm{d}}{\mathrm{d}t}V_{rr}(t)\right]-\mathcal{L}_{\mathrm{i}\omega}\left[\frac{\mathrm{d}}{\mathrm{d}t}V_{rx}(t)\right]}{\mathcal{L}_{\mathrm{i}\omega}\left[\frac{\mathrm{d}}{\mathrm{d}t}V_{rr}(t)\right]+\mathcal{L}_{\mathrm{i}\omega}\left[\frac{\mathrm{d}}{\mathrm{d}t}V_{rx}(t)\right]} \tag{2.6}$$

In Eq. 2.6, $V_{rx}(t)$ and $V_{rr}(t)$ represent the relative time dependent reflection intensities of the sample and the reference, respectively.[83,84] The relative reflection coefficient is related to the dielectric properties by the working equation,

$$\hat{\rho}_{xr} = \frac{\hat{\eta}_x\cdot\hat{z}_r\cot(\hat{z}_r)-\hat{\eta}_r\cdot\hat{z}_x\cot(\hat{z}_x)}{\hat{z}_r\cot(\hat{z}_r)\hat{z}_x\cot(\hat{z}_x)+g^2\cdot\hat{\eta}_x\hat{\eta}_r(\omega l/c)^2} \tag{2.7}$$

with

$$\hat{z}_x = \frac{\omega l}{c}\sqrt{\hat{\eta}_x} \quad\text{and}\quad \hat{z}_r = \frac{\omega l}{c}\sqrt{\hat{\eta}_r} \tag{2.8}$$

Numerical solution of Eq. 2.7 with a Newton-Raphson procedure and Tailor series expansion of $\hat{z}\cdot\cot\hat{z}$ yields $\hat{\eta}_x(\omega)$.[85]

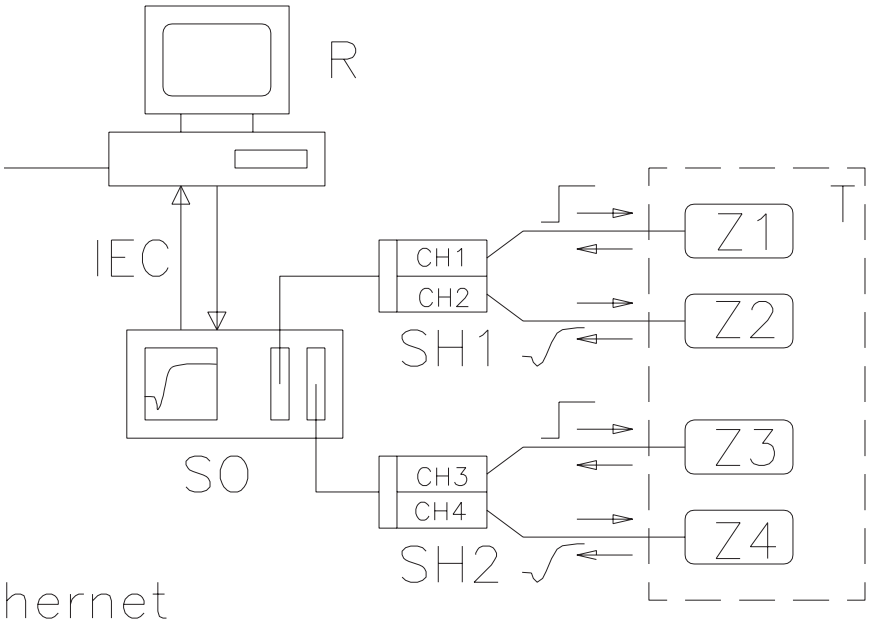

Figure 2.2: Schematic representation[83] of the time-domain reflectometer: **SO** digital sampling scope; **SH1,SH2** SD-24 sampling heads; **Z1-Z4** cutoff cells; **T** precision thermostat; **R** personal computer with access to other computers for data analysis.

Experimental setup Figure 2.2 shows the experimental TDR setup. The sampling scope (TEK 11808; Tektronix) is connected to sampling heads (SD24), which generate a square wave signal at 200 kHz with a fast rise time (typically 17.5 ps). Each sampling head has two independent channels which are used for the measurement of two cells of the cutoff-type. This dual channel configuration allows to monitor and correct the inevitable time drifts (e.g. due to thermal expansion of the cables) as one trace is used for the actual sample measurement, the other one as a time reference to account for these drifts. Traces are recorded with a resolution of 5120 points and averaged over 256 single measurements, to improve the signal to noise ratio. Several cells of different dimensions and pin-lengths are available, resulting in different impedances to optimize the signal for different frequency ranges and dielectric properties. Further details are described in literature.[82,86,87] In the presented study various cut-off type cells were tested (see Table 2.2) in order to obtain smooth data over the required frequency range.

Table 2.2: Different cutoff cells tested in the present work with following characteristic parameters: mechanical pin-length, l, electrical pin-length, l_{el}, and ratio of the feeding line impedance to the impedance of the empty cell, g.

Cutoff cell	l/ mm	l_{el}/ mm	g
T9	0.7	1.118	0.4282
TX	5.35	5.987	1.0018
TS3	6.0	6.05	0.4282
TS1	25	26.377	0.82258

2.2.2 Interferometry

For the determination of the complex permittivity of materials below 50 GHz, various well established methods are available[25,88,89] while for the frequencies in the far infrared region (>300 GHz or 10 cm^{-1}) such data is accessible by the dispersive Fourier transform spectroscopy[90,91]. For the measurements in the intermediate frequency region however, due to technical issues the application of both waveguide techniques and free space optical methods is difficult. In the presented study waveguide interferometers (IFM, capable of detecting the signal amplitude only) based on the method of traveling waves are used for this frequency range.

Theory The experimentally accessible quantities through IFM measurements are the attenuation coefficient, α, and the wavelength, λ_{m}, of the radiation of frequency, ν, transmitted in the sample, which are obtained for each required frequency via several steps. After filling of the measurement cell and determination of the start position for the measurement, full destructive interference is established at an appropriate probe position $z_0^{'}$ with the help of attenuators and phase shifters, as the receiver detects only amplitude of the signal, this procedure is necessary to obtain the phase information.
The time-dependence of a harmonically oscillating field propagating through the reference beams is described by

$$\hat{E}_1(t) = E_0 \exp(\mathrm{i}\omega t) \tag{2.9}$$

For a full destructive interference, the phases, φ, of the interfering waves are shifted by

$$\Delta\varphi = (2n+1)\pi \quad \text{with } n \in \mathbb{Z} \tag{2.10}$$

If z_0 is assumed to be the absolute optical path length of the transmission cell then the difference between z_0 and $z_0^{'}$ would be considered as $x = z_0 - z_0^{\prime}$, the relative distance from the interference minimum. The electromagnetic wave passing through the sample beam can be expressed as

$$\hat{E}_2(t,x) = E_0 \exp(-\alpha x) \exp\left[\mathrm{i}(\omega t + \pi - \beta x)\right] \tag{2.11}$$

where $\beta = 2\pi/\lambda_\mathrm{m}$ is the phase coefficient. Since both reference and sample beams are combined at the receiver, their superposition yields

$$\hat{E}(t,x) = \hat{E}_1(t) + \hat{E}_2(t,x) = \hat{E}_0 \exp(\mathrm{i}\omega t)\,[1 + \exp(-\alpha x)\exp(\mathrm{i}(\pi - \beta x))] \tag{2.12}$$

The power P of the detected signal is experimentally accessible and is defined as

$$P = \hat{E} \cdot \hat{E}^* = E_0^2 \cdot I(x) \tag{2.13}$$

where E_0 is the amplitude of $\hat{E}$ and $I(x)$ is the interference function, which can be defined as

$$\begin{aligned} I(x) &= [1 + \exp(-\alpha x)\exp(\mathrm{i}(\pi - \beta x))] \cdot [1 + \exp(-\alpha x)\exp(\mathrm{i}(\pi - \beta x))] && (2.14)\\ &= 1 + \exp(-2\alpha x) + \exp(-\alpha x) \cdot 2\cos(-\pi + \beta x) && (2.15) \end{aligned}$$

The signal-level measured by the receiver, $A(x)$, is commonly expressed in decibel (dB), i.e. the relative attenuation of the signal power on a logarithmic scale. It is defined as

$$A(x) = 10 \lg \frac{P(x)}{P_\mathrm{ref}} \tag{2.16}$$

Since P_ref is not known, $A(x)$ is normalized by A_0, the relative intensity of the signal passing through the sample beam at position z_0'

$$A_0 = 10 \lg \frac{P_0}{P_\mathrm{ref}} \tag{2.17}$$

and it follows

$$\begin{aligned} A_\mathrm{rel}(x) &= A(x) - A_0 \\ &= 10 \lg \frac{P(x)}{P_\mathrm{ref}} - 10 \lg \frac{P_0}{P_\mathrm{ref}} \\ &= 10 \lg \frac{P(x)}{P_0} \\ &= 10 \lg \frac{E_0^2 \cdot I(x)}{E_0^2} \end{aligned} \tag{2.18}$$

The recorded interferogram $A(z_0 - z_0')$ can be fitted by the expression[92]

$$\begin{aligned} A(z_0 - z_0') = A_0 + 10 \lg \Big\{ & 1 + \exp\left[-2p\alpha_\mathrm{dB}(z_0 - z_0')\right] \\ & - 2\cos\left(\frac{2\pi}{\lambda_\mathrm{m}}(z_0 - z_0')\right) \cdot \exp\left[-p\alpha_\mathrm{dB}(z_0 - z_0')\right] \Big\} \end{aligned} \tag{2.19}$$

In above equation p is a conversion factor

$$p = \left(20 \lg \mathrm{e} \cdot \frac{\mathrm{dB}}{\mathrm{Np}}\right)^{-1} \tag{2.20}$$

Eq. 2.19 yields the power attenuation coefficient, α_{dB} (in dB/m), and λ_{m}. These quantities are related to $\hat{\eta}(\nu)$ via

$$\eta'(\nu) = \left(\frac{c_0}{\nu}\right)^2 \left[\left(\frac{1}{\lambda_{\mathrm{c},10}^{\mathrm{vac}}}\right)^2 + \left(\frac{1}{\lambda_{\mathrm{m}}(\nu)}\right)^2 - \left(\frac{\alpha(\nu)}{2\pi}\right)^2\right] \qquad \text{and} \tag{2.21}$$

$$\eta''(\nu) = \left(\frac{c_0}{\nu}\right)^2 \frac{\alpha(\nu)}{\pi\lambda_{\mathrm{m}}(\nu)} \tag{2.22}$$

Where $\lambda_{\mathrm{c},10}^{\mathrm{vac}}$ is the limiting vacuum frequency, a characteristic quantity for a particular waveguide.

Experimental setup Figure 2.3 shows a block diagram of the E-band setup where a computer-controlled system of transmission lines is used. Phase lock oscillators are used to generate signals of desired frequency. The signal coming from the source is then split by a directional coupler to feed the measuring and reference branches. The sample is placed in a cell consisting of mica window, a piece of waveguide and a gold-plated (5 µm, to suppress corrosion) ceramic probe with variable, motor-controlled position. Variable precision phase shifters and attenuators are integrated in the branches. Signals are recombined by directional couplers and then after passing through the isolator, harmonic mixer and millimeterwave to micrometerwave converter the signal is detected at a precision attenuation receiver. Two types of double-beam interferometers were used for measurement of the dielectric properties at high GHz frequencies[92] namely A-band ($27 \leq \nu/\mathrm{GHz} \leq 40$) and E-band ($60 \leq \nu/\mathrm{GHz} \leq 89$). For the A-band measurements, however interferometer was connected to the VNA (see section 2.2.3) to enable continuous frequency scans[93], whereas the temperature was controlled by a Julabo FP 50 or a Lauda RK 20 thermostat and monitored by a Pt-100 resistance with a precision of $\pm 0.02\,^{\circ}\mathrm{C}$ and an overall accuracy of $\pm 0.05\,^{\circ}\mathrm{C}$. Prior to the filling the cells were properly washed and dried with a spray of dry nitrogen. It should be noted that the IFM measurements do not require any calibration and the obtained data is considered absolute.

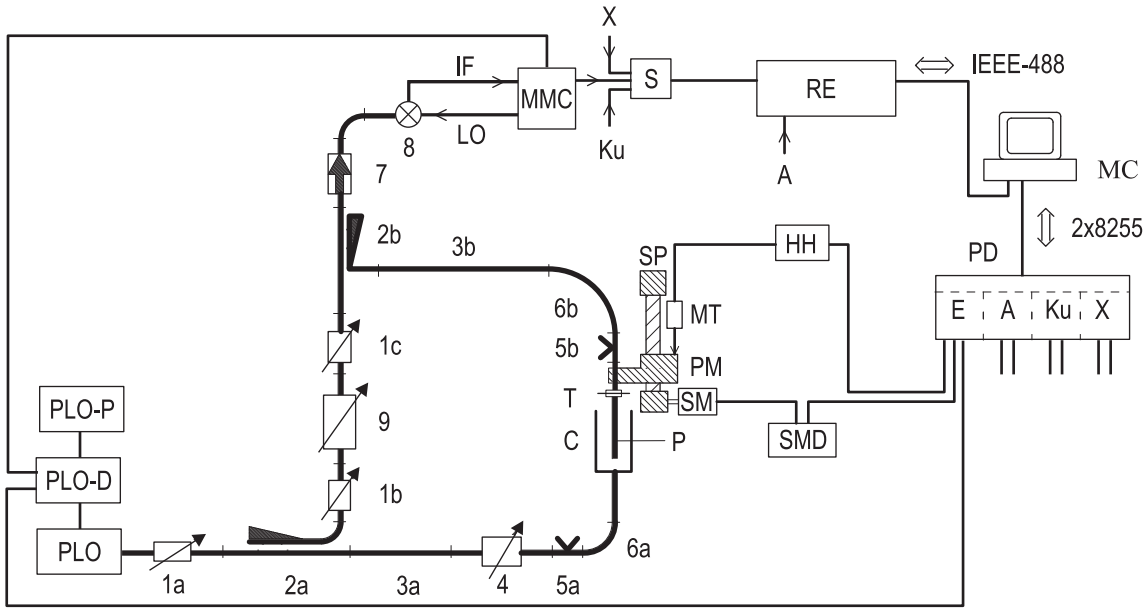

Figure 2.3: Block diagram of the E-band equipment:[92] **1a**, **b**, **c** represent variable attenuators; **2a**, **b** directional couplers; **3a**, **b** waveguide sections; **4** precision phase shifter; **5a**, **b** E/H tuners; **6a**, **b** flexible waveguides; **7** isolator; **8** harmonic mixer; **9** variable precision attenuator; **C** cell, **HH** bidirectional counter; **MC** microcomputer; **MMC** millimeter-wave to microwave converter; **MT** digital length gauge; **P** probe; **PD** parallel interface unit; **PLO** phase locked oscillators; **PLO-D** PLO-control unit; **PLO-P** PLO-power supply; **PM** probe mount; **RE** precision receiver; **S** electromechanical switch; **SM** stepping motor; **SMD** stepping motor control unit; **SP** spindle and spindle mount; **T** tapered transmission; double lines represent waveguides, thick lines semi-rigid microwave cables and normal lines symbolize data transfer connections (analog or digital).

2.2.3 Vector network analysis

Due to the need of maximum power transfer at higher frequencies, the coaxial lines are preferably used. Commercially available devices (vector network analyzers, VNA, capable of analyzing both magnitude and phase of the component signals in electrical networks) are able to operate upto 110 GHz. For the characterization of a two-port device, an arbitrary electrical network is analyzed by determining the reflection and transmission of electrical signals which yields the scattering parameter matrix, $\hat{S}$, that can be defined as

$$\begin{pmatrix} \hat{b}_1 \\ \hat{b}_2 \end{pmatrix} = \begin{pmatrix} \hat{S}_{11} & \hat{S}_{12} \\ \hat{S}_{21} & \hat{S}_{22} \end{pmatrix} \begin{pmatrix} \hat{a}_1 \\ \hat{a}_2 \end{pmatrix}$$

where $\hat{a}_j$ and $\hat{b}_j$ are the incident and reflected power waves at the port j, respectively. For one-port measurements (reflection studies) the instrument has to be calibrated with at least three reference materials (conventionally open, short and 50 Ω are used) in order to correct the errors in directivity, $\hat{e}_d$, frequency response, $\hat{e}_r$, and source match, $\hat{e}_s$. The obtained scattering parameter by the VNA, $\hat{S}^m_{jj}$ can be defined as

$$\hat{S}^m_{jj} = \hat{e}_d + \frac{\hat{e}_r \hat{S}^a_{jj}}{1 - \hat{e}_s \hat{S}^a_{jj}} \tag{2.23}$$

where $\hat{S}^a_{jj}$ is the actual scattering parameter at the plane of interest.
For one-port reflection measurements on an electrical network, consisting of an impedance step varying from $\hat{Z}_1$ to $\hat{Z}_2$, the complex scattering parameter $\hat{S}_{11}$, is defined as

$$\hat{S}_{11} = \frac{1 - \hat{Y}}{1 + \hat{Y}} \tag{2.24}$$

In Eq. 2.24, $\hat{Y} = \hat{Z}_2/\hat{Z}_1$, is the normalized terminating impedance.

Open-ended coaxial probes

Dielectric data of aqueous solutions of ChCl, ClChCl, NH_4Cl, ChC12, ChDS, and NaC12, in the frequency range $0.2 \leq \nu/\mathrm{GHz} \leq 50$ was recorded with Agilent E8364B VNA connected to an electronic calibration module (Ecal, Agilent N4693A) and a dielectric probe kit (85070E). The use of Ecal module ensures the efficiency and accuracy of VNA setup as it measures the well known reflection standards during the measurement and thus compensates for the systematic drifts, e.g., phase error due to possible thermal expansion of the coaxial lines. This setup requires the use of two different open-ended coaxial probes namely "high temperature" probe and "performance" probe in the frequency range $0.2 \leq \nu/\mathrm{GHz} \leq 20$ (with 61 equidistant frequency data points on logarithmic scale) and $1 \leq \nu/\mathrm{GHz} \leq 50$ (with 51 equidistant frequency data points on logarithmic scale), respectively (in principle the frequency limit of theses probes is 0, but due to small aperture

capacitances data were practically reproducible down to 0.2 GHz and 1 GHz for high temperature and performance probe, respectively). However, during the fitting procedure, in order to have an equal density of data points throughout, the data of the performance probe was used in frequency range $15 \lesssim \nu/\mathrm{GHz} \leq 50$ only. Both probe heads were mounted in two different temperature controlled cells as described by Hunger.[93] The temperature was controlled with a Huber CC505 thermostat and measured with a Agilent 34970A datalogger, using a platinum resistance thermometer (PT-100) in 4-wire configuration.
The complex dielectric parameter $\hat{\eta}$ was calculated from the normalized aperture impedence of the probe head, $\hat{Y}$ by using a simplified coaxial aperture opening model[94,95] and numerical solution of the equation

$$\hat{Y} = \frac{\mathrm{i}\hat{k}^2}{\pi \hat{k}_\mathrm{c} \ln(D/d)} \left[\mathrm{i} \left(I_1 - \frac{\hat{k}^2 I_3}{2} + \frac{\hat{k}^4 I_5}{24} - \frac{\hat{k}^6 I_7}{720} + \ldots \right) + \left(I_2 \hat{k} - \frac{\hat{k}^3 I_4}{6} + \frac{\hat{k}^5 I_6}{120} - \ldots \right) \right] \tag{2.25}$$

In Eq. 2.25, $\hat{k}_\mathrm{c} = \omega\sqrt{\hat{\eta}_\mathrm{c}\varepsilon_0\mu_0}$ and $\hat{k} = \omega\sqrt{\hat{\eta}\varepsilon_0\mu_0}$ are the propagation constants within the dielectric material of the coaxial probe head (*index* c) and within the sample, respectively. A theoretical approach yields the probe constants $I_1 \ldots I_{28}$[95], whereas D and d are radii of outer and inner conductor of coaxial line, respectively.
Calibration of the VNA was performed according to Eq. 2.23 with respect to the probe-sample interface. A standard three point calibration using air (open), mercury (short) and a pure liquid (load, with accurately known dielectric properties) was used. Prior to use mercury was purified according to the procedure described by Wölbl;[96] minor scum formation was removed by 'pin-hole' filtration (paper filter). Since dielectric properties of the third calibration material should be close to those of the studied sample so, water was adopted as a third reference material. At least two independent calibrations were performed (for each probe head type) to obtain a set of consistent spectra for each of the studied system.

Generally a complex Padé approximation,[86,97] is used for the correction of VNA data, if the dielectric properties of the sample deviate considerably from that of reference liquid. This approach was also tested in the present studies for the selected systems, using water, propylene carbonate (PC, Sigma-Aldrich, 99.7 %) and N,N-dimethylacetamide (DMA, Fluka, $>$ 99.8 %) as secondary calibration standards. No significant improvement of the VNA spectra was observed after doing Padé calibration (Figure 2.4), in addition the uncorrected data was in excellent agreement with the corresponding IFM measurements (absolute data, do not require any calibration), so this approximation was not applied to the presented studies.

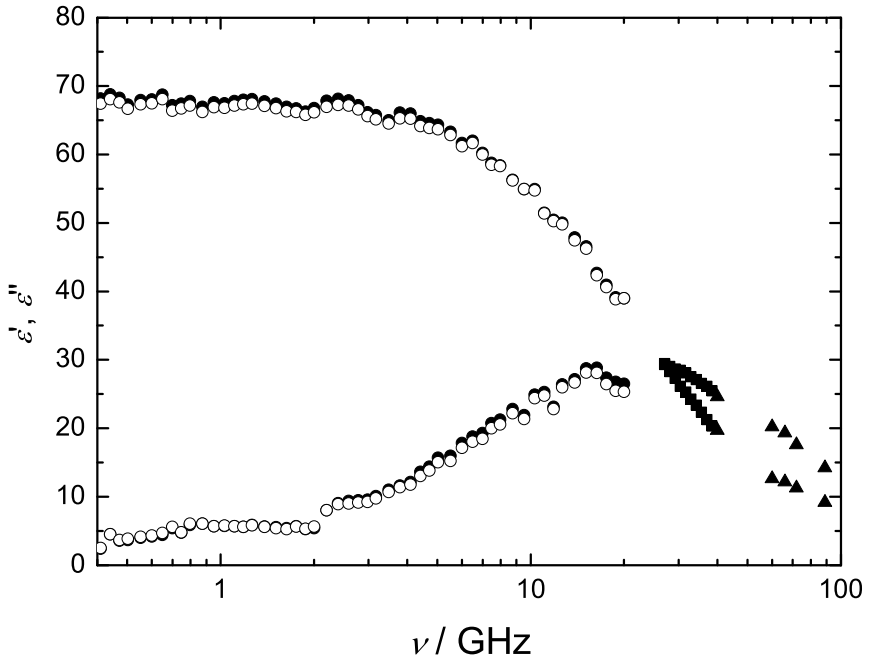

Figure 2.4: Dielectric permittivity and loss spectrum of c = 1.10M NH_4Cl in water (κ = 12.21 S·m^{-1}) Circles, squares and triangles (filled) represent data obtained with 20 GHz probe head, A-band and E-band IFM, respectively. Open symbols show corrected data with a complex Padé approximation[86,97] using water, PC and DMA as secondary calibration standards.

Cut-off type coaxial cells

Because of the break down of sampling scope during the course of presented work, it was not possible to use TDR set up any more. Therefore, reflection coefficients of the cut-off type coaxial cells, as used in the TDR experiment, were also measured with the Agilent E8364B VNA.
The normalized impedence of the cell is given by[81]

$$\hat{Y} = \left[-2\pi Z_{\mathrm{L}} \ln\left(\frac{d}{D}\right) \sqrt{\frac{\varepsilon_0}{\mu_0} \cdot \hat{\eta}(\omega)} \tanh\left(\frac{\mathrm{i}\omega l}{c}\sqrt{\hat{\eta}(\omega)}\right) + \mathrm{i}\omega\hat{\eta}(\omega) Z_{\mathrm{L}} C_{\mathrm{s}} \right]^{-1} \tag{2.26}$$

where Z_{L} is the wave resistance of the feeding line (typically 50 Ω) and C_{s} the discontinuity capacity of the coaxial to circular waveguide transition. In case of C_{s} =0 the electrical model becomes equal to the model used in the TDR experiment (see section 2.2.1).[85,87] Eqs. 2.24 and 2.26 are solved numerically to obtain the generalized complex permittivity of the sample, $\hat{\eta}(\nu)$.
This set up requires calibration of VNA, which is performed by an open-short-load calibration of the cable at the connector plugged to the cell, and the remaining part (connector-

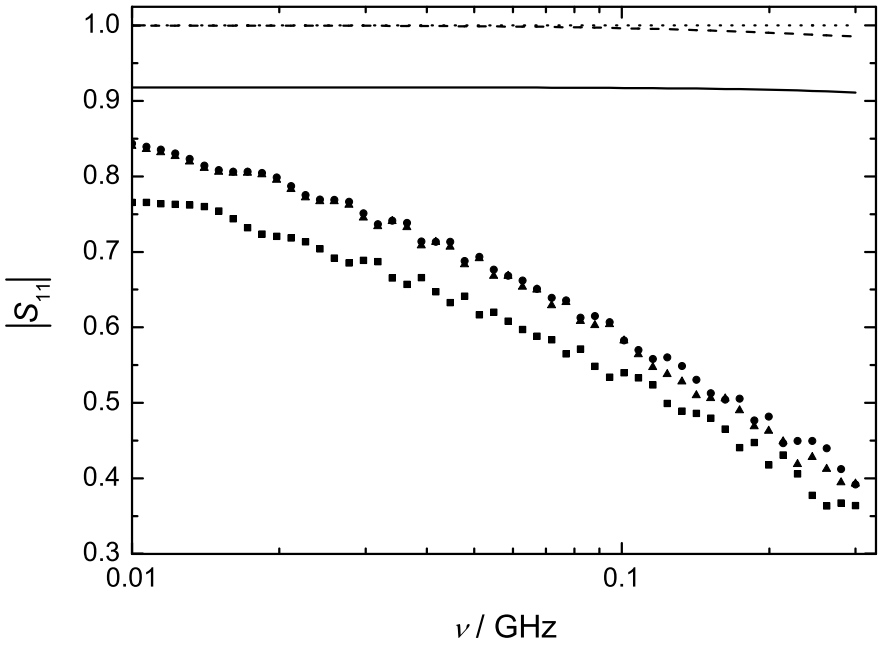

Figure 2.5: Modulus of the complex scattering parameter $|\hat{S}_{11}|$ of three standards at 25 °C : air (●, dotted line), water (▲, dashed line) and 5 mol·kg^{-1} NaCl(aq) (■, full line) obtained by using TS3 cell. Symbols represent values at the connector plane, lines correspond to the theoretical values at the coaxial-sample interface (Eqs. 2.24 and 2.26).

sample plane) is treated as an ideal coaxial line[81]. In actual practice, however, as can be seen in Figure 2.5, the difference between the scattering parameter measured at the connector plane and the calculated $\hat{S}_{11}$ values at the sample-coaxial line interface is far from being due to an ideal coaxial line. Thus, it is essential to calibrate the VNA with respect to the sample-coaxial line interface with three reference materials. As a first approximation, the calibration standards should be roughly comparable to the short-load-open standards, to reliably obtain the three errors in directivity, frequency response and source match. For short calibration NaCl (aq, m $\sim$ 0.2 mol·kg^{-1}) or NaCl (aq, m $\sim$ 5 mol·kg^{-1}) were used.[98]Although the dielectric relaxation behavior is less accurately known,[98] the conductivity can be determined very accurately, which is the main contribution to $\hat{\eta}(\nu)$ at the relevant frequencies. It was found that the dielectric parameters are not crucial as long as κ is sufficiently high and accurately determined. For open calibration air was used while water was used as a third reference material. However, the choice of appropriate cell for the studied systems was restricted due to electrode polarization[99,100] (Figure 2.6).

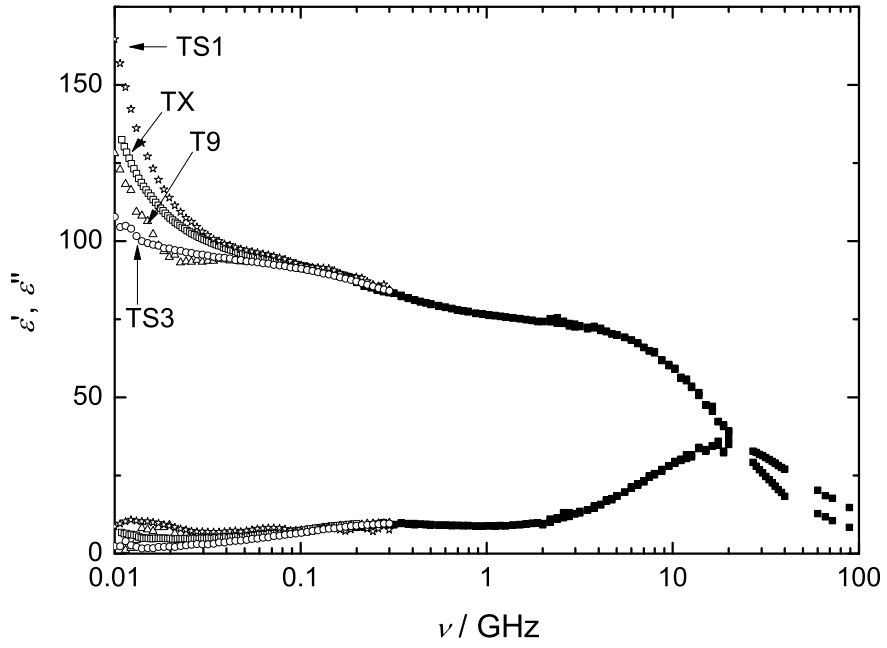

Figure 2.6: Depiction of electrode polarization in the low-frequency region (where data points are represented with hollow symbols) of DRS spectrum of 0.11M NaC12 (obtained by using different cut-off cells, of variable characteristics). Also shown is the data of high temperature probe, A-band and E-band interferometer, using filled symbols.

Wave guide transmission cells

Since the VNA is able to detect amplitude and phase simultaneously, hence, it is not necessary to record interference curves at each frequency separately as described in section 2.2.2. Therefore, the waveguide-transmission cell of A-band was connected to the Agilent E8364B VNA. With this transmission setup the complex scattering parameter, $\hat{S}_{12}$, is recorded as a function of the relative optical path length at all relevant frequencies simultaneously, which is advantageous for being time saving.

The procedure involves measurements of the z position of the wave guide probe with a personal computer by controlling the stepper motor, VNA and the precision gauge, whereas the calibration of the VNA at the 2.4 mm connector planes has to be refreshed occasionally manually. Absorption coefficient α_{dB} and medium wavelength λ_{M} were obtained from the slopes of the linear regression of the phase and of the magnitude of $\hat{S}_{12}$. Regression coefficients R^2 were generally 0.99980 or better. λ_{M} and α_{dB} were converted to complex permittivity values via Eqs. 2.21 and 2.22. For most of the studied systems, the data from A-band measurements, using this set up was preferred over the data of "performance" probe as quite often the data of performance probe in its low frequency range were scattered and

the scattering become worst for the data at high temperatures and for high conducting samples, this surely depicts the need for having some appropriate calibration materials (with $\kappa >> 0$) for the highly conducting systems.

2.2.4 Data analysis

Once the dielectric data at the spot frequencies are obtained, a frequency-continuous description via a suitable model has to be found. It is preferred to analyze $\hat{\varepsilon}(\nu)$ data after correcting for dc conductivity rather than $\hat{\eta}(\nu)$ as this may lead to biasing of the resulting parameters, due to large values of η'' at low ν as weights are higher at low ν than at high ν. Therefore, the spectra were first corrected for the measured conductivity, κ, as a starting approximation. The κ was varied slightly in order to improve the fit quality (Eq. 2.27). The difference between the experimental conductivity from low-frequency measurements in the Hz-kHz region and adjusted κ values reflects errors in the measurement setup and/or in mathematical model for the equipment.[101,102]
Furthermore, the measured data triples (ν_i, ε_i', ε_i'') have to be fitted by the relaxation models (or superpositions) as already described in preceding chapter. However, due to the broadness of relaxation modes in the condensed phase finding the right model is not trivial, and also the successful formal description does not automatically imply that the resolved modes have a physical meaning or that they are independent of each other. Thus, few basic rules should be obeyed:
Firstly, the parameters obtained have to be physically meaningful. Second, the normalized variance of the fit, χ_r^2, defined as

$$\chi_r^2 = \frac{1}{2N - m - 1}\left[\sum_{i=1}^{N} w_{\varepsilon'}(\nu_i)\delta\varepsilon'(\nu_i)^2 + \sum_{i=1}^{N} w_{\varepsilon''}(\nu_i)\delta\varepsilon''(\nu_i)^2\right] \tag{2.27}$$

should be small. In above equation, $\delta\varepsilon'(\nu_i)$ and $\delta\varepsilon''(\nu_i)$ are the residuals, N is the number of data triples $[\nu_i, \varepsilon'(\nu_i), \varepsilon''(\nu_i)]$ and m the number of the adjustable parameters; $w_{\varepsilon'}(\nu_i)$ and $w_{\varepsilon''}(\nu_i)$ are the weights; only unweighted fits, $w_{\varepsilon'}(\nu_i) = w_{\varepsilon''}(\nu_i) = 1$, were performed in the analysis of the spectra presented here.
Additionally, the number of parameters should be as small as possible and the relaxation model should not vary in a concentration or temperature series measurements, unless there are some specific physical reasons.
It should also be noted that the model seeming to be most appropriate for a studied system can depend on the measured frequency range as well as on the precision and the "density" of the spot frequency, hence special care should be taken regarding the density, meaning that the number of data points should be comparable over the whole frequency range.
Different relaxation models were tested for each of the studied systems in the presented work, by simultaneously fitting $\varepsilon'(\nu)$ and $\varepsilon''(\nu)$ (as is advisable) using the MWFIT program. A non-linear least-squares routine based on the method of Levenberg and Marquardt is used in this program.[103] However, due to the nonlinear nature of the fitting process, assignment of statistically meaningful standard uncertainties to the individual fit parameters is not possible but the square root of the diagonal elements of the covariance matrix can be used as a measure for the certainty of the resulting parameters.[103,104]

In order to further check the validity of an accepted model, another fitting procedure and computer code was used for the evaluation of a discrete analog of relaxation time distribution functions[105]. Due to unbiased nature of this fitting technique no prior knowledge of number of modes, characteristic times of the modes, relaxation amplitudes or the relaxation time distribution function is required for the Zasetsky method. This fitting procedure is based on a quasi-linear procedure with constraints for least squares fitting of experimental complex dielectric permittivity spectra in the frequency domain. The solution of linear least square minimization problem with constraints[105,106] provides information on relaxation time distribution functions. The procedure involves the linearization of non-linear least square fitting of dielectric spectra by pre-computing (based on the Debye model of relaxation) a set of basis spectra, modifications can be done for the non-debye type relaxation modes[105]. However, it must be noted that both of the above mentioned fitting routines do not *a priori* reflect the actual molecular level mechanism behind the resolved relaxation modes.

2.3 Auxiliary measurements

2.3.1 Densimetry

Solution densities, ρ, were measured with an accuracy of $\sim \pm 0.05\,\mathrm{kg{\cdot}m^{-3}}$ using a vibrating-tube densimeter (Anton Paar DMA 60/601 HT) according to the method described in literature[107]. The instrument measures the period of vibration, τ, of a glass tube filled with the sample. Sample density is related to this τ as

$$\rho = \mathrm{A} \times \left(\tau^2 - \mathrm{B}\right) \tag{2.28}$$

where A and B are the intrument-related constants that were determined via calibration using degassed Millipore MILLI-Q water and purified nitrogen at atmospheric pressure, assuming densities from standard sources[108]. The temperature was kept constant to $\pm 0.003\,^{\circ}\mathrm{C}$ with an overall accuracy of $\pm 0.02\,^{\circ}\mathrm{C}$ using a Braun Thermomix 1480 thermostat in combination with a thermostated heat sink (Lauda RK 20).
However, later on due to availablity of new instrument, the densities for rest of studied systems were measured with a densimeter DMA 5000 M (Anton Paar), which measures τ of a U-shaped borosilicate glass tube filled with the sample, for this instrument τ is related to the ρ as

$$\rho = \mathrm{A} \times \left(\frac{\tau}{\tau_{\mathrm{ref}}}\right)^2 \times \mathrm{f_1} - \mathrm{B} \times \mathrm{f_2} \tag{2.29}$$

where τ_{ref} is the period of oscillation of the reference oscillator, A and B are the instrument constants, and $\mathrm{f_1}$ and $\mathrm{f_1}$ are the correction terms for temperature, viscosity and nonlinearity, respectively.
The temperature was kept constant to $\pm 0.001\,^{\circ}\mathrm{C}$ with an overall accuracy of $\pm 0.01\,^{\circ}\mathrm{C}$ with a built-in thermoelectric temperature control. The precision of the measurements was $\pm 0.001\,\mathrm{g{\cdot}L^{-1}}$. The accuracy stated by the manufacturer is $\pm 0.005\,\mathrm{g{\cdot}L^{-1}}$. Before starting actual measurements "water check" was performed to check the accuracy while "air check" was performed quite often to ensure that the measuring cell was clean and properly dried. The obtained density data (at $25\,^{\circ}\mathrm{C}$) was used to calculate molar concentrations, c, of the studied systems, in addition for ChCl(aq), ClChCl(aq) and NH_4Cl(aq) ρ were recorded at $5\,^{\circ}\mathrm{C}$, $15\,^{\circ}\mathrm{C}$, $25\,^{\circ}\mathrm{C}$, $35\,^{\circ}\mathrm{C}$ and $45\,^{\circ}\mathrm{C}$ for various concentrations of each electrolyte. For ChCl(aq) and ClChCl(aq) such data was used to calculate apparent molar volume, ϕ_{v}.

2.3.2 Conductivity

For the determination of electrical conductivities, κ, the Wheatstone-bridge equipment described previously,[109–111] was used (with precision of $\pm 0.2\,\%$ and an accuracy of $\pm 0.5\,\%$). The temperature was controlled with a home-built precision thermostat stable to $\pm 0.003\,\mathrm{K}$ in combination with a thermostated heat sink (Lauda Kryomat K 90 SW). A set of different two-electrode capillary cells with cell constants, C, ranging from 25 to $360\,\mathrm{cm^{-1}}$ were used. The cells were calibrated with aqueous solutions of KCl.[112] The cell resistance, $R(\nu)$, was measured manually as a function of the applied AC frequency, ν, between $120\,\mathrm{Hz}$ and $10\,\mathrm{kHz}$. To overcome possible effects of electrode polarization, the conductivity of

each sample was obtained as $\kappa = C/R_\infty$ where $R_\infty = \lim_{\nu\to\infty} R(\nu)$ was obtained by extrapolation using the empirical function $R(\nu) = R_\infty + A/\nu^a$, where A is specific to the cell and a was found to be in the range $0.5 \lesssim a \lesssim 1$.[113]

Later on, another computer-controlled setup for the conductivity measurements was established in our lab and was used to record the conductivity data for some of the studied systems[114]. This setup involves use of a Huber, unistat 705 as the thermostat (temperature stability $< 0.005\,\mathrm{K}$), a high-precision LCR-bridge* (HAMEG, HM8118) for the measurement of $R(\nu)$ (relative uncertainty ≤ 0.0005), and a switchboard to address the capillary cells mounted on the thermostat lid. Parasitic impedances were eliminated by an open/short calibration of LCR-bridge and switchboard prior to each measurement.
Measurement temperatures were recorded with an uncertainty of $\pm 0.01\,\mathrm{K}$ with a MIST traceable Pt-100 resistance thermometer (ASL). The conductivities were obtained in the same way as mentioned above.

2.3.3 Viscometry

The dynamic viscosities, η, of aqueous solutions (of selected systems) were measured using an automated rolling-ball viscometer (Anton Paar AMVn) at 5 °C, 15 °C, 25 °C, 35 °C and 45 °C (with a temperature uncertainty $\leq 0.01\,\mathrm{K}$) as

$$\eta = \mathrm{K_1} \times (\rho_\mathrm{K} - \rho) \times \mathrm{t_1} \tag{2.30}$$

where $\mathrm{K_1}$ is the calibration constant of the measuring system, ρ_K is the density of the falling ball, ρ is the density of the measured sample and $\mathrm{t_1}$ is the the rolling time of the ball.
The manufacturer-stated relative uncertainty of the instrument is ≤ 0.005. The repeatability and reproducibility of the viscosity measurements are $< 0.1\,\%$ and $< 0.5\,\%$, respectively.

2.3.4 MOPAC calculations

In order to validate the experimental results pertaining to molecular properties, semiempirical quantum mechanical calculations (MOPAC2009[115]) were performed for various ions and ion-pairs using the PM6 Hamiltonian.[116] Dipole moments were calculated assuming the geometric center (i.e. the center of the longest axis of the ion/ion-pair) as pivot. The geometry of the ions was optimized using the eigenvector-following (EF) routine[117] and for the ion-pairs, in order to avoid geometry reorganization, the 1SCF method was preferably used. Molecular diameters, d_max, were obtained by taking the longest distance between two atoms and adding the Van der Waals radii of the atoms[118], whereas the Van der Waals volumes, V_vdW, were obtained from the optimized geometry of the ions/ion-pairs using WINMOSTAR[119].

*The measurable frequency range of the LCR-bridge is from 20 Hz to 200 kHz.

Chapter 3

Investigation of electrolyte solutions

Knowledge pertaining to ion-association and ion-hydration is crucial in determining various properties of electrolyte solutions which in case of biological ions, can be correlated to various ongoing processes in living systems. Thus, whether it be strong ion-ion interactions (resulting in ion-pairing or aggregation) or strong ion-solvent interactions (giving rise to a specific hydration pattern), both are the area of peculiar interest for electrolyte solution chemists, so a huge body of data is available on these phenomena, and their importance in areas ranging from geochemistry to various biological processes and large scale technical applications has been widely recognized.[120,121]

Present work deals with the study of ammonium (NH_4^+), choline (Ch^+, chemically 2-hydroxyethyl trimethyl ammonium ion, vitamin B4) and chloro-choline ion (Cl-Ch^+, 2-chloroethyl trimethyl ammonium ion) through dielectric relaxation spectroscopy (DRS). Solvation studies of NH_4^+ ion are important in the environmental chemistry of pollutants and soil contamination[122] in addition NH_4^+ ion is an important chemical species that serves as a simple model for solvated amides[123,124] while high-temperature density data of NH_4Cl is needed for the problem of material transport and solid deposition in steam generator systems.[125]

Choline is an important dietary component[2,3] which is required for the normal brain functioning in human. Moreover choline keeps the constituency of cell membranes, is involved in cholinergic neurotransmission[4] and is an important part of pulmonary surfactants.[126] Recently choline based ionic liquids[9] and surfactants[127,128] have attracted increased attention in many fields. It is also known to form a deep eutectic solvent (DES) with urea,[129] and Chloro-choline chloride is known to be an effective plant growth regulator.[130]

Since the structure and functioning of biomolecules mainly depend on the presence and structuring of water molecules around them so it is of crucial importance to study the properties of these molecules in aqueous environment. As far as the study of hydration behaviour of biomolecules is concerned several techniques, each having its own limitations have been employed so far. Nuclear magnetic resonance (NMR) and X-ray diffraction are powerful techniques to study the specific hydration sites with atomic resolution.[131–133] Calorimetry studies mainly deal with the macroscopic amount of water and solute and lacks the data at the molecular level.[134,135] In contrast to bulk methods such as calorimetry, X-ray crystallography, and NMR, molecular simulations provide a way to study individual

steps of hydration.[136]
In this regard DRS, which probes the interaction of matter with electromagnetic radiation in the microwave region, has outstanding capabilities for the study of electrolyte solutions.[87,137,138] Owing thanks to the advances in measurement and related technologies, modern DRS can provide useful information about the nature of the species present in electrolyte solutions. In many cases DRS can provide detailed information about the thermodynamics, kinetics and sometimes even structures of ion pairs (DRS has a unique sensitivity for detecting solvent-separated ion pairs in solution). The information regarding the hydration stoichiometry of cholinergic ions is important, as the water which is bound to these ions has got a role in interaction with certain enzymes.[139] This is accomplished through the analysis of the solvent contributions to DR spectra which yields data on the solvation of the ions.[140]
The present chapter is further partitioned into two sections: first (section 3.1) deals mainly with the physical properties and second (section 3.2) presents detailed broadband DRS studies of investigated electrolyte systems.

3.1 Physical properties of choline chloride, chlorocholine chloride and ammonium chloride

Most of the material presented in this section makes the basis of the manuscript:

Shaukat, S.; Buchner, R. *'Densities, Viscosities [from (278.15 to 318.15) K] and Electrical Conductivities (at 298.15 K) of Aqueous Solutions of Choline Chloride and Chloro-Choline Chloride.' J. Chem. Eng. Data*, **2011**, *56*, 4944.

Physical properties, namely electrical conductivity, κ, at 298.15 K, as well as density, ρ, at (278.15, 288.15, 298.15, 308.15 & 318.15) K, of aqueous solutions of choline chloride (ChCl), chloro-choline chloride (Cl-ChCl), and ammonium chloride (NH_4Cl) were measured according to the procedure described in section 2.3. Data for the dynamic viscosity, η, at (278.15, 288.15, 298.15, 308.15 & 318.15) K are also provided for ChCl and Cl-ChCl. Aqueous solutions of ChCl and Cl-ChCl have been measured in the concentration (molality) range ($0.02 \lesssim m/\mathrm{mol \cdot kg^{-1}} \lesssim 2.1$), whereas for NH_4Cl(aq) data are presented upto saturation limit.

3.1.1 Results and discussion

Electrical Conductivity. Electrical conductivities have been recorded with the equipment described in section 2.3.2. The obtained electrical conductivities are summarized in Table 3.1 and Figures 3.1 & 3.2. Consistent with the slightly smaller partial molar volume of this compound (see later) $\kappa(m)$ is always larger for ChCl compared to Cl-ChCl, whereas NH_4Cl being smallest of all studied salts has highest $\kappa(m)$ values. The dependence of κ on salt molality is well described by the empirical Casteel-Amis equation[141]

$$\kappa = \kappa_{\max}(\frac{m}{m_{\max}})^a \exp[-bm_{\max}^2(\frac{m}{m_{\max}} - 1)^2 - a(\frac{m}{m_{\max}} - 1)] \tag{3.1}$$

where κ_{max} is the maximum conductivity reached at molality m_{max} while a and b are shape parameters. Since for none of the studied electrolytes κ_{max} was reached in the investigated concentration range $b = 0$ was assumed in the fit.[142] The resulting parameters are summarized in Table 3.2.
To the best of our knowledge literature data for conductivity are only available for ChCl at 298.15 K.[143] As can be seen from Figure 3.1 the agreement with our conductivities is good with deviations $\delta_\kappa = |\kappa_{fit} - \kappa_{lit}| < 0.03\,S \cdot m^{-1}$. For NH_4Cl, experimental data is compared with the literature values[144,145] and, as can be seen from Figure 3.2 the agreement of the literature data with our conductivity values is good with deviations, $\delta_\kappa = |\kappa_{fit} - \kappa_{lit}| < 0.3$ and $< 0.1\,S \cdot m^{-1}$ for reference data of Wishaw and McCleskey, respectively[144,145].

Table 3.1: Electrical Conductivities, κ, of Aqueous Solutions of ChCl, Cl-ChCl, and NH_4Cl at 298.15 K [a]

ChCl(aq)		Cl-ChCl(aq)		NH_4Cl(aq)	
m	κ	m	κ	m	κ
0.0272	0.279	0.0277	0.265	0.0230	0.506
0.0500	0.492	0.0514	0.490	0.0538	0.704
0.1000	0.919	0.1003	0.898	0.0790	1.04
0.2500	2.03	0.2497	1.97	0.1518	1.92
0.3500	2.67	0.3502	2.58	0.3523	4.24
0.5000	3.55	0.5001	3.36	0.4974	5.88
0.6500	4.37	0.6509	4.10	0.7446	8.68
0.7500	4.79	0.7498	4.51	1.1533	12.2
0.9000	5.44	0.8997	5.07	1.4989	15.4
1.2048	6.54	0.9998	5.42	1.9981	19.7
1.5047	7.43	1.2117	6.08	2.4997	23.7
1.9945	8.53	1.5070	6.81	3.3934	30.1
		1.9980	7.67	4.3981	36.3
				5.0023	39.5
				5.4929	41.8
				6.4884	45.9
				7.3958	48.8

[a] Units: m in $mol \cdot kg^{-1}$, κ in $S \cdot m^{-1}$.

Density. The obtained ρ values (see section 2.3.1) are given in Table 3.3 and data are plotted in Figures 3.3, 3.4 & 3.5. Also included in Table 3.3 are literature data[146] for the density of pure water at the investigated temperatures. The latter deviate from our results by $0.007\,kg{\cdot}m^{-3}$ at maximum, lending credit to the stated reproducibility of the instrument ($\pm 0.005\,kg{\cdot}m^{-3}$) and to the quality of the used water sample.
The density data for ChCl(aq), Cl-ChCl(aq) and NH_4Cl(aq) at all temperatures can be well fitted ($\sigma_{fit} \leq 0.12\,kg{\cdot}m^{-3}$ for ChCl(aq), $0.06\,kg{\cdot}m^{-3}$ for Cl-ChCl(aq) and $0.13\,kg{\cdot}m^{-3}$

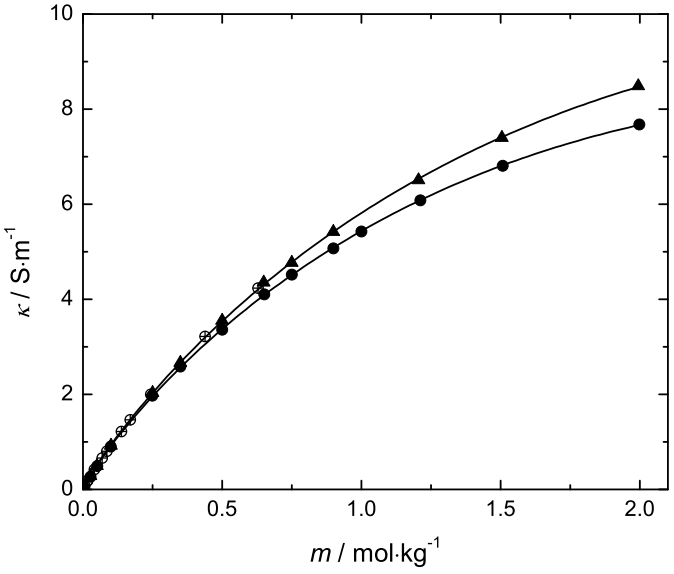

Figure 3.1: Electrical conductivities, κ, of aqueous solutions of ChCl (▲, this work; ⊕, Reference 143) and Cl-ChCl (●) at 298.15 K as a function of solute molality, m. Solid lines represent fits with the Casteel-Amis equation, Eq. 3.1.

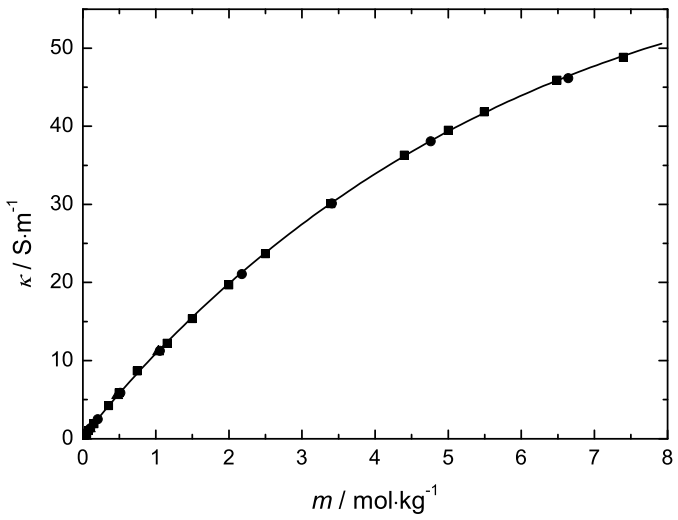

Figure 3.2: Electrical conductivities, κ, of aqueous solutions of NH_4Cl(aq) as a function of molality, m from this work (■), Reference 144 (●), and Reference 145 (▲), at 25 °C. Solid line represents fit of Eq. 3.1.

Table 3.2: Maximum Conductivity, κ_{max}, Corresponding Electrolyte Molality, m_{max}, and Shape Parameter, a, of Eq. 3.1 ($b = 0$ fixed) for Aqueous Solutions of ChCl, Cl-ChCl, and NH_4Cl at 298.15 K. Also Included is the Corresponding Standard Error of the Fit, σ_{fit}[a]

Electrolyte	κ_{max}	m_{max}	a	σ_{fit}
ChCl(aq)	9.75 ± 0.10	3.71 ± 0.09	0.891 ± 0.008	0.02
Cl-ChCl(aq)	8.42 ± 0.06	3.30 ± 0.06	0.883 ± 0.007	0.02
NH_4Cl(aq)	58.87 ± 0.87	14.72 ± 0.45	0.960 ± 0.010	0.16

[a] Units: κ_{max} in $S \cdot m^{-1}$, m_{max} in $mol \cdot kg^{-1}$, σ_{fit} in $S \cdot m^{-1}$.

for NH_4Cl(aq)) with a polynomial in solute molality

$$Y = \sum_{j=0}^{n} a_j m^j \tag{3.2}$$

where $Y = \rho$ and $n = 3$. The obtained parameters, a_j, are summarized in Table 3.4 together with the corresponding standard deviation of the fit, σ_{fit}; fit curves are shown in Figures 3.3, 3.4 & 3.5 for ChCl, Cl-ChCl and NH_4Cl, respectively. Compared to the deviations of the present densities for pure water from corresponding literature data,[146] which do not exceed $\leq 0.007\,kg\,m^{-3}$, the fit standard errors for the solutions are considerably larger. This almost certainly reflects the uncertainty in m. For a comparison of solution densities again only data of Fleming[143] for ChCl(aq) at 298.15 K are available (Figure 3.3). The agreement is good with relative deviations $\leq 5.5 \times 10^{-4}$. It is aimed that the presented density data can serve as an updated addition to the existing literature data for the density of NH_4Cl(aq)[147–152]. Comparison is made between our density data and the literature values[149,150] at 25 °C only and the agreement is generally good with both of the literature data with relative deviations $\leq 2.4 \times 10^{-4}$.

Table 3.3: Densities, ρ, of Aqueous Solutions of ChCl, Cl-ChCl, and NH_4Cl at Molality, m, and Temperature, T [a]

	ρ at Different T				
m	278.15	288.15	298.15	308.15	318.15
			ChCl(aq)		
0[b]	999.964	999.099	997.043	994.029	990.208
0	999.961	999.092	997.036	994.023	990.206
0.0540	1000.967	1000.031	997.931	994.893	991.063
0.1087	1001.952	1000.950	998.810	995.745	991.902
0.2554	1004.503	1003.333	1001.088	997.961	994.085
0.5004	1008.705	1007.266	1004.844	1001.614	997.683
0.6512	1011.014	1009.433	1006.921	1003.633	999.672
0.7484	1012.676	1010.996	1008.420	1005.091	1001.109
1.2030	1019.283	1017.228	1014.403	1010.921	1006.860
1.5035	1022.746	1020.505	1017.560	1014.000	1009.901
1.9924	1028.852	1026.308	1023.157	1019.473	1015.308
			Cl-ChCl(aq)		
0.0506	1001.453	1000.522	998.426	995.387	991.452
0.1009	1002.888	1001.900	999.762	996.694	992.837
0.2364	1006.793	1005.646	1003.397	1000.252	996.273
0.5010	1013.917	1012.479	1010.021	1006.724	1002.683
0.6523	1017.877	1016.276	1013.698	1010.315	1006.203
0.7529	1020.456	1018.745	1016.090	1012.650	1008.516
1.1995	1031.176	1029.024	1026.042	1022.358	1018.058
1.4973	1038.126	1035.683	1032.481	1028.632	1024.208
1.9862	1048.245	1045.386	1041.866	1037.775	1033.173
			NH_4Cl(aq)		
0.0230	1000.808	999.911	997.841	994.822	991.004
0.0538	1001.093	1000.183	998.103	995.081	991.259
0.0790	1001.581	1000.648	998.557	995.529	991.699
0.1518	1002.886	1001.900	999.778	996.735	992.894
0.3523	1006.367	1005.225	1003.012	999.821	996.006
0.4974	1008.826	1007.581	1005.312	1002.199	998.302
0.7446	1012.830	1011.420	1009.054	1005.896	1002.037
1.1533	1019.105	1017.456	1014.946	1011.718	1007.792
1.4989	1024.101	1022.276	1019.659	1016.379	1012.240
1.9981	1030.918	1028.863	1026.114	1022.764	1018.828
2.4997	1037.323	1035.068	1032.194	1028.783	1024.886
3.3934	1047.759	1045.208	1042.151	1038.646	1034.725
4.3981	1058.402	1055.579	1052.347	1048.748	1044.802
5.0023	1064.241	1061.275	1057.951	1054.300	1050.342
5.4929	1068.754	1065.683	1062.289	1058.600	1054.628
6.4884	1077.246	1074.127	1070.572	1066.810	1062.812
7.3958			1077.343	1073.466	1069.512

[a] Units: m in $\mathrm{mol \cdot kg^{-1}}$, ρ in $\mathrm{kg \cdot m^{-3}}$, T in K. [b] Reference 146.

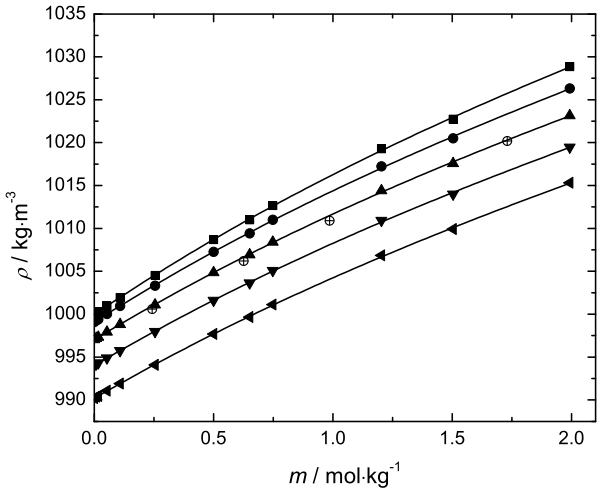

Figure 3.3: Densities, ρ, of aqueous ChCl as a function of solute molality, m, at (■, 278.15; ●, 288.15; ▲, 298.15; ▼, 308.15 and ◄, 318.15) K. Solid lines represent fits of Eq. 3.2 ($Y = \rho$; $n = 3$). For comparison the data (⊕) of Fleming[143] at 298.15 K are included.

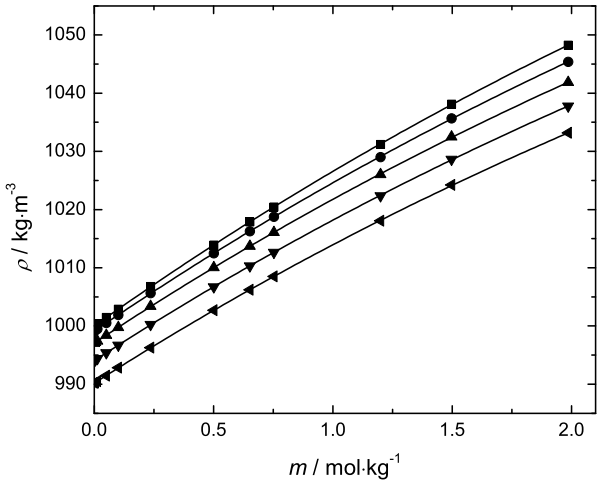

Figure 3.4: Densities, ρ, of aqueous solutions of Cl-ChCl as a function of solute molality, m, at (■, 278.15; ●, 288.15; ▲, 298.15; ▼, 308.15 and ◄, 318.15) K. Solid lines represent fits of Eq. 3.2 ($Y = \rho$; $n = 3$).

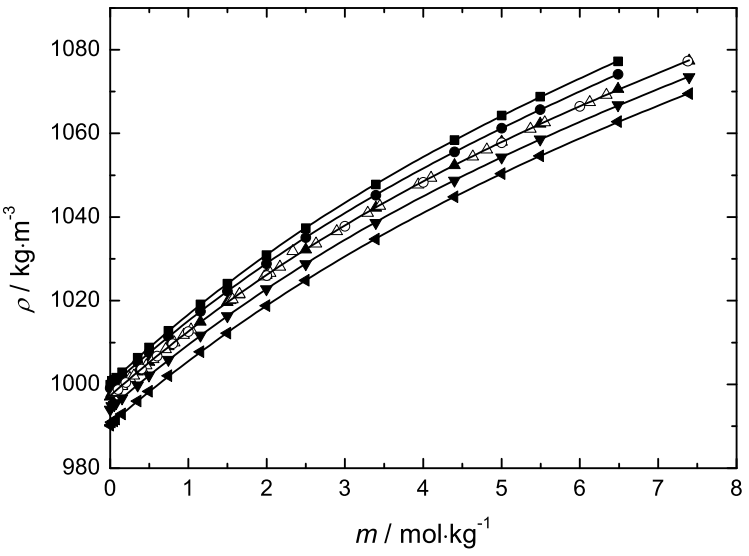

Figure 3.5: Densities, ρ, of aqueous solutions of NH_4Cl(aq) as a function of solute molality, m, at (■, 278.15; ●, 288.15; ▲, 298.15; ▼, 308.15 and ◀, 318.15) K. The data of References 149 (○), and 150 (△) are also given for comparison. Solid lines represent fit of Eq. 3.2 ($Y = \rho$; $n = 3$).

Table 3.4: Coefficients, a_j ($j = 0 \ldots 3$), of Eq. 3.2 for the Densities, $Y = \rho$, of Aqueous Solutions of ChCl, Cl-ChCl, and NH_4Cl and Corresponding Standard Deviation of the Fit, σ_{fit} [a]

T	a_0	a_1	a_2	a_3	σ_{fit}
		ChCl(aq)			
278.15	999.946	18.876	-2.900	0.348	0.12
288.15	999.078	17.600	-2.604	0.311	0.12
298.15	997.024	16.786	-2.429	0.290	0.11
308.15	994.012	16.306	-2.344	0.283	0.11
318.15	990.182	16.103	-2.344	0.292	0.11
		Cl-ChCl(aq)			
278.15	999.984	29.139	-2.697	0.134	0.06
288.15	999.113	27.964	-2.616	0.137	0.06
298.15	997.057	27.145	-2.588	0.143	0.06
308.15	994.046	26.578	-2.598	0.155	0.06
318.15	990.167	26.254	-2.635	0.162	0.06
		NH_4Cl(aq)			
278.15	1000.227	17.694	-1.272	0.058	0.12
288.15	999.345	16.956	-1.191	0.055	0.11
298.15	997.311	16.383	-1.065	0.043	0.13
308.15	994.288	16.171	-1.038	0.041	0.13
318.15	990.468	16.043	-1.005	0.038	0.12

[a] Units: T in K, a_0 in $\text{kg} \cdot \text{m}^{-3}$, a_1 in $\text{kg}^2 \cdot \text{m}^{-3} \cdot \text{mol}^{-1}$, a_2 in $\text{kg}^3 \cdot \text{m}^{-3} \cdot \text{mol}^{-2}$, a_3 in $\text{kg}^4 \cdot \text{m}^{-3} \cdot \text{mol}^{-3}$, σ_{fit} in $\text{kg} \cdot \text{m}^{-3}$

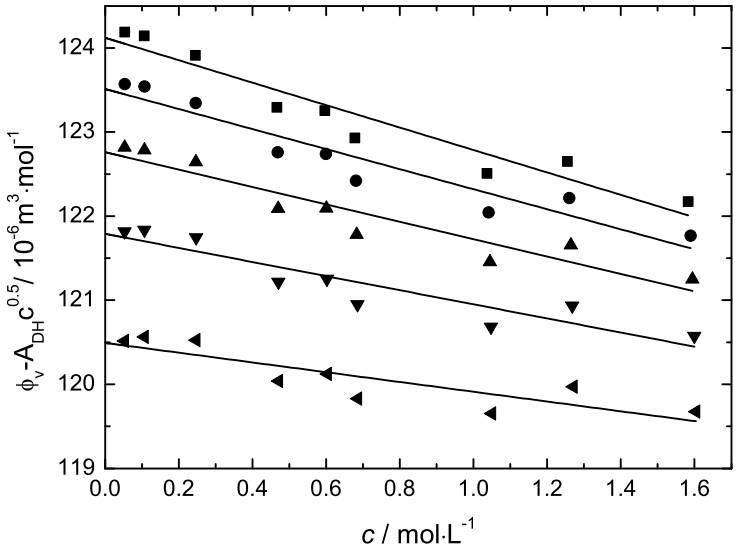

Figure 3.6: Apparent molar volume, ϕ_v, of ChCl in aqueous solution as a function of salt concentration, c, at (◀, 278.15; ▼, 288.15; ▲, 298.15; ●, 308.15 and ■, 318.15) K. Solid lines represent fits of Eq. 3.4.

From ρ the corresponding apparent molar volumes, ϕ_v (Figures 3.6 & 3.7), were calculated for ChCl and Cl-ChCl only as sufficient literature data is available for NH_4Cl[147–149] in this regard. Following equation was used to calculate ϕ_v[153]

$$\phi_v = \frac{M}{\rho(m)} + \frac{\rho(0) - \rho(m)}{m\rho(0)\rho(m)} \tag{3.3}$$

where M is the molar mass (ChCl: 0.13962 kg·mol^{-1}; Cl-ChCl: 0.15807 kg·mol^{-1}). According to Redlich and Meyer[154] for electrolyte solutions the dependence of ϕ_v on solute concentration c ($= \rho(m) \cdot m/(1 + Mm)$) should follow the relation

$$\phi_v = \phi_v^0 + A_{DH}c^{1/2} + hc \tag{3.4}$$

where ϕ_v^0 is the limiting partial molar volume of the solute and A_{DH} is the Debye-Hückel limiting slope (constant for all 1:1 electrolytes in a given solvent at a certain T). The empirical "deviation parameter", h, of Eq. 3.4 is thought to measure ion-ion interactions in the chosen system.[155] The fits obtained with A_{DH} values taken from literature data of Archer and Wang[156] (converted to molarity scale) are shown in Figure 3.6 for ChCl and 3.7 for Cl-ChCl; the derived limiting partial molar volumes, ϕ_v^0, and h values are summarized in Table 3.5.

As expected from the larger van der Waals volume of the chlorine atom compared to the OH group, ϕ_v^0(Cl-ChCl) > ϕ_v^0(ChCl). The present result for the limiting partial molar volume of ChCl at 298.15 K, ϕ_v^0(ChCl) = 122.8 × 10^{-6} m^3·mol^{-1}, is slightly smaller than

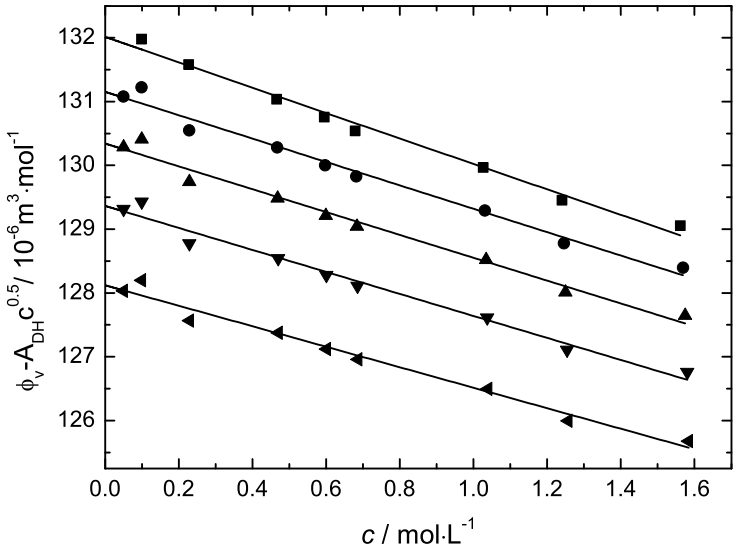

Figure 3.7: Apparent molar volume, ϕ_v, of Cl-ChCl in aqueous solution as a function of salt concentration, c, at (◀, 278.15; ▼, 288.15; ▲, 298.15; ●, 308.15 and ■, 318.15) K. Solid lines represent fits of Eq. 3.4.

the value published by Fleming[143] ($124.9 \times 10^{-6}\,\mathrm{m^3{\cdot}mol^{-1}}$). This is mainly due to the slightly smaller densities of Reference 143 but the different A_{DH} parameters used there also contribute to the difference.
For ChCl and Cl-ChCl ϕ_v^0 increases with increasing temperature according to the relation

$$\phi_v^0 = a_0^\phi + a_1^\phi(T - T_0) + a_2^\phi(T - T_0)^2 \tag{3.5}$$

where $T_0 = 298.15\,\mathrm{K}$.[157] The obtained parameters, a_j ($j = 0, \ldots, 2$), collected in Table 3.6, permit calculation of the limiting apparent molar expansibility

$$\phi_E^0 = (\frac{\partial\phi_v^0}{\partial T})_p = a_1^\phi + 2a_2^\phi(T - T_0) \tag{3.6}$$

of ChCl and Cl-ChCl in water (Table 3.5) and of the corresponding Hepler's constant,[158] $(\partial^2\phi_v^0/\partial T^2)_p = 2a_2^\phi$ ($= (-0.0023 \pm 0.0002) \times 10^{-6}\,\mathrm{m^3mol^{-1}K^{-2}}$ for ChCl; $(-0.0013 \pm 0.0004) \times 10^{-6}\,\mathrm{m^3mol^{-1}K^{-2}}$ for Cl-ChCl).
Similar to aqueous NaCl solutions[159] the deviation parameter, h, is negative and decreases with rising temperature for both ChCl(aq) and Cl-ChCl(aq). This suggests that ion-pairing is weak and ion-ion interactions decrease further with increasing thermal motions.[159] The rather small concentration dependence of ϕ_v^0 (and thus small $|h|$ values) for ChCl suggests that both ions well fit into the water structure, whereas the fairly negative h for Cl-ChCl may indicate mutual salting-in of the ions, as discussed by Desnoyers and Arel for some n-alkylamine hydrobromides.[153]

Table 3.5: Limiting Partial Molar Volumes, ϕ_v^0, Debye-Hückel Parameters, A_{DH},[156] and Sensitivity Parameters, h, of Eq. 3.4 for Aqueous Solutions of ChCl and Cl-ChCl at Temperature, T. Also Included are the Corresponding Limiting Apparent Molar Expansibilities, ϕ_E^0 [a]

T	ϕ_v^0	A_{DH}[b]	h	ϕ_E^0
		ChCl(aq)		
278.15	120.49 ± 0.11	1.5498	-0.59 ± 0.13	0.137
288.15	121.79 ± 0.11	1.6728	-0.82 ± 0.13	0.113
298.15	122.76 ± 0.11	1.8332	-1.01 ± 0.13	0.090
308.15	123.51 ± 0.11	2.0259	-1.18 ± 0.14	0.066
318.15	124.12 ± 0.12	2.2499	-1.34 ± 0.14	0.043
		Cl-ChCl(aq)		
278.15	128.12 ± 0.07	1.5498	-1.62 ± 0.09	0.124
288.15	129.37 ± 0.07	1.6728	-1.71 ± 0.09	0.110
298.15	130.34 ± 0.08	1.8332	-1.77 ± 0.09	0.096
308.15	131.15 ± 0.08	2.0259	-1.82 ± 0.09	0.082
318.15	132.01 ± 0.08	2.2499	-2.00 ± 0.09	0.068

[a] Units: T in K, ϕ_v^0 in $10^{-6}\mathrm{m}^3 \cdot \mathrm{mol}^{-1}$, A_{DH} in $10^{-6}\mathrm{m}^3 \cdot \mathrm{L}^{1/2} \cdot \mathrm{mol}^{-3/2}$, h in $10^{-6}\mathrm{m}^3 \cdot \mathrm{L} \cdot \mathrm{mol}^{-2}$, ϕ_E^0 in $10^{-6}\mathrm{m}^3 \cdot \mathrm{mol}^{-1} \cdot \mathrm{K}^{-1}$. [b] Converted to molarity scale with the water densities of Reference 146.

Table 3.6: Temperature Coefficients, a_i^ϕ $(j = 0, 1, 2)$, of Eq. 3.5 for the Limiting Partial Molar Volumes, ϕ_v^0, of ChCl(aq) and Cl-ChCl(aq) and Corresponding Fit Standard Errors, σ_{fit} [a]

Electrolyte	a_0^ϕ	a_1^ϕ	a_2^ϕ	σ_{fit}
ChCl(aq)	122.77 ± 0.03	0.0898 ± 0.0014	-0.00117 ± 0.00011	0.04
Cl-ChCl(aq)	130.34 ± 0.05	0.0959 ± 0.0023	-0.00071 ± 0.00019	0.07

[a] Units: a_0 in $10^{-6}\mathrm{m}^3 \cdot \mathrm{mol}^{-1}$, a_1 in $10^{-6}\mathrm{m}^{-3} \cdot \mathrm{mol}^{-1} \cdot \mathrm{K}^{-1}$, a_2 in $10^{-6}\mathrm{m}^{-3} \cdot \mathrm{mol}^{-1} \cdot \mathrm{K}^{-2}$, σ_{fit} in $10^{-6}\mathrm{m}^3 \cdot \mathrm{mol}^{-1}$.

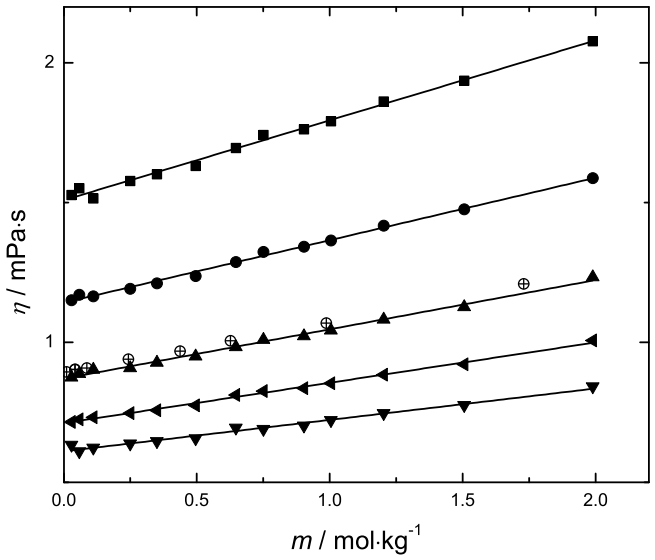

Figure 3.8: Dynamic viscosities, η, of aqueous ChCl as a function of solute molality, m, at (■, 278.15; ●, 288.15; ▲, 298.15; ◀, 308.15 and ▼, 318.15) K. Solid lines are the linear fits of Eq. 3.2 ($Y = \eta$; $n = 1$). For comparison the data (⊕) of Fleming[143] at 298.15 K are included.

Viscosity. Dynamic viscosities, η, of aqueous solutions of ChCl (Figure 3.8), Cl-ChCl (Figure 3.9) and NH_4Cl (Figure 3.10) were measured as a function of solute molality, m, at different temperatures, T. Dynamic viscosities determined for ChCl(aq) and Cl-ChCl(aq) are summarized in Table 3.7.* To the best of our knowledge only the data of Fleming[143] for ChCl(aq) at 298.15 K are available for comparison (Figure 3.8). These are slightly larger than the present results with relative deviations $\leq 3.4 \times 10^{-2}$.
For ChCl(aq) plots of $\eta = f(m)$ are linear over the entire range of m (Figure 3.8), whereas a notable curvature was found for Cl-ChCl(aq) (Figure 3.9). The data can be well-fitted with Eq. 3.2 where $Y = \eta$, $n = 1$ for ChCl, and $n = 2$ for Cl-ChCl. The obtained parameters are summarized in Table 3.8.

For liquids and solutions far from the glass-transition temperature, as should be the case for the present samples, the temperature dependence of η is generally well-described by the Arrhenius equation

$$\ln \eta = \ln \eta_\infty + E_a/(RT) \tag{3.7}$$

where η_∞ is the limiting viscosity for $T \to \infty$, R the gas constant, and E_a the activation energy of viscous flow.

*Unfortunately, measured η data for NH_4Cl were scattered (Figure 3.10) and none of the available capillaries was helpful to obtain reproducible set of viscosity data. Hence, data for NH_4Cl are not shown in Table 3.7 and also further analysis for this system is not appropriate.

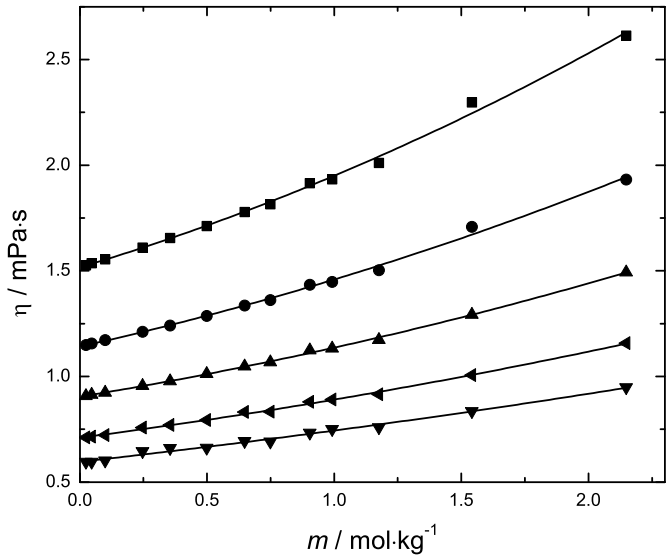

Figure 3.9: Dynamic viscosities, η, of aqueous Cl-ChCl as a function of solute molality, m, at (■, 278.15; ●, 288.15; ▲, 298.15; ◀, 308.15 and ▼, 318.15) K. Solid lines are the fits of Eq. 3.2 ($Y = \eta$; $n = 2$).

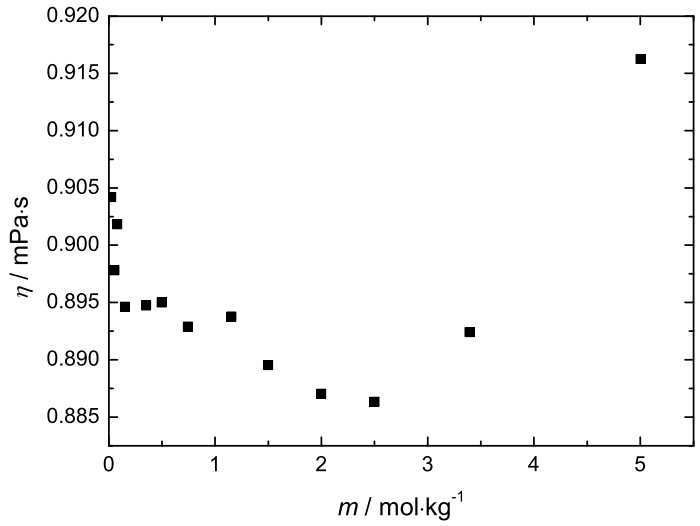

Figure 3.10: Dynamic viscosities, η, of aqueous NH_4Cl as a function of solute molality, m, at 278.15 K.

Table 3.7: Dynamic Viscosities, η, of Aqueous Solutions of ChCl and Cl-ChCl at Molality, m, and Temperature, T [a]

	η at Different T				
m	278.15	288.15	298.15	308.15	318.15
			ChCl(aq)		
0.0293	1.527	1.151	0.875	0.715	0.633
0.0580	1.551	1.170	0.888	0.724	0.610
0.1113	1.515	1.164	0.903	0.732	0.623
0.2495	1.577	1.192	0.908	0.746	0.638
0.3505	1.601	1.211	0.928	0.757	0.646
0.4956	1.631	1.237	0.950	0.774	0.656
0.6473	1.695	1.287	0.984	0.811	0.694
0.7512	1.741	1.323	1.009	0.826	0.690
0.9030	1.762	1.342	1.023	0.835	0.702
1.0049	1.791	1.364	1.043	0.854	0.721
1.2029	1.862	1.417	1.082	0.884	0.747
1.5060	1.936	1.476	1.127	0.921	0.776
1.9896	2.077	1.587	1.234	1.007	0.843
			Cl-ChCl(aq)		
0.0236	1.526	1.148	0.907	0.711	0.596
0.0464	1.536	1.156	0.913	0.714	0.595
0.0994	1.555	1.172	0.924	0.722	0.602
0.2464	1.610	1.211	0.955	0.757	0.645
0.3552	1.656	1.241	0.977	0.770	0.660
0.4990	1.712	1.286	1.012	0.793	0.661
0.6479	1.778	1.335	1.047	0.831	0.694
0.7493	1.815	1.362	1.069	0.833	0.691
0.9041	1.914	1.433	1.124	0.879	0.733
0.9927	1.933	1.447	1.133	0.890	0.750
1.1758	2.010	1.502	1.173	0.915	0.759
1.5415	2.298	1.708	1.292	1.005	0.835
2.1484	2.612	1.932	1.493	1.158	0.948

[a] Units: m in mol $\cdot$ kg^{-1}, η in mPa $\cdot$ s, T in K.

Figure 3.11 shows the activation energies obtained from the present viscosity data along with the calculated E_a value of pure water using literature data[160]. For ChCl(aq) E_a is essentially independent of solute molality over the entire concentration range, yielding an average value of 16.9 kJ·mol^{-1}, whereas E_a appears to increase linearly for Cl-ChCl(aq). However, these results have to be taken with a grain of salt. Error bars for E_a are rather large, and a close inspection of the fits (Figures 3.12 & 3.13) reveals that especially at low

Table 3.8: Coefficients a_j of Eq. 3.2 ($Y = \eta$) for the Viscosity, η, of Aqueous Solutions of ChCl ($n = 1$) and Cl-ChCl ($n = 2$) at temperature, T [a]

T	a_0	a_1	a_2
	ChCl(aq)		
278.15	1.508 ± 0.006	0.286 ± 0.007	
288.15	1.142 ± 0.004	0.223 ± 0.004	
298.15	0.870 ± 0.004	0.176 ± 0.004	
308.15	0.711 ± 0.003	0.144 ± 0.003	
318.15	0.610 ± 0.004	0.112 ± 0.004	
	Cl-ChCl(aq)		
278.15	1.516 ± 0.012	0.360 ± 0.029	0.073 ± 0.014
288.15	1.141 ± 0.008	0.268 ± 0.021	0.049 ± 0.010
298.15	0.904 ± 0.003	0.196 ± 0.008	0.036 ± 0.004
308.15	0.800 ± 0.004	0.157 ± 0.009	0.024 ± 0.004
318.15	0.596 ± 0.006	0.134 ± 0.014	0.013 ± 0.007

[a] Units: T in K, a_0 in mPa·s, a_1 in $\mathrm{mPa \cdot s \cdot kg \cdot mol^{-1}}$, a_2 in $\mathrm{mPa \cdot s \cdot kg^2 \cdot mol^{-2}}$.

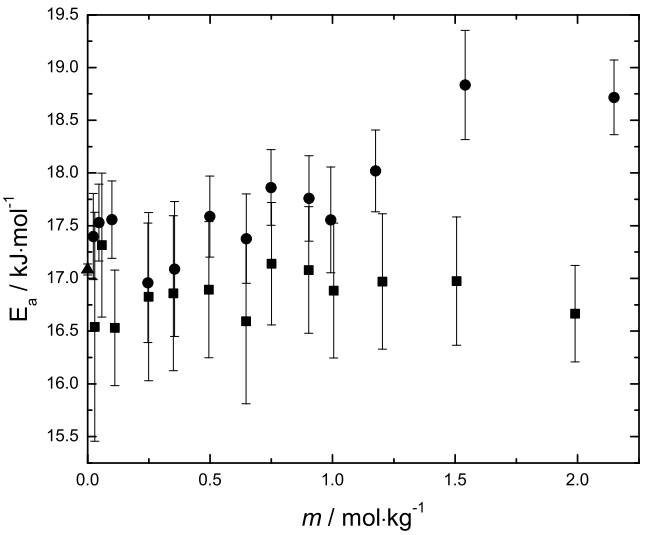

Figure 3.11: Arrhenius activation energy, E_a, of of viscous flow for aqueous solutions of ■, ChCl and ●, Cl-ChCl as a function of solute molality, m. The E_a value of pure water ▲, calculated from the data of Reference 160 is also shown.

concentrations, and more pronounced for ChCl (Figure 3.12), $\ln \eta(T)$ shows a small but

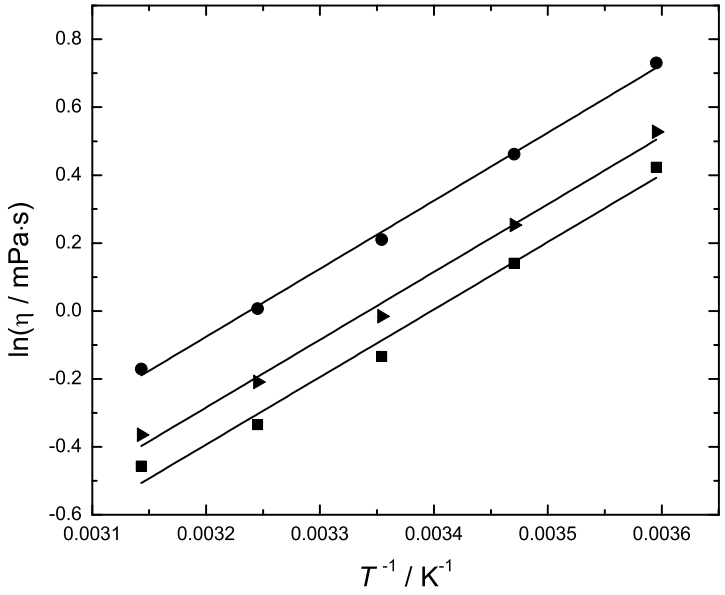

Figure 3.12: Arrhenius plot, $\ln \eta = f(T^{-1})$, of aqueous solutions of ChCl with $m =$ (■, 0.0292; ▶, 0.6473 and ●, 1.9896) mol·kg^{-1}. Solid lines are the fits of Eq. 3.7.

significant positive curvature, possibly indicating Vogel-Fulcher-Tamann (VFT) behaviour already around room temperature. However, a larger temperature range than that covered in the present investigation [(278.15 to 318.15) K] is required for a thorough determination of the curvature.

According to Walden's rule,[121] $\Lambda\eta =$ constant, the product of viscosity and molar conductivity, Λ ($= \kappa/c$), should be independent of concentration as long as ion association is negligible. Since the values obtained for the h parameter of Eq. 3.4 suggest only weak ion association, which is in accordance with dielectric relaxation studies (section 3.2), it is therefore surprising to find a rather large decrease of $\Lambda\eta$ with increasing m for both ChCl(aq) and Cl-ChCl(aq) (Figure 3.14). However, it should be kept in mind that also changes in ion solvation with rising concentration may cause deviation from Walden's rule.

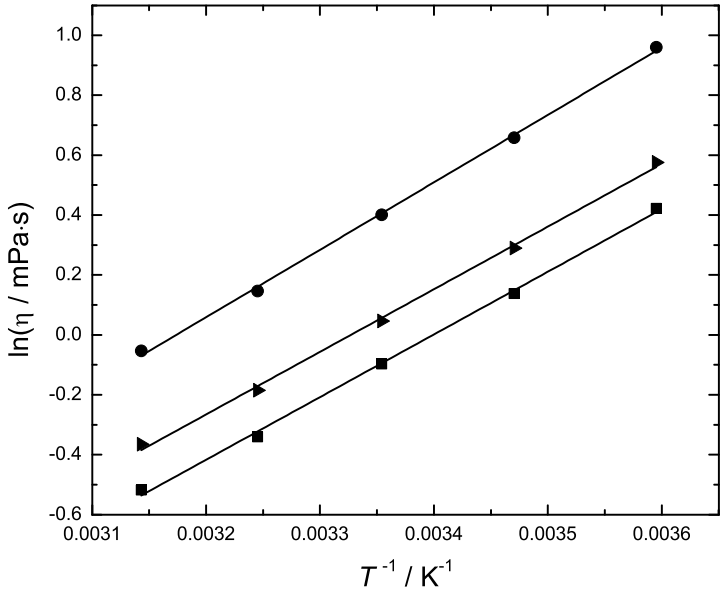

Figure 3.13: Arrhenius plot, $\ln \eta = f(T^{-1})$, of aqueous solutions of Cl-ChCl with $m =$ (■, 0.0236; ►, 0.6479 and ●, 2.1484) mol·kg^{-1}. Solid lines are the fits of Eq. 3.7.

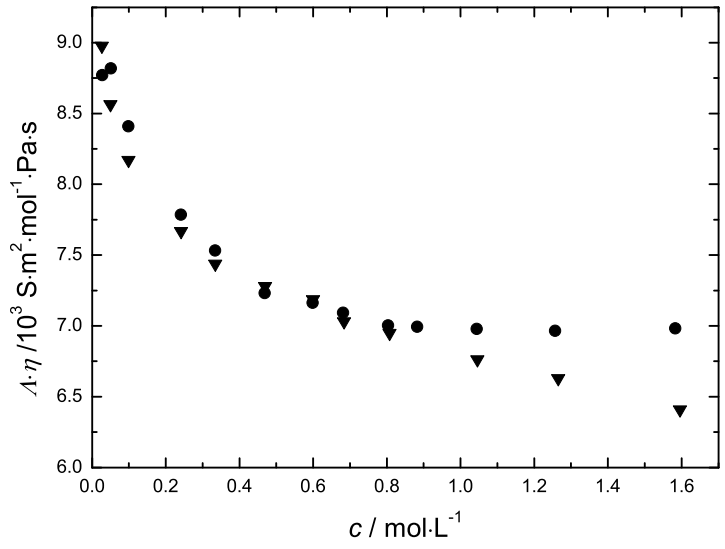

Figure 3.14: Walden product, $\Lambda\eta$, of aqueous solutions of ▼, ChCl and ●, Cl-ChCl at 298.15 K.

3.2 DRS of choline chloride, chlorocholine chloride and ammonium chloride

Most of the material presented in this section makes the basis of the manuscript:

Shaukat, S.; Buchner, R. *'Dielectric Relaxation Spectroscopy of Hydration and Ion-pairing in Aqueous Solutions of Choline Chloride, Chlorocholine Chloride, and Ammonium Chloride.' Phys. Chem. Chem. Phy*, In preparation.

The present section deals with broadband DRS study of aqueous solution of ammonium chloride, choline chloride and chloro-chlone chloride. DR spectra were measured over the frequency range of ∼0.2 GHz to 89 GHz upto fairly high concentrations at 25 °C. Additionally, spectra of 0.280 mol · kg^{-1} of ChCl(aq) were measured at 5, 15, 25, 35, 45, 55 and 65 °C.
The data in the frequency range $0.2 \leq \nu/\text{GHz} \leq 50$ were recorded with Agilent E8364B VNA (section 2.2.3) and high frequency data, $60 \leq \nu/\text{GHz} \leq 89$ was recorded using E-band interferometer (section 2.2.2).

3.2.1 Choice of fit model

The combined $\hat{\varepsilon}(\nu)$ data were analyzed by simultaneously fitting the in-phase ($\varepsilon'(\nu)$, Figures 3.15a - 3.18a) and out-of-phase ($\varepsilon''(\nu)$, Figures 3.15b & 3.18b) components of the complex permittivity to various relaxation models with n distinguishable relaxation processes using Eq. 1.66. Only simplified variants of Eq. 1.66, i.e., CD, CC, and D models were considered.[21] The quality of the fit was evaluated via χ^2_r values.[103] Along with the minimum variance, the choice of accepted model was also based on one offering least number of modes which are physically explainable. All fitting parameters obtained from the present spectra are summarized in Tables 3.9 and 3.10.
The method devised by Zasetzky and Buchner[105] was used additionally to check the validity of accepted model for each of the studied salt. Typical results of that analysis are shown in Figure 3.19.

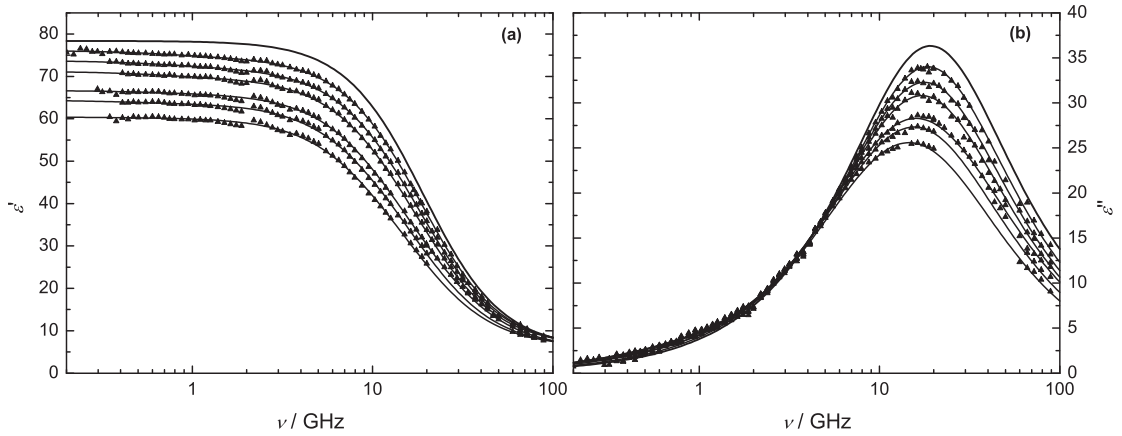

Figure 3.15: Permittivity, $\varepsilon'(\nu)$ (**a**), and dielectric loss, $\varepsilon''(\nu)$ (**b**), spectra for ChCl(aq) at 25 °C and concentrations, c / M = 0, 0.2419, 0.4696, 0.6843, 1.0457, 1.2653 and 1.5957 (top to bottom). Symbols show experimental data; lines represent the D+D+D fit

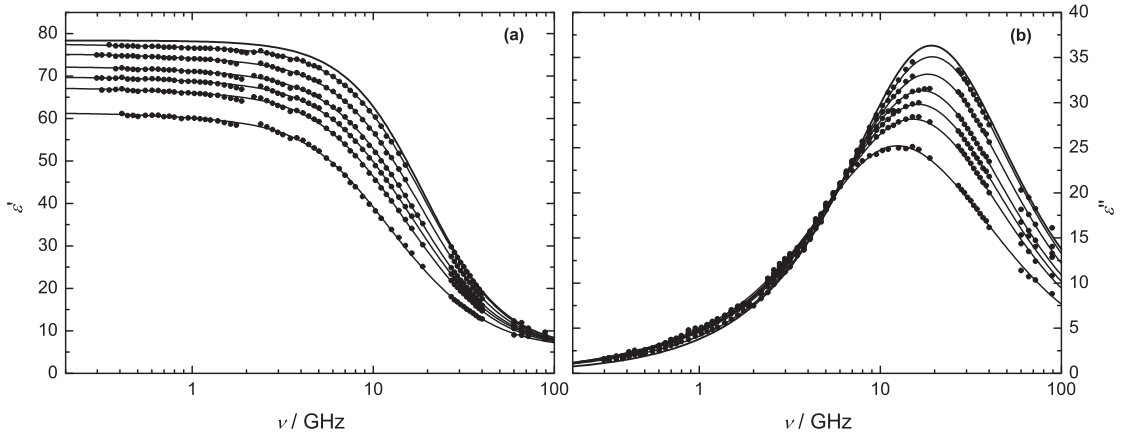

Figure 3.16: Permittivity, $\varepsilon'(\nu)$ (**a**), and dielectric loss, $\varepsilon''(\nu)$ (**b**), spectra for Cl-ChCl(aq) at 25 °C and concentrations, c / M = 0, 0.0987, 0.3339, 0.5982, 0.8030, 1.0438 and 1.5825 (top to bottom). Symbols show experimental data; lines represent the D+D+D fit.

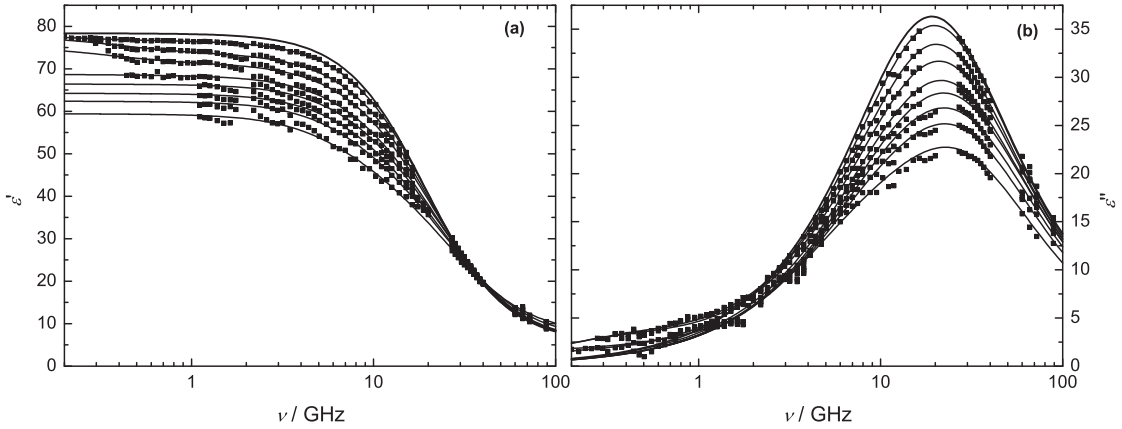

Figure 3.17: Permittivity, $\varepsilon'(\nu)$ (**a**), and dielectric loss, $\varepsilon''(\nu)$ (**b**), spectra for NH_4Cl(aq) at 25 °C and concentrations, c / M = 0, 0.0229, 0.3468, 0.7226, 1.1025, 1.4150, 1.8524, 2.2759 and 2.9931 (top to bottom). Symbols show experimental data; lines represent either a D+D+D or a D+D fit.

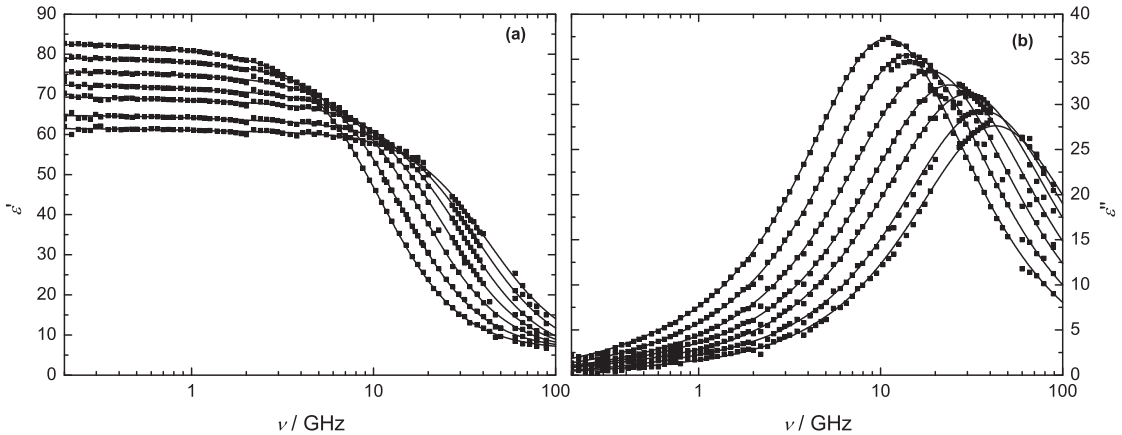

Figure 3.18: Permittivity, $\varepsilon'(\nu)$ (**a**), and dielectric loss, $\varepsilon''(\nu)$ (**b**), spectra for $0.280\,\mathrm{mol}\cdot\mathrm{kg}^{-1}$ of ChCl(aq) at temperature, T / °C = 5, 15, 25, 35, 45, 55 and 65 (top to bottom). Symbols show experimental data; lines represent the D+D+D fit.

Table 3.9: Densities, ρ; Electrical Conductivities, κ; Limiting Permittivities, ε_j; Relaxation Times, τ_j; and Reduced Error Function Values, χ^2_r, for ChCl(aq), Cl-ChCl(aq) and NH_4Cl(aq) at Concentration c and 25 °C[a,b]

c	ρ	κ	ε	τ_1	ε_2	τ_2	ε_3	τ_3	ε_∞	χ^2_r
					ChCl					
0[c]			78.37					8.32	3.48	0.048
0.0270	0.99751	0.279	78.08	811.9	77.62	12F	76.85	8.27	5.89	0.057
0.0501	0.99782	0.492	77.91	468.5	77.21	12.3F	75.37	8.23	5.72	0.050
0.0993	0.99865	0.919	77.72	357.2	76.52	12.5F	72.45	8.24	5.74	0.082
0.2419	1.0009	2.03	76.07	215.4	74.52	13F	67.85	8.25	6.03	0.084
0.3342	1.0024	2.67	75.13	212.1	73.56	13.9	65.54	8.25F	6.23	0.054
0.4696	1.0046	3.55	73.69	215.8	72.00	14.0	61.05	8.27	6.38	0.118
0.5998	1.0067	4.37	71.91	195.7	70.53	14.6	57.23	8.25F	6.39	0.149
0.6843	1.0080	4.79	71.17	241.8	69.69	14.8	54.87	8.20F	6.35	0.134
0.8074	1.0100	5.44	69.15	166.1	68.38	14.8	51.28	8.27	6.66	0.177
1.0457	1.0140	6.54	66.51	232.3	66.07	16.5	47.60	8.00F	6.33	0.130
1.2653	1.0176	7.43	64.39	370.2	63.61	16.1	41.97	8.00F	5.94	0.105
1.5957	1.0228	8.53	60.41	388.9	60.22	15.8	34.98	8.00F	6.10	0.129
					Cl-ChCl(aq)					
0.0275	0.99776	0.265	78.24	527.7	77.77	15.3F	76.22	8.27	5.65	0.027
0.0509	0.99844	0.490	78.06	515.5	77.44	15.3F	72.36	7.95	5.36	0.041
0.0987	0.99973	0.898	77.55	382.8	76.83	15.3F	69.22	7.80	5.36	0.068
0.2411	1.0037	1.97	76.26	242.6	74.93	15.3F	65.28	7.96	5.68	0.070
0.3339	1.0062	2.58	75.19	213.5	73.97	15.3F	60.31	7.78	5.50	0.054
0.4681	1.0099	3.36	73.66	203.4	72.45	15.3F	56.05	7.82	5.70	0.084
0.5982	1.0136	4.10	72.18	203.1	70.90	15.3F	53.24	8.00	5.87	0.067
0.6810	1.0160	4.51	71.23	207.1	70.00	15.3F	49.67	7.91	5.94	0.056
0.8030	1.0194	5.07	69.76	205.1	68.68	15.3F	44.80	7.71	5.87	0.078
0.8821	1.0217	5.42	69.04	240.1	67.82	15.3F	41.55	7.56	5.82	0.073
1.0438	1.0264	6.08	67.19	263.3	66.07	15.3F	35.53	7.18	5.75	0.068
1.2566	1.0324	6.81	64.92	291.2	63.70	15.3F	28.93	6.72	5.67	0.081
1.5825	1.0422	7.67	61.29	211.2	60.03	15.3F	20.20	6.01	5.85	0.077
					NH_4Cl(aq)					
0.0229	0.99784	0.506	78.26	797.8	76.60	26.8	75.58	8.00F	5.40	0.068
0.0536	0.99810	0.704	78.23	480.8	76.76	20.8	75.50	8.00F	5.48	0.067
0.0785	0.99856	1.04	77.76	460.9	75.92	25.1	74.32	7.80F	5.15	0.114
0.1505	0.99978	1.92	77.72	342.1	75.44	18.5	72.80	7.75F	5.32	0.149
0.3468	1.0030	4.24	77.65	413.9	73.63	17.0	68.17	7.50F	5.54	0.138
0.4870	1.0053	5.88	76.88	412.8	72.58	15.3	64.42	7.30F	5.64	0.281
0.7226	1.0090	8.68	75.17	450.8	71.24	15.4	60.20	6.87F	5.45	0.220
1.1025	1.0149	12.2	68.68	231.7	68.39	15.1	53.39	6.35F	5.35	0.216
1.4149	1.0196	15.4	66.39			14.9	49.33	5.90F	5.08	0.362
1.8523	1.0261	19.7	64.21			15.4	46.70	5.75F	5.45	0.272
2.2759	1.0322	23.7	62.34			16.9	45.75	5.68	6.29	0.352
2.9931	1.0422	30.1	59.38			20.5	44.41	5.73	7.34	0.604

[a] Parameter values followed by the letter F were held constant during the fitting procedure. [b] Units: c in M; ρ in $kg\,L^{-1}$; κ in $\Omega^{-1}\,m^{-1}$; τ_j in $10^{-12}\,s$. [c] Reference 86.

Table 3.10: Limiting Permittivities, ε_j; Relaxation Times, τ_j; and Reduced Error Function Values, χ^2_r, for 0.28 mol $\cdot$ kg^{-1} ChCl(aq) at Different Temperatures[a]

T	ε_1	τ_1	ε_2	τ_2	ε_3	τ_3	ε_∞	χ^2_r
5	82.59	231	80.81	17.7	72.56	14.2	6.31	0.120
15	79.13	208	77.75	17.4	70.71	10.7	6.21	0.101
25	75.64	203	74.37	16.6	68.21	8.11	5.85	0.151
35	72.37	208	70.87	14.0	65.10	6.31	5.29	0.097
45	69.46	251	68.16	12.3	62.82	5.05	4.38	0.127
55	64.73	148	63.46	6.80	60.66	4.25	4.73	0.246
65	61.49	197	60.76	4.12	60.43	3.72	5.54	0.359

[a] Units: T in °C; τ_j in 10^{-12} s.

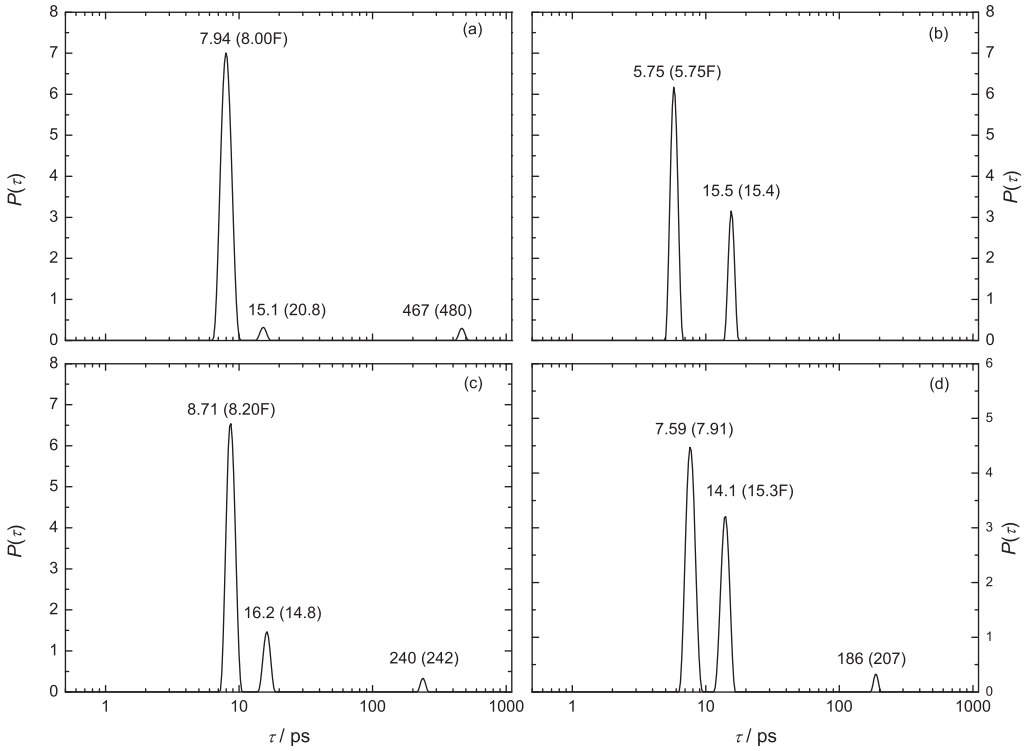

Figure 3.19: Relaxation time distribution function, $P(\tau)$, at, c / M of: NH_4Cl(aq) (a) 0.0536, (b) 1.8523, ChCl(aq) (c) 0.6843 and Cl-ChCl(aq) (d) 0.6811 at 25 °C.

3.2.2 Resolution of DR spectra and assignment of relaxation modes.

The obtained DRS spectra of all studied electrolytes were best fitted by a superposition of three Debye-type relaxation processes, D+D+D model (D+D model for NH_4Cl

at $c > 1.1025\,\mathrm{M}$), see Figures 3.15 - 3.21. The assignment of the dominant process appearing in the spectra of all studied electrolyte solutions (at ∼18 GHz) to the bulk water (with amplitude, S_b and relaxation time, τ_b) is unambiguous, as is known to be specific to the cooperative dynamics of the hydrogen-bonded network of water molecules.[64] For the aqueous solutions of ChCl, $\tau_\mathrm{b} \approx 8.2\,\mathrm{ps}$ (for pure water, $\tau_\mathrm{b} \approx 8.3\,\mathrm{ps}$[64]), remains virtually invariant of the solute concentration, c. However, unlike ChCl(aq) a decreasing trend of τ_b is observed for Cl-ChCl(aq) and this decrease is more pronounced in NH_4Cl(aq).

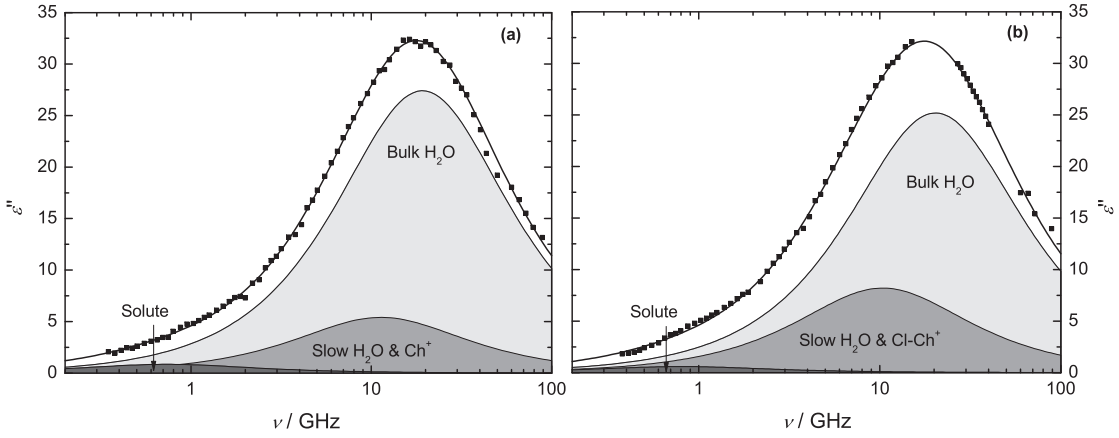

Figure 3.20: Dielectric loss spectrum, $\varepsilon''(\nu)$, of **(a)** 0.4696 M ChCl(aq) and **(b)** 0.4681 M Cl-ChCl(aq) at 25 °C. Symbols represent experimental data, the line represents the D+D+D fit, and shaded areas indicate the contributions of the three relaxation modes

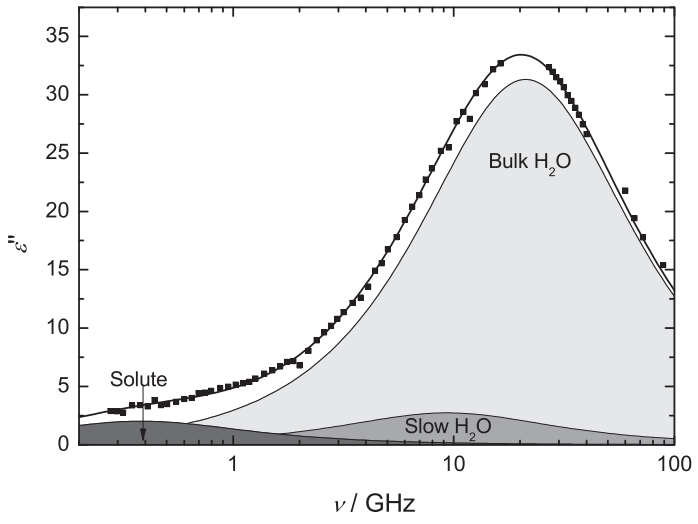

Figure 3.21: Dielectric loss spectrum, $\varepsilon''(\nu)$, of 0.3468 M NH_4Cl(aq) at 25 °C. Symbols represent experimental data, the line represents the D+D+D fit, and shaded areas indicate the contributions of the three relaxation modes

A common feature of the DR spectra of both ChCl(aq) and Cl-ChCl(aq) is the shifting of experimental loss peak towards low frequency (with increasing concentration) and its corresponding broadening with increasing c of the respective electrolyte (Figures 3.15 and 3.16) while opposite trend is observed for NH_4Cl(aq) solutions where the experimental loss peak shifts slightly towards higher frequencies with increasing concentration (Figure 3.17). Resolution of DR spectra yielded another mode at ∼12 GHz which is designated to be a "composite mode" (with amplitude S_c and relaxation time τ_c) with an average relaxation time $\tau_c \approx 14$ and 15 ps for ChCl(aq) and Cl-ChCl(aq) respectively, arising due to the incidentally overlapping relaxations of "slow" water molecules hydrating the cations (with amplitude S_s and relaxation time τ_s) and of the reorienting Ch^+ or Cl-Ch^+ ions (with amplitude S_+ and relaxation time τ_+), respectively. Such species of slow water molecules are known to exist in the solutions of hydrophobic solutes[12,161] or moderately hydrophillic anions.[74,162] The inclusion of cation relaxation process in the composite mode is based on the fact that both Ch^+ and Cl-Ch^+ ions have significant dipole moments ($\mu_{Ch^+} = 3.32$ D and $\mu_{Cl-Ch^+} = 7.81$ D, MOPAC[115] values calculated for the ions in gas phase) so their contribution should appear in the DR spectra but since no separate relaxation peaks are observed for any of these cations so it is reasonable to assume that the process occurring at ∼12 GHz is a composite mode. For aqueous solutions of NH_4Cl, however, this intermediate mode is assigned solely to the "slow" water molecules.

A very small amplitude, low frequency process detected at <1 GHz (in all studied salts) is fairly recognized to be a solute-related mode. However, due to low-amplitude, although for aqueous solutions of NH_4Cl the amplitude of this mode has quite significant magnitude, the presence of this low-frequency mode in the studied systems could be *suspected* as an artifact which *may* appeared due to experimental or analytical problems. This conviction, however, could be counter argued through some logical explanations, first culprit in this regard could be the *arbitrary* conductivity correction of the DRS spectra but as already mentioned, this correction is infact not arbitrary as during the fitting procedure always the experimental κ value is chosen to be a starting value for the correction and if required more correction is made but the difference between the experimental and the adjusted κ values is never let exceed 3% and if it did not work the chosen model is discarded for the studied system. Secondly there is no reason to consider any role of electrode polarization in the spectra of all studied salts as the amplitude of the low-frequency process decreases after $c \lesssim 0.5$ for each studied salt, which of course could not be the case for electrode polarization. Similarly as far as the choice of primary calibration standards is concerned, their suitability is always cross checked by a secondary calibration with well studied molecular liquids i.e., liquids having well-defined DRS parameters, such as propylene carbonate and *N,N*-dimethylacetamide. Moreover this process, if neglected, results in large variance of the spectral fits as well as lack of internal consistency of the obtained parameters. The origin of this low-amplitude process, hence could be assigned to two possible phenomena i.e., ion-pairs and/or ion-cloud relaxation in all studied electrolyte solutions (amplitude S_1 and relaxation time τ_1) which are discussed separately in following sections.

No fast water dynamics[98,163] is observed in the presented DR spectra of ChCl(aq), Cl-ChCl(aq) and NH_4Cl(aq), nevertheless, the obtained values of 'infinite-frequency' permittivity, ε_∞, are considerably larger than the literature values (Table 3.9 and 3.10) which

indicates that even being unresolvable the fast-water dynamics is still making a minor contribution in spectra of all studied salts. Also it should be noted that since the value of ε_∞ is experimentally reached in the far-IR region (∼1 - 30 THz) and its precise determination is difficult, so in the presented study this is treated as an adjustable parameter and for some calculations its value was assumed to be same as for pure water (as mentioned in literature[73]) at corresponding temperature (section 3.2.4). It is interesting to note that the number of modes and their corresponding relaxation times are in good agreement (Figure 3.19) with those predicted by the Zasetsky method[105].

3.2.3 Solute dispersion.

Ion-cloud relaxation.

As indicated in Figures 3.20 and 3.21, the spectra of all studied electrolyte exhibited a low-amplitude process centered at <1 GHz that is assigned to the ion-pairs and/or ion-cloud relaxation.
The relaxation time of ion-cloud relaxation was theoretically calculated according to Eq. 1.100 assuming $c\Lambda_\infty \sim \kappa$. It is evident from Figure 3.22 that the relaxation amplitude of the lowest frequency process increases for some initial concentrations (true for all three studied electrolytes), reaches to a maximum at c ∼0.5 M and then decreases again, same was observed for the aqueous solutions of some other 1:1 electrolytes[73–75]. Here, it should be noted that for NH_4Cl(aq) this low frequency process disappears after c >1.1 M. This behavior definitely demands for the rigorous judgement of the underlying mechanisms of this mode and one logical and simple approach would be to consider this mode as a combined mode originating possibly from two sources, i.e., ion-cloud and ion-pair relaxations in the systems. Further clarity to assign this mode comes from the apparent behavior of this low-frequency mode in terms of its relaxation time, as can be seen from Figure 3.23 where a comparison is made between the calculated (using Eq. 1.100) and experimentally observed values of τ_1. For all of the studied salts at c <0.4 M the τ_1 decreases sharply, whereas after c >0.4 M the τ_1 could be considered as a constant value in the studied concentration ranges of the respective salt. Thus it is reasonable to assume that in the region of lower concentrations ($c \lesssim 0.4$ M) both ion-cloud and ion-pair relaxations are contributing to this low-frequency process while for higher concentrations (where τ_1 reaches a constant value) only ion-pair relaxation is dominant.

Ion-pair relaxation.

Presence of ion pairs in aqueous solutions of ChCl is supported by the MD simulations[164] while apparent molar volume studies of ChCl(aq) and Cl-ChCl(aq) also suggest ion pairing[114] whereas the literature results for the association and ion-pair formation in aqueous solutions of NH_4Cl vary, as we find an indication of ion-pairs formation in aqueous solutions of NH_4Cl[165,166] along with no obvious proof of ion pairing at ambient temperature.[125]
DRS in principle is able to detect all the species with a non-zero dipole moment, $\mu_i > 0$ provided the life time of the relaxing species to be at least comparable to the rotational correlation time.

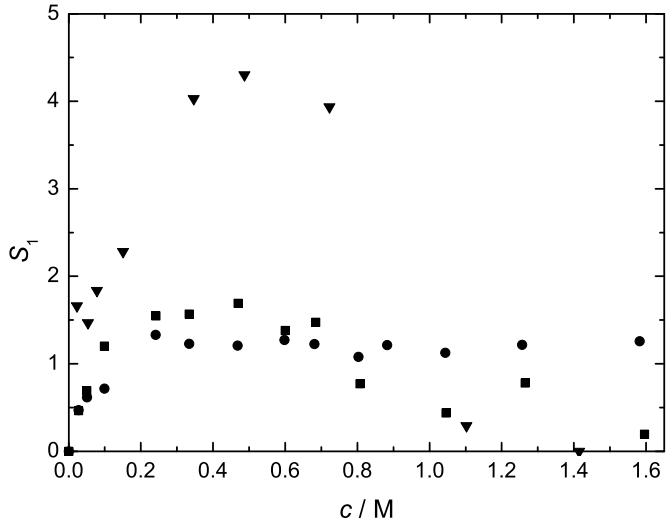

Figure 3.22: Concentration dependence of ion-pair and/or ion cloud-relaxation amplitude, S_1, at 25 °C for ChCl(aq) (■), Cl-ChCl(aq) (●), and NH_4Cl(aq) (▼).

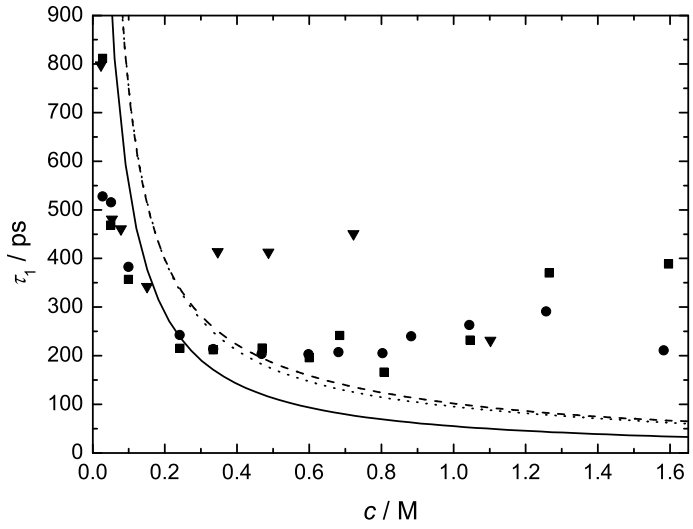

Figure 3.23: Concentration dependence of ion-pair and/or ion cloud-relaxation time, τ_1, of ChCl(aq) (■), Cl-ChCl(aq) (●), and NH_4Cl(aq) (▼), at 25 °C, whereas the calculated ion-cloud relaxation time (using Eq. 1.100) is presented as solid line for NH_4Cl(aq), dotted line for ChCl(aq) and dashed line for Cl-ChCl.

An initial decrease in the τ_1 followed by a rise at higher concentrations is observed for all electrolytes, Figure 3.23. For ChCl(aq) and Cl-ChCl(aq), S_1 remains small in the studied c range, however for NH_4Cl(aq) the amplitude of this lowest frequency process is pretty large (Figure 3.22). MD simulations of ChCl(aq) suggest the presence of solvated ion pairs and also the plausible location of chloride ion to be more nearer to the hydroxyl group of cation than to the partially positive nitrogen due to the steric shielding of nitrogen.[164] By assuming that the lowest frequency process in spectra of all studied electrolyte solutions is solely due to ion-pair relaxation (i.e., no contribution from ion-cloud relaxation is considered), a quantitative description of ion-pairing has been done by relating the amplitude of the lowest frequency mode (S_1) to the concentration of various possible ion-pair types, c_{IP}, using the Cavell equation (Eq. 1.72). Required polarizabilities and dipole moment of different types of ion pairs were calculated from MOPAC.[115] Calculations were done considering different types of ion-pair structures including CIP (contact ion-pairs), SIP (solvent-shared ion-pairs) and 2SIP (double solvent-separated ion-pairs).
The ion-pair association constant were determined for all studied electrolytes and for different possible types of ion-pairs using Eq. 1.99.

Table 3.11: Ion-Pair Dipole Moments, μ_{IP}; and Resulting Parameters log K^0_A, B_K, and C_K of Eq. 1.99; Experimental τ_{rot} of Eq. 1.80; τ'_{slip} and τ'_{stick} of Eq. 1.85 for Different Ion-Pair Models of ChCl(aq), Cl-ChCl(aq) and NH_4Cl(aq)[a]

Model	μ_{IP}	logK^0_A	B_K	C_K	τ_{rot}	τ'_{slip}	τ'_{stick}
			ChCl				
CIP	10.14	2.87±0.10	-6.61±0.76	3.14±0.72		32	134
SIP	24.36	1.23±0.17	-4.85±1.28	2.19±1.21	220	74	192
2SIP	36.43	0.76±0.17	-4.42±1.26	1.92±1.19		141	274
			Cl-ChCl				
CIP	9.60	2.12±0.10	-5.65±0.76	3.11±0.72		39	147
SIP	24.04	1.27±0.17	-6.06±1.28	3.53±1.21	195	90	216
2SIP	36.17	0.83±0.17	-5.66±1.26	3.27±1.19		167	309
			NH_4Cl				
SIP	21.28	1.67±0.33	-2.67±2.22	-0.31±1.98	306	26	67
2SIP	33.24	0.82±0.11	-5.66±0.58	3.27±0.46		65	114

[a] Units: μ_{IP} in Debye (1 D = 3.3356 × 10^{-30} C·m.); B_K in L·mol^{-1}; C_K in L$^{3/2}$·mol$^{-3/2}$; τ in 10^{-12} s.

The various parameters obtained through Eq. 1.99 are given in the in Table 3.11 and from this data unreasonably high values of the association constants are obtained for the CIP for all salts, however K_A values obtained for SIP (17.0 and 18.6 M^{-1} for ChCl(aq) and Cl-ChCl(aq) respectively) and 2SIP (5.75, 6.76 and 18.3 M^{-1} for ChCl(aq), Cl-ChCl(aq) and NH_4Cl(aq) respectively) are in reasonable range, see Figure 3.24. However for ChCl(aq)

and Cl-ChCl(aq)the possibility of formation of SIP can be taken as to be more likely than 2SIP as it is already known that the Cl^- ion hydrates weakly due to similar strength of water-water and Cl^--water interactions[167].

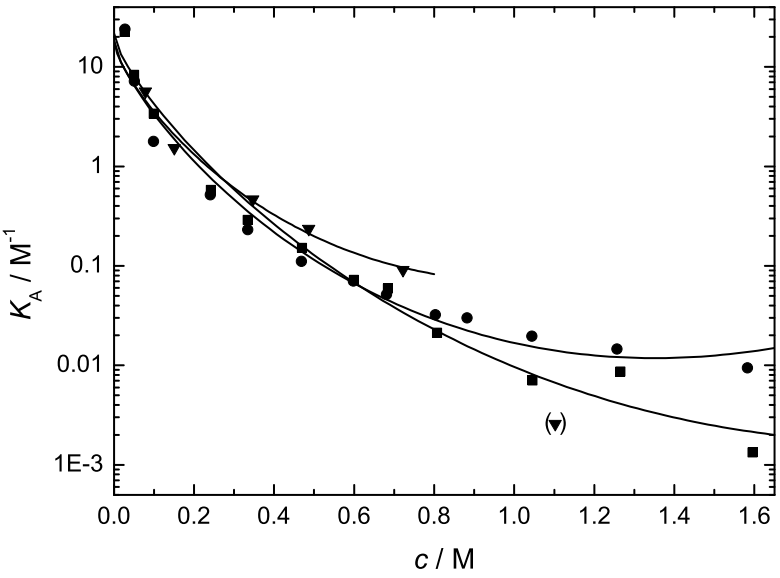

Figure 3.24: Ion association constant, K_A, as a function of the concentration, c, of ChCl(aq) (■), Cl-ChCl(aq) (●), and NH_4Cl(aq) (▼), at 25 °C (SIP Model for ChCl(aq) and Cl-ChCl(aq); 2SIP for for NH_4Cl(aq)). Lines represent fits according to Eq. 1.99.

Another approach was tested which could possibly help to establish the types of ion pairs existing in the studied electrolyte solutions, this is based on finding the microscopic rotational correlation time, τ_{rot} from the experimentally obtained macroscopic τ_1, DRS values ($=\tau$ in Eq. 1.80) through the Powles-Glarum equation, see Eq. 1.80. The obtained τ_{rot} can be compared with the theoretical microscopic correlation time, τ' that can be calculated from the Stokes-Einstein-Debye equation[47](Eq. 1.85).
In Eq. 1.85, η of pure water (= 0.8903mPa·s[168]) was used so that the calculated relaxation times correspond to the limit of infinite dilution. Calculations were done by approximating the ion-pairs to be prolate ellipsoids and the approach of Dote and Kivelson[47] was followed (using both *stick*, $C = 1$ and *slip*, $C = 1\text{-}f^{-\frac{2}{3}}$ boundary conditions) whereas the geometric parameters needed to estimate f were calculated from MOPAC.[115] Usually the *slip* boundary conditions are taken as to be more likely than the *stick* boundary conditions,[10,49,169] however for both ChCl(aq)and Cl-ChCl(aq) solutions it seems that SIP rotating under *stick* boundary condition are the more plausible species (Table 3.11), moreover presence of CIP can be over ruled (for both ChCl(aq)and Cl-ChCl(aq)) as both τ'_{slip} and τ'_{stick} values are much lower than the corresponding τ_{rot}. Unfortunately, from the data of NH_4Cl(aq) no such conclusion can be made, rather it is more logical to assume here that in aqueous solutions of NH_4Cl the slowest process corresponds mainly to the ion-cloud relaxation and

ion-pair relaxation has possibly negligible contribution.

3.2.4 Solvent dispersion.

Bulk-water process.

DR spectrum of pure water demonstrates two types of dispersion peaks. First peak centers around 20 GHz while other in the sub-picosecond region.[98,163] The first relaxation corresponds to the hydrogen-bonded network of bulk water having a characteristic relaxation time,τ_b, which is essentially the dwelling time of a water molecule in a particular configuration until all except one of its H-bond are broken.
The other high frequency process represents a new configuration where the broken H-bond is replaced by a new one in an alternative configuration and its relaxation time, τ_{f} is the time that a water molecule needs (after the breakage of atleast one H-bond) to get into a new configuration. For the present systems however, no fast water dynamics is observed.

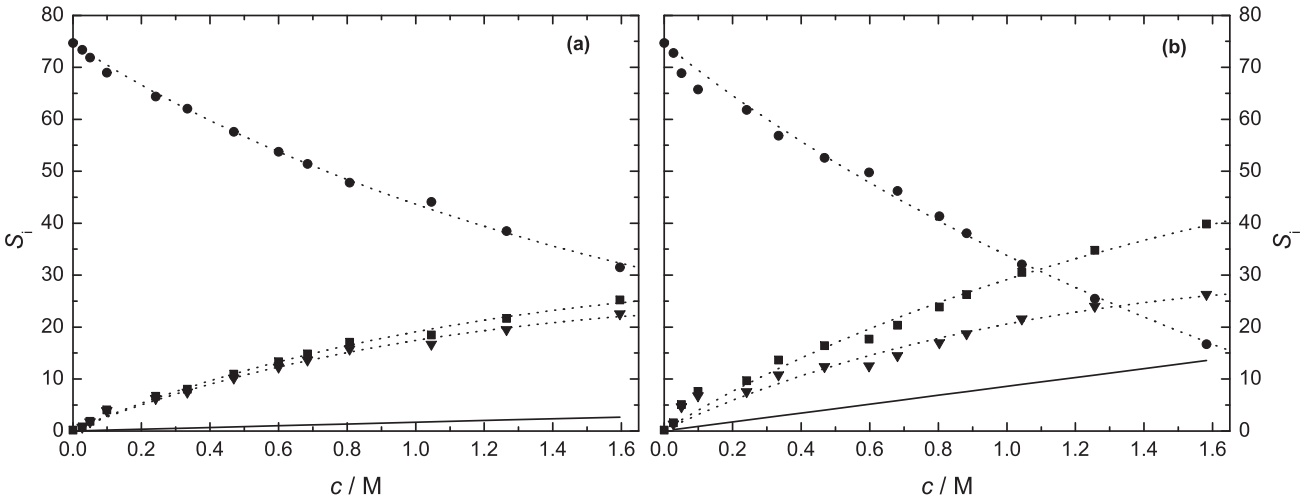

Figure 3.25: Concentration dependence for (a) ChCl(aq) and (b) Cl-ChCl(aq) at 25 °C of the relaxation amplitudes of bulk water, S_{b} (●), the composite mode, $S_{\mathrm{s}} + S_{+}$ (■), and slow water, S_{s} (▼). The solid lines represent S_{+}, calculated via Eq. 1.72; the dotted lines are included for visual aid only.

Figures 3.15-3.17, 3.25 & 3.26 reveal that upon concentration rise both the bulk-water relaxation amplitude, S_{b}(c), and the static permittivity, ε, decrease for the presently studied three sets of salt solutions. This effect can be split into the contribution from: the dilution effect due to the decrease of $c_{\mathrm{w}}(c)$; "freezing" of solvent molecules in the hydration shells of ions; kinetic depolarization (kd) and possible slowing of water[87]. Thus, the S_{b}(c) has to be corrected for the kd effect as

$$S_{\mathrm{b}}^{\mathrm{eq}}(c) = S_{\mathrm{b}}(c) + \Delta_{\mathrm{kd}}\varepsilon(c) \tag{3.8}$$

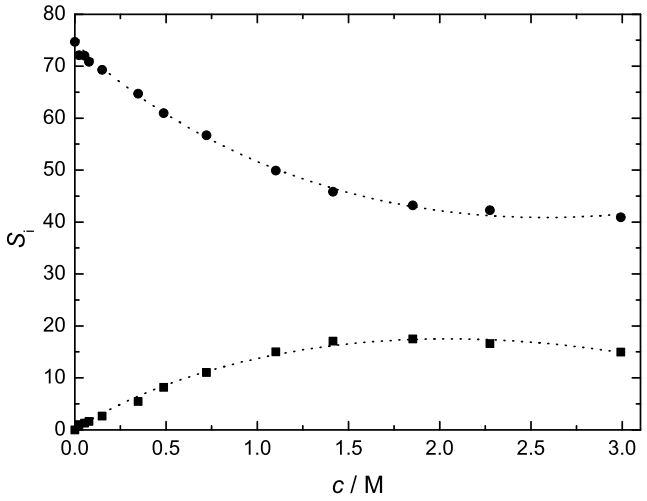

Figure 3.26: Concentration dependence of the relaxation amplitudes of bulk water, S_b (●), and slow water, S_s (■), at 25 °C for NH_4Cl(aq). Dotted lines are included for visual aid only.

For a solvent with Debye-type relaxation behavior, kd can be expressed as

$$\Delta_{kd}\varepsilon(c) = \xi\kappa(c) \tag{3.9}$$

and

$$\xi = p \times \frac{\varepsilon(0) - \varepsilon_\infty(0)}{\varepsilon(0)} \times \frac{\tau(0)}{\varepsilon_0} \tag{3.10}$$

in Eq. 3.10, $\varepsilon(0)$ is the static permittivity and $\tau(0)$ is the relaxation time of pure water.[170–172] The parameter p characterizes the hydrodynamic boundary conditions with $p = 1$ for *stick* and $p = 2/3$ for *slip* type of ionic motion.
Here it should be noted that the relaxation time of bulk water mode, τ_b remains fairly constant (Figure 3.27) for ChCl(aq) and decreases (Figures 3.27 & 3.28) for Cl-ChCl(aq) and NH_4Cl(aq) which stems that bulk water dynamics is not affected by the solute in case of ChCl(aq) while presence of Cl-ChCl and NH_4Cl in water do have an effect on the bulk water dynamics hence Cl-Ch^+ and NH_4^+ ions affect the water molecules even beyond their hydration shells, as claimed in literature[10,173] for certain electrolytes in water.

Composite process.

As described before in section 3.2.2, the intermediate dispersion mode in case of ChCl(aq) and Cl-ChCl(aq) is assumed to be a "composite mode" which has contribution from slow water as well as respective cations in the salt. For NH_4Cl(aq), however, this mode is assigned solely to the "slow" water molecules. Quantitative description of this composite mode has been done with an equation analogous to the Eq. 1.72.

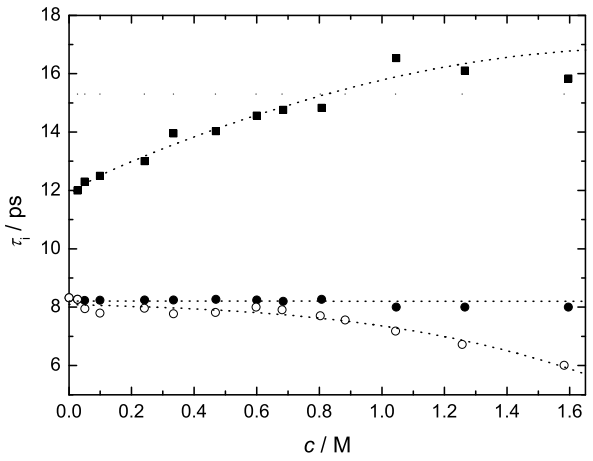

Figure 3.27: Concentration dependence of the relaxation time of composite mode, τ_c, of ChCl(aq) (■), bulk-water mode, τ_b, of ChCl(aq) (●), and bulk-water mode, τ_b, of Cl-ChCl(aq)(○), at 25 °C. Dotted lines are visual aid only.

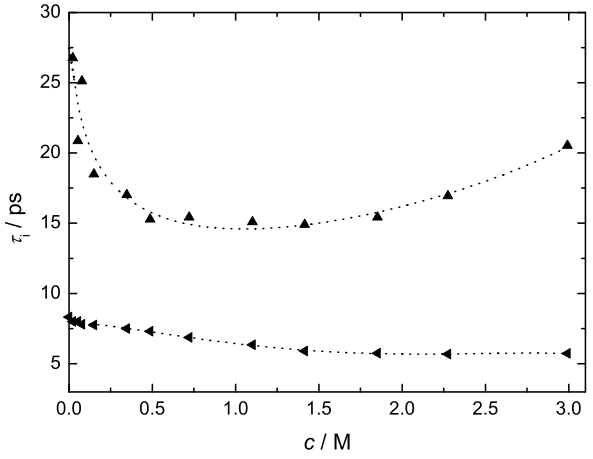

Figure 3.28: Concentration dependence of the relaxation time of slow-water mode, τ_s, (▲), and bulk-water mode, τ_b, (◀), of NH_4Cl(aq) at 25 °C. Dotted lines are visual aid only.

The amplitude of this mode can be split into its constituents as

$$S_c = S_+ + S_s \tag{3.11}$$

where S_+ is the relaxation amplitude due to the rotation of the dipolar Ch^+ or $Cl - Ch^+$ ions and S_s is the relaxation amplitude of the "slow" water molecules hydrating the cation. Similar splitting of the τ_c is however not permissible as the relaxation rates, τ_+^{-1} and τ_s^{-1} can not be assumed to be concentration independent, also the τ_c^{-1} can not be considered

as the amplitude-weighted average of the two contributing processes in the composite mode.[73] Unfortunately, this hinders the calculation of the activation parameters for slow-water relaxation process, which would be of considerable interest. For Cl-ChCl(aq) system, the τ_c is fixed to a value 15.3 in the fitting routine in order to get internally consistent parameters of the fits. This number is the average value of various τ_c obtained for different concentrations and without fixing any parameter. To calculate S_+ for both systems Eq. 1.72 can be used, hence the S_c can also be evaluated from Eq. 3.11. It is evident from Fig. 3.25 that the S_+ for $\mathrm{Cl-Ch^+}$ is greater than S_+ for $\mathrm{Ch^+}$ at all the studied concentrations and this corresponds to the greater dipole moment of $\mathrm{Cl-Ch^+}$ ion compared to the $\mathrm{Ch^+}$ ion.

3.2.5 Ion hydration.

If the strength of ion-solvent interactions is much greater (strong ion-dipole forces) than the solvent-solvent interactions and the kinetics of exchange between the water molecules in the hydration shell(s) of ion and the bulk water is too slow, then these water molecules (bounded to ions) become effectively immobalized on DRS time scale and are said to be 'frozen' or 'irrotationally bound', hence cannot be detected by DRS anymore. This effect can be seen for the ions with high surface-charge density in all solvent classes and is major cause of decrease in the solvent dispersion amplitude with increasing concentration of electrolyte.[11] In order to calculate the number of frozen water molecules per unit of salt an effective solvation number, Z_{ib}, can be defined as

$$Z_{\mathrm{ib}} = (c_{\mathrm{w}}^{\mathrm{o}} - c_{\mathrm{b}}^{\mathrm{ap}} - c_{\mathrm{s}}^{\mathrm{ap}})/c \tag{3.12}$$

In a moderate situation, however the water dynamics is not frozen but only slowed down compared to the bulk-water dynamics. For large hydrophobic solutes such slow-water molecules in the primary hydration shell are detectable as a separate relaxation process with $\tau_{\mathrm{s}} \approx 3\,\tau_{\mathrm{b}}$.[12,161,162] The number of water molecules which have been slowed down per salt molecule, Z_{s}, can be evaluated as

$$Z_{\mathrm{s}} = c_{\mathrm{s}}^{\mathrm{ap}}/c \tag{3.13}$$

Two different types of hydration numbers obtained in this way are shown in Figures 3.29 & 3.30. No irrotational bounding of water molecules is observed in aqueous solutions of NH_4Cl while for both ChCl(aq) and Cl-ChCl(aq) the observed number of frozen-water molecules per respective salt molecule at infinite dilution is found to be similar i.e., ∼5, this value for each system corresponds to the total salt hence, in order to find individual ionic contributions the value was split by assuming $Z_{\mathrm{ib}}(\mathrm{Cl^-}, \mathrm{aq}) = 0$. This assumption is made due to the observation that $Z_{\mathrm{ib}}(\mathrm{R_4NCl}, \mathrm{aq}) \approx 0$ when R = methyl (Me) or ethyl (Et) group.[12]
It is worthwhile here to compare our results with the literature data pertaining to some tetra-*n*-alkylammonium ions[12], where it was observed that Me_4NBr, Et_4NCl, Et_4NBr, Pr_4NBr, Bu_4NBr and Pe_4NBr do not freeze water molecules in their hydration shells whereas only Pr_4NBr, Bu_4NBr and Pe_4NBr show 'hydrophobic hydration' (with $Z_{\mathrm{s}} \sim 18.8$, 36.3 and 44.1, respectivly). MD simmulations of ChCl suggest the formation of weak hydrogen bonds between cation's –OH and the water.[164] Based on these observations it would

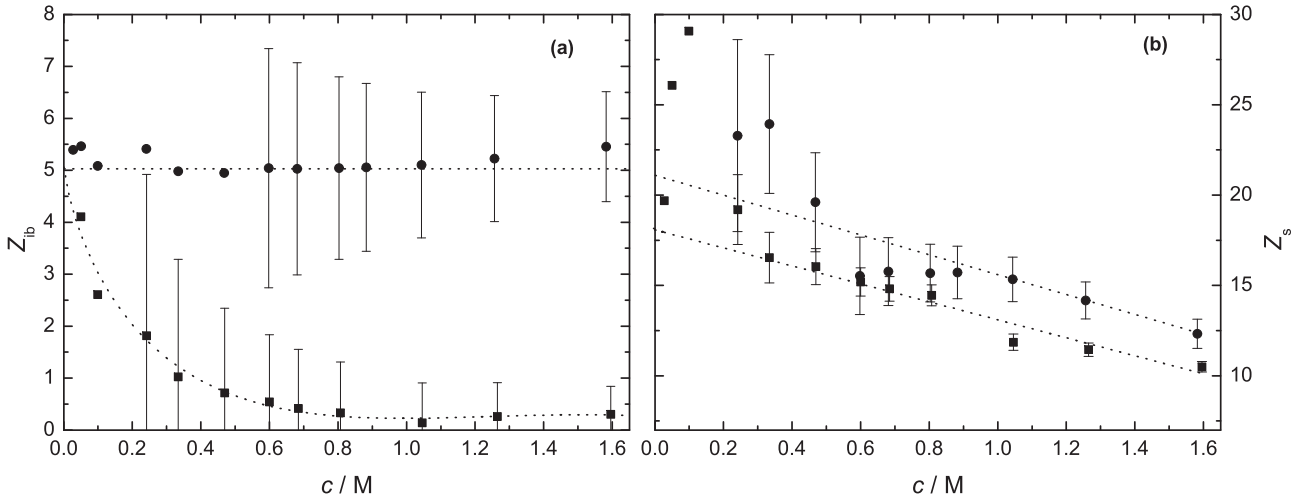

Figure 3.29: Concentration dependence of (**a**) effective hydration numbers, Z_{ib}, and (**b**) slow-water hydration numbers, Z_{s}, at 25 °C for ChCl(aq) (■), and Cl-ChCl(aq) (●) . Dotted lines are included as a visual guide only (few of the error bars[174] are omitted for visual clarity).

be reasonable to assume that the frozen water molecules are located nearer to the OH or Cl moiety then to the bulky positively charged nitrogen head group. The Z_{ib} of ChCl shows a negative concentration dependence and no variation is observed for Cl-ChCl, this may suggest interacting hydration spheres of choline ion, this in principle should also explain the the difference in the Waldon product obtained for ChCl and Cl-ChCl at 298.15 K.[114] Fleming found hydration number of 2.1 for ChCl[175] which is in agreement with our Z_{ib} value of ChCl. At infinite dilution Z_{s} ∼18, ∼22 and ∼13 is obtained for ChCl and Cl-ChCl (their value is very similar to the one obtained for Pr_4NBr i.e., ∼ 18.8[12]) and NH_4Cl respectively, (calculated via Eq. 3.13). These values for ChCl and Cl-ChCl are in excellent agreement with the MD simmulations of Shao et al[176] on two ultralow fouling zwitterionic materials, namely poly carboxybetaine methacrylate (polyCBMA) and poly sulfobetaine methacrylate (polySBMA), their results indicated similar hydration behaviour of the positive head group ($N^+(CH_3)_3$) of both polyCBMA and polySBMA with coordination number of ∼18, having similar coordination shell size and very similar water-solute distance distribution, however the water molecules around the $N^+(CH_3)_3$ group were found to be less ordered than the negatively charged groups on polyCBMA and polySBMA. Again by referring to the literature data of Me_4NBr and Et_4NCl[12], it seems that the assignment of the slow-water mode to only $N^+(CH_3)_3CH_2CH_2-$ group of either ChCl or Cl-ChCl is not straight forward, thus interpretation of Z_{s} as 'hydrophobic hydration' could also be not justified. In this regard however, it would be useful to obtain DRS data of asymmetric TAA ions (like $N^+(CH_3)_3CH_2CH_2-$). Our result for $Z_{\mathrm{s}} \sim 13$ for NH_4Cl is in excellent agreement with literature data for the aqueous solutions of NH_4Cl suggesting hydration numbers of 8[177] and 13[178]. Dang found a tetrahedral coordination of ammonium ion by

the water molecules in the first hydration shell.[179]

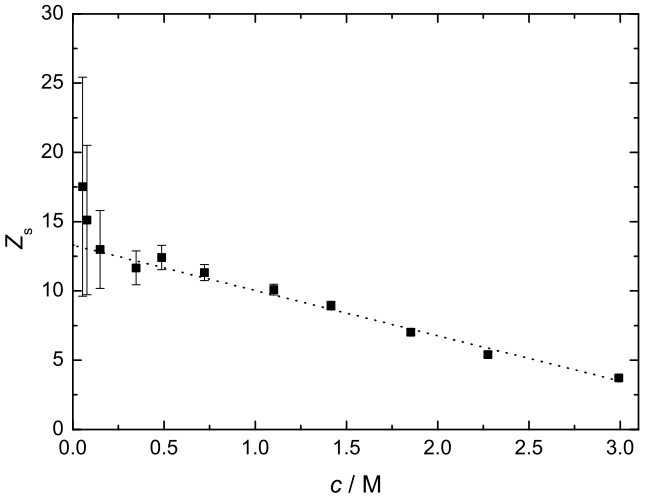

Figure 3.30: Concentration dependence of slow-water hydration number, Z_s, for NH_4Cl(aq) at 25 °C. Dotted lines are included as a visual guide only.

Decrease in the Z_s with increasing concentration is observed for all studied electrolytes. It should be noted that the emergence of slow-water dispersion (in the composite mode) is not assumed to be due to the strengthening of H-bonds in the vicinity of solute but to the increase in number and life time of H-bonds adjacent to the solute.[11] NMR studies of Kenneth and his coworkers showed that addition of water to the lowest liquid hydrates (saturated solutions) of ChCl resulted in larger and looser hydration shell with the composition $ChCl{\cdot}10H_2O$ (secondary clathrates),[180] all these observations point that the hydration shell of ChCl and Cl-ChCl is labile, also the MD simulation of hydrated NH_4^+ ion[181] suggest a rather flexible solvation structure around the ion hence a highly labile NH_4^+ hydrate.

3.2.6 Temperature dependence of bulk water dynamics.

For the detailed analysis of dynamics of ChCl solutions, spectra of 0.28 molal ChCl were measured at at 5, 15, 25, 35, 45, 55, and 65 °C. All the spectra fitted well in D+D+D model. The rise in temperature is accompanied with the decrease in amplitudes of all DR modes, where the composite mode can be just detected at 65 °C. Vanishing slow water contribution in the composite mode with temperature rise can be justified as dynamics get faster, this further implies that the contribution of cation relaxation to the composite mode is very weak and is always dominated by the slow water process. This can be seen in Figure 3.25a (at 25 °C) where S_+ has weak contribution to S_c. Relevant spectra are shown in Figure 3.18 whereas Figure 3.31 refer to the changes in the various relaxation times with the changes in the temperature. No significant changes in the τ_1 were observed but the τ_c and τ_b decrease significantly as expected due to faster dynamics of solvent molecules at

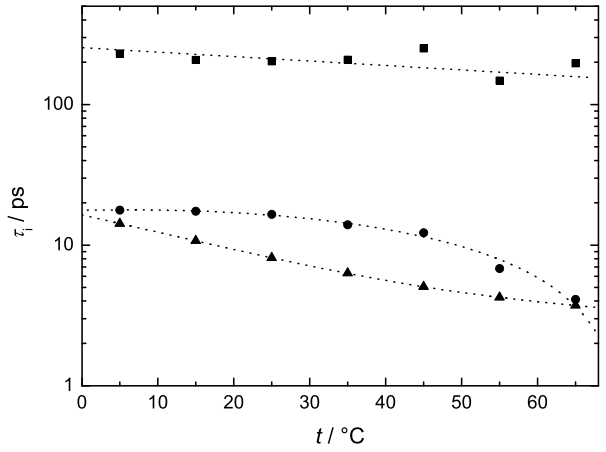

Figure 3.31: Temperature dependence of ion-pair and/or ion cloud-relaxation time, τ_1, (■), composite-mode relaxation time, τ_c, (●), and bulk-water relaxation time, τ_b, (▲), of $0.280\,\mathrm{mol}\cdot\mathrm{kg}^{-1}$ ChCl. Dotted lines are visual guide only.

Table 3.12: Enthalpy of activation, $\Delta H^{\neq}$, Entropy of activation, $\Delta S^{\neq}$, and average number of H-bonds per water molecule, $\bar{n}_{HB}$, of 0.28 $\mathrm{mol}\cdot\mathrm{kg}^{-1}$ ChCl[a]

Property	Bulk water	Pure water
$\Delta H^{\neq}$	15.2±0.6	15.9±0.2
$\Delta S^{\neq}$	18.5±1.9	20.4±0.7
$\bar{n}_{HB}$	2.40±0.08	2.46±0.12

[a] Units: $\Delta H^{\neq}$ in $\mathrm{kJ.mol}^{-1}$; $\Delta S^{\neq}$ in $\mathrm{J.K}^{-1}.\mathrm{mol}^{-1}$.

higher temperatures. The temperature dependence of τ_b can be analyzed in terms of the Arrhenius plot and Eyring, see section 1.5. Table 3.12 summarizes the values of obtained activation parameters. The obtained activation enthalpy, $\Delta H^{\neq}$(T) can be linked to the average number of H-bonds per water molecule as

$$\bar{n}_{HB} = \frac{\Delta H^{\neq}}{\Delta_{HB} H} + 1 \tag{3.14}$$

In Eq. 3.14, $\Delta_{HB}H = (10.9 \pm 0.4)\,\mathrm{kJ\,mol}^{-1}$ gives the strength of water-water H-bond in the pure solvent (for water $\bar{n}_{HB} = 2.402$)[182]. As already mentioned, further analysis of τ_c is not done due to inseparable τ_s and τ_+. The obtained parameters $\Delta H^{\neq}$, $\Delta S^{\neq}$ and $\bar{n}_{HB}$ are summarized in Table 3.12 together with the literature data for water at 25 °C.[98] It is evident from the Table 3.12 that the activation enthalpy and the activation entropy (less accurate) and $\bar{n}_{HB}$ obtained for ChCl(aq) coincide (within error limits) with the value of

pure water, this is also supported by the constant τ_b of ChCl(aq) (section 3.2.2), thus, for ChCl(aq) ions do not affect the dynamics of bulk-water molecules.

Chapter 4

Investigation of micellar systems

Owing to their amphiphilic nature and special properties like adsorption and self-aggregation, surfactants are widely used in detergents, foaming agents, dispersants, emulsifiers, textile, food industry and formulations. Among natural surfactants, the alkali soaps (sodium and potassium carboxylates) are the oldest and are known since centuries and were prepared from tallow and alkali hydroxides.[6] Among different classes of surfactants, anionics, with carboxylates, -CO_2^-, sulfates, -OSO_3^-, and sulfonates, -SO_3^-, as headgroups are used more frequently as they are easy to prepare and are more economical, on the other hand cationics, with tetramethylammonium ions, -$N^+(CH_3)_3$, as headgroups are employed as surface modifiers, anticorrosion agents, flotation collectors, bactericides and fabric softeners.[183]

The solubility of a surfactant is a critical parameter as far as its practical application is concerned and generally the clearing temperature of 1 wt% surfactant solution, known as Krafft point,[184] is used as a criterion for surfactant's solubility. It is known that Krafft points of sodium carboxylates are higher, as it ranges from 25 °C for sodium laurate, NaC12, to 45 °C for sodium myristate, NaC14, 60 °C for sodium palmitate, NaC16,[13,185,186] and 71 °C for sodium stearate, NaC18.[186] Since surfactants with longer alkyl chain have better detergency[187] and other properties compared to those with short chains, compromising not on these properties but still attaining lower Krafft points was a matter of challenge. At one hand this problem can be solved by modifying the structure of headgroup or alkyl chain but this generally has negative effects on biodegradability of surfactant.[8] It was observed that the choice of counterion is critical in achieving this goal[188] and tetraalkylammonium ions, TAA, were found to be a better choice than sodium with carboxylates.[189,190] It is claimed that surfactants having choline as counter-ions are able to substitute those with tetraalkylammonium counter-ions as TAA ions are toxic, whereas choline is non-toxic and biologically degradable.[14] It should be noted that choline is also part of a natural surfactant, dipalmitoylphosphatidylcholine which is crucial for the normal lung functioning. In addition to choline carboxylates, another biocompatible surfactant, choline dodecylsulfate, was prepared and patented by the University of Regensburg.[7]

Figure 4.1 taken from the literature data of Vlachy et al.[191] represents the suitability of coupling among various types of headgroups and cations. In principle, choline ion (Ch^+) could be the next member of this cationic series, i.e. $Li^+..\rightarrow..NH_4^+ \rightarrow Ch^+$, hence softest among the displayed cations. As expected the binding between carboxylate headgroup

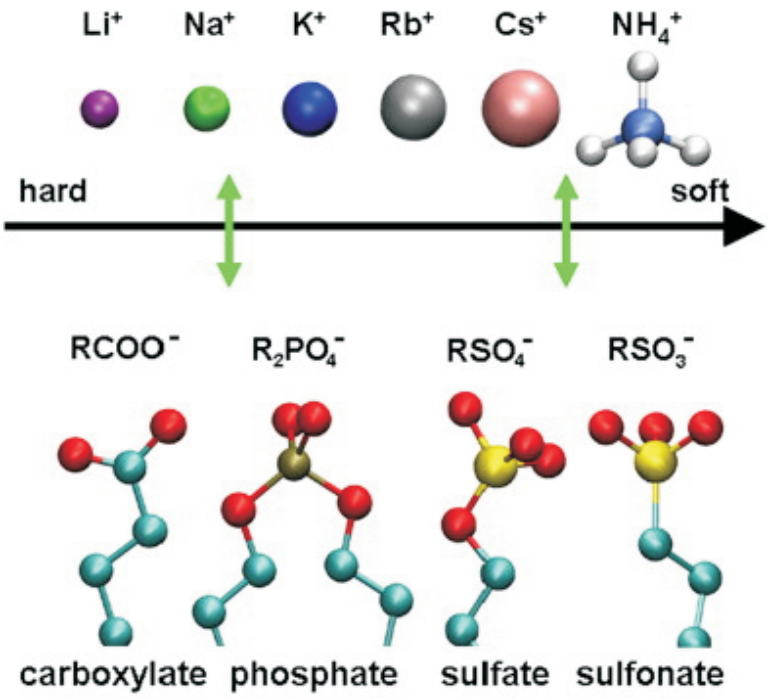

Figure 4.1: Scheme of preferred surfactant-counterion interactions (taken from Reference 191) between hard-hard and soft-soft ions whereas combination of hard-soft ions will yield surfactant of high counterion dissociation.

Table 4.1: Physicochemical properties of NaC12, ChC12 & ChDS: critical micelle concentration, *cmc*; Krafft temperature, T_K; Degree of counterion attachement, β; and Radius of the micelle, R_{mic}, for comparison data of SDS is also included.

	cmc/ mM	T_K/ °C	β	R_{mic}/ nm
NaC12	26 [192]	25 [13,185]	0.73 [193]	≤2.37 [193]
ChC12	25.5 [14]	<0 [14]	0.67 [14]	2.10 [194]
ChDS	5.99 [8]	0 [8]	0.75 [8]	2.0 [8]
SDS	8.3 [195]	14.1 [8]	0.73 [196]	2.64 (at cmc) [15]

and choline ion is weak (hard-soft binding). This is beneficial in one regard as this makes choline carboxylate surfactants, ChC*m* more water soluble. However, this also lends them sensitive to the addition of common alkali impurities. Furthermore, solutions of ChC*m* surfactants are alkaline with pH ranging between 10-11,[8] which is of course undesirable. The newly synthesized choline dodecylsulfate (ChDS) surfactant should in principle be able to overcome both theses problems associated with ChC*m* surfactants, their low salt

sensitivity is however, yet to be proven.
The present study focusses on the DR measurements of aqueous solutions of ChC12 and ChDS surfactants. Since dielectric data of sodium dodecylsulfate (SDS) is already available in literature[15] hence sodium dodecanoate (sodium laurate) is measured as well so that comparison can be made between surfactants with same headgroups, either carboxylate or sulfate but different counterions, sodium or choline. Table 4.1 includes values of various micelle-related parameters pertaining to studied systems, theses values are then used for further analysis.

4.1 Aqueous solutions of sodium laurate

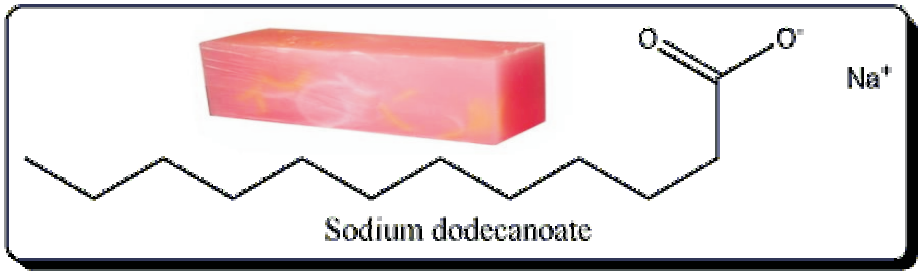

This part of the dissertation presents a detailed DRS study of aqueous solutions of sodium laurate (NaC12, $C_{11}H_{23}C00Na$) at 25 °C up to ~0.1077 M concentration, over the frequency range $0.01 \lesssim \nu/\text{GHz} \leq 89$. Low-frequency measurements, i.e., $0.01 \lesssim \nu/\text{GHz} \leq 0.3$ were performed using four different cutoff cells with different cell constants, attached to the Agilent E8364B VNA (section 2.2.3) and the data obtained from TS3-type cut off cell was finally selected as it generated the required data in the optimal frequency range and offered least "electrode polarization" (Figure 2.6). The data in the frequency range $0.2 \leq \nu/\text{GHz} \leq 20$ was recorded with Agilent E8364B VNA using high temperature probe, while A & E-band interferometers (sections 2.2.2 and 2.2.3) were used to record the DR data in the frequency range of $27 \leq \nu/\text{GHz} \leq 89$.
The DR spectra of the presented system appear to be bimodal, Figure 4.2b. The low frequency region in the range $0.01 \lesssim \nu/\text{GHz} \leq 1$ was primarily occupied by solute as the mode(s) in this frequency domain becomes more pronounced with increasing concentration of sodium laurate. The higher frequency region was however, recognized as solvent related. The position of loss peaks in both of the above mentioned regions remained invariant of c (Figure 4.2b). The obtained spectra were analyzed using different mathematical models and the obtained solute-related modes were further analyzed using Grosse model (section 1.6.3) and the resulting parameters were rationalized. Similarly the solvent-related relaxations were put to further quantitative analysis to find different types of effective hydration numbers in variation with the concentration of sodium laurate. For comparison

purpose, obtained hydration numbers for all studied surfactants are discussed at the end of ongoing chapter.

4.1.1 Resolution of DR spectra

The complex dielectric spectra including both dispersion and loss curves ($\varepsilon'(\nu)$ & $\varepsilon''(\nu)$), as shown in Figures 4.2a & 4.2b were simultaneously fitted to various possible relaxation models using band shape defined by the Debye (D), the Cole-Cole (CC), the Davidson-Cole (DC) and the Havriliak-Negami (HN) functions. The selection of the most appropriate model was based on the criteria of minimum variance, χ^2_{r},[103] and internally consistent set of resulting parameters. The best fits were obtained with a four-Debye model i.e. each spectrum was characterized with the superposition of four Debye-type relaxations, a D+D+D+D model, Figure 4.3. All fitting parameters along with the experimentally obtained data of densities and conductivities are presented in Tables 4.2.

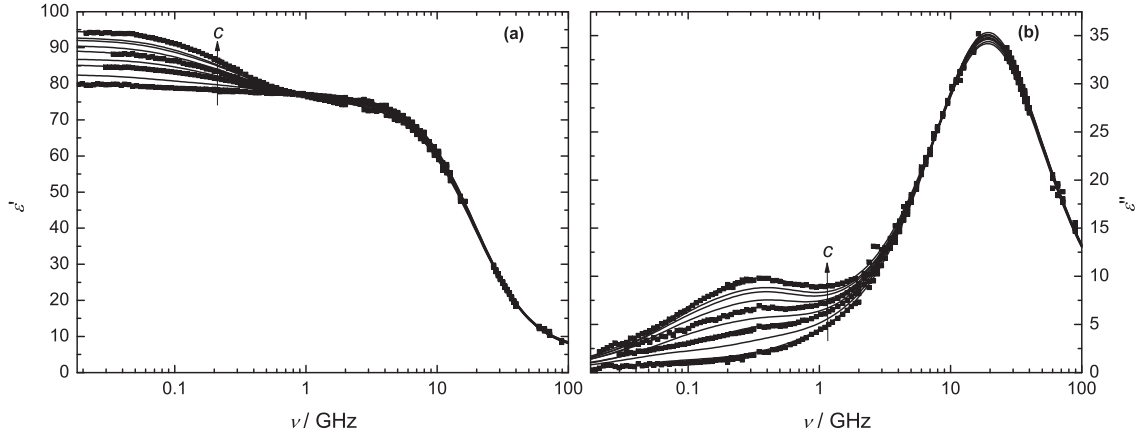

Figure 4.2: Permittivity, $\varepsilon'(\nu)$ (**a**), and dielectric loss, $\varepsilon''(\nu)$ (**b**), spectra for NaC12(aq) at 25 °C and concentrations c/M = 0.0297, 0.0396, 0.0493, 0.0591, 0.0688, 0.0784, 0.0881, 0.0977, and 0.1077 (bottom to top). Symbols show experimental data (for some samples, symbols are omitted for visual clarity) and lines represent the D+D+D+D fit.

Table 4.2: Densities, ρ; Electrical Conductivities, κ; Limiting Permittivities, ε_j; Relaxation Times, τ_j; and Reduced Error Function Values, χ^2_r, for NaC12(aq) at Concentrations, c; and 25 °C[a,b]

c	ρ	κ	ε	τ_1	ε_2	τ_2	ε_3	τ_3	ε_4	τ_4	ε_∞	χ^2_r
0[c]			78.37							8.32	3.48	
0.02974	0.99767	0.156	79.67	1968	78.14	231	76.78	17.7F	74.76	8.09	5.74	0.084
0.03956	0.99781	0.179	82.56	2353	80.20	384	76.82	17.7F	73.05	7.99	5.91	0.050
0.04934	0.99794	0.209	85.33	2460	82.70	444	76.63	17.7F	73.63	8.11	5.92	0.055
0.05911	0.99806	0.232	86.87	1377	82.58	404	76.41	17.7F	71.34	7.84	5.50	0.050
0.06878	0.99818	0.256	89.23	2079	85.44	462	76.12	17.7F	70.85	7.85	5.57	0.043
0.07844	0.99826	0.280	90.59	1506	85.21	421	75.80	17.7F	71.00	7.90	5.57	0.045
0.08808	0.99841	0.305	92.19	1532	86.52	424	75.48	17.7F	70.64	7.89	5.52	0.061
0.09770	0.99853	0.330	92.82	1357	86.08	397	75.07	17.7F	69.67	7.82	5.49	0.054
0.10773	0.99866	0.357	94.66	1464	88.70	438	75.10	17.7F	67.95	7.76	5.51	0.084

[a] Parameter values followed by the letter F were held constant during the fitting procedure.
[b] Units: c in M, κ in $\Omega^{-1}\,m^{-1}$; τ_j in 10^{-12} s. [c] Reference 86.

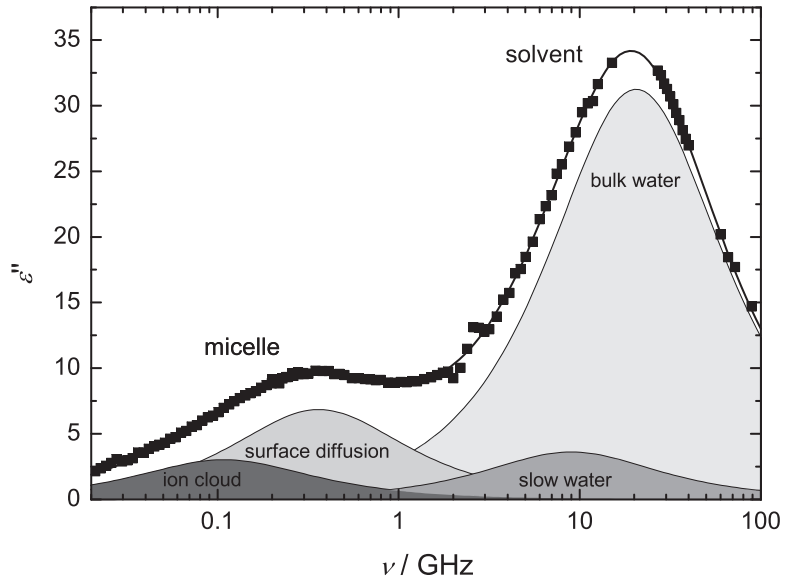

Figure 4.3: Dielectric loss spectrum, $\varepsilon''(\nu)$, of 0.1077 M NaC12(aq) at 25 °C. Symbols represent experimental data, the line represents the D+D+D+D fit, and shaded areas indicate the contributions of the different relaxation modes to the overall spectrum.

The validity of the accepted D+D+D+D model was also checked with the method devised by Zasetzky and Buchner[105] and as depicted by Figure 4.4, the analysis reinforces the fitting results with the similar number of relaxation processes, furthermore the relaxation times obtained via this method and MWFIT program[103] are in good agreement with each other.

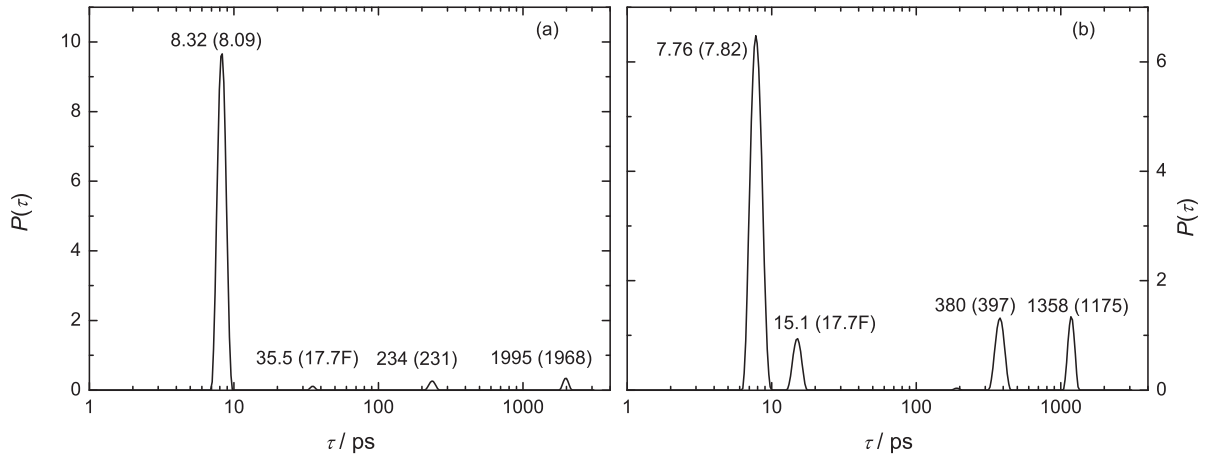

Figure 4.4: Relaxation time distribution function, $P(\tau)$, of NaC12(aq) at 25 °C at concentrations c / M of: **(a)** 0.02974, and **(b)** 0.09770 obtained with the bias-free fitting procedure of Zasetzky and Buchner.[105] Relaxation times for the resolved modes are indicated together with the corresponding values from Table 4.2 (in brackets).

4.1.2 Assignment of micelle-specific modes

As already shown in Figure 2.6, DR spectra of NaC12(aq) showed distinct "electrode polarization" effect. This unwanted feature was removed by roughly estimating the permittivity contribution coming from the electrode polarization, using the empirical relation as

$$\varepsilon'_{\mathrm{EP}} = \mathrm{A}\nu^{-\alpha} + \mathrm{B} \tag{4.1}$$

In Eq. 4.1 $\varepsilon'_{\mathrm{EP}}$ is calculated from the difference of uncorrected permittivity and the permittivity data of "high temperature" probe extrapolated to the lowest frequency, whereas A, B and α are the empirical constants. In doing so, however, the chances of "over correction" of the permittivity data at lower frequency region can not be neglected and this may lead to somewhat too low static permittivity and relaxation times values of the micellar modes. The two low-frequency processes appearing in all the DR spectra of NaC12(aq) are recognized as micelle-related. The process occurring at ∼0.1 GHz (amplitude, S_1 and relaxation time, τ_1) is attributed to the radial charge fluctuations of the diffuse ion cloud around the micelles whereas the relaxation mode appearing at ∼0.4 GHz, is assigned to the tangential motion of the bound Na^+ ions at the surface of NaC12 micelles and hence reflects the

interfacial polarization. The associated parameters S_2 and τ_2 reflect the amount and mobility of these adsorbed Na^+ ions at the surface of micelle. The latter can be interpreted as hopping of bound Na^+ ions between adjacent headgroups, i.e., surface conductance of the presented system. Presence of these micelle-related modes are responsible for a steady increase of the static permittivity of the solutions from $\varepsilon = 78.37$ (value for pure water) to 94.7 at 0.1 M, Figure 4.2a, this increment is already observed for some other colloidal systems.[15,197]

The dielectric properties of colloidal systems can be modeled with the theory of Grosse[79] and the model presented by Pauly and Schwan,[198] however in the presented study only Grosse model is used and is considered superior over the model of Pauly and Schwan as both models in principle give complementary results but Grosse model requires less number of adjustable parameters to fit the relaxation times and relaxation amplitudes of the micelle-specific modes. Furthermore, only interfacial polarization is accounted by the theory of Pauly of Schwan and not the ion-cloud relaxation.

First step in the data analysis involved direct inclusion of experimentally obtained micelle-related relaxation times and relaxation amplitudes (τ_1, τ_2, S_1 & S_2) into Grosse's equations. The input parameters were the static permittivity of water, ε_m=78.37, core permittivity, ε_p=2, and neglecting the minor contributions from free anions and concentration changes, the diffusion coefficient of the Na^+ ion at infinite dilution, $1.334\times10^{-9}m^2s^{-1}$,[121] was used for D. The resulting output quantities were namely, the radius, R_G, surface conductance, λ_s, volume fraction, ϕ_{mic}, and Debye length, χ^{-1}, of the micelle obtained by inserting the data in Eqs. 1.102, 1.105, 1.106, & 1.103, respectively.

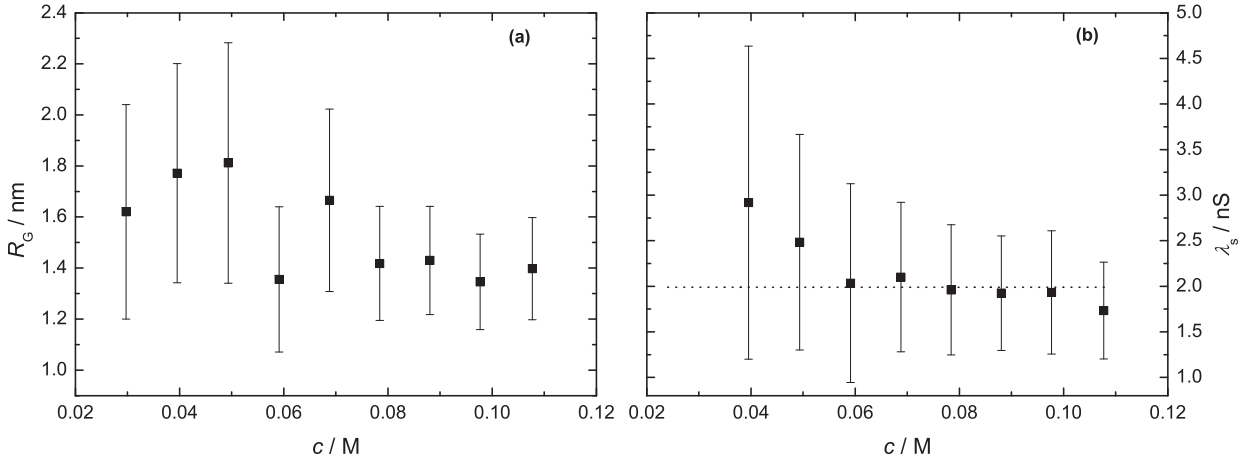

Figure 4.5: Concentration dependence of; Grosse radius, R_G (**a**), and λ_s (**b**), of NaC12(aq) at 25 °C. Dotted line represents λ_s values obtained via Eq. 4.3.

As illustrated in Figure 4.5b, within the error limits the surface conductance of NaC12 micelle is nearly constant which signifies that the counterion-headgroup interactions do not vary with increasing concentration of the surfactant. The direct calculation of R_G from

the experimental τ_1 values results in values ranging between 1.2 and 1.8 nm (Figure 4.5a), which is considerably smaller than experimental data from small-angle neutron scattering (SANS) method ranging from 2.37 nm at 0.16 M to 2.58 nm at 0.53 M.[193] Due to this reason the obtained values of R_G (Figure 4.5a) were not used for further calculations, rather R_G was used as an adjustable parameter for further calculations. Furthermore, it was observed that the χ^{-1} values, obtained from the fitting of experimental data into Eq. 1.103, in the studied concentration range could be presented as

$$\chi^{-1} = [0.57 + 2.20 \times c] \text{ nm} \tag{4.2}$$

The obtained ϕ_{mic} values are shown in Figure 4.8. In the next step of analysis the simultaneous fitting of micelle-related relaxation times and relaxation amplitudes was performed by using two adjustable parameters namely the micellar radius, R_G and tangential diffusion coefficient of the sodium ions condensed on the micellar surface, D_+^s, and from the equations of reference 79, following relation was employed to evaluate λ_s.

$$D_+^s = \frac{4\pi k_B T \lambda_s R_G^2}{e^2 \beta N_{ag}} \tag{4.3}$$

Where β denotes the degree of counterion attachment and e is the elementary charge. Eq. 4.3 & Eq. 1.101 alone were employed to obtain another set of values for λ_s and ϕ_{mic}, hence do not involve the use of experimental amplitudes or relaxation times. The corresponding results are displayed in the form of dotted lines in Figures 4.5b & 4.8.
A constant value of micellar aggregation number, N_{ag} of 89 was taken from literature.[199] It should be noted that the molecular dynamics study of the sodium laurate plus water system does show the progression from spherical through elongated and worm micelles to lamellar phases.[200] However, upto 10% (weight percent) only spherical micelles prevail and for the presented work, where the concentration was not more than 2.4%, N_{ag} can be used as a constant, hence similar argument can be used for the constant R_G. Also, it was assumed that above critical micelle concentration, *cmc* the concentration of free monomers, c_f is equal to the *cmc*. In addition to the use of R_G and D_+^s as adjustable parameters, experimental conductivities were used as κ_m, while a core conductivity of κ_c=0 was used as the inner core of the micelle is considered as pure hydrocarbon. Moreover, χ^{-1} values represented by Eq. 4.2 and Eq. 1.104 were also used in the data analysis and the results obtained from both equations were then compared. The rest of input parameters were same as already mentioned in preceding paragraph, i.e., standard values of ε_m, ε_p and D, together with the degree of counterion attachment, β=0.73, estimated from the literature data of Caponetti et al.[193] The micellar radius was adjusted to the value of 2.50 nm as this value yielded excellent description of S_1 & S_2 and τ_2 over the entire concentration range (Figures 4.6 & 4.7).
The experimental values of τ_1 always lie below the Grosse's predicted values which might be due to under estimation of ion-cloud relaxation times resulting from the correction for "electrode polarization". After correcting the adjusted value of R_G for the radius of Na^+ ion (0.12 nm[18]) as $R_G = R_{mic} + R_{Na^+}$, the micellar radius agrees well with the literature data,[193] hence, it can be reasonably inferred that the counter sodium ions are in direct contact with the carboxylate headgroup of the NaC12 micelle (Figures 4.26). this

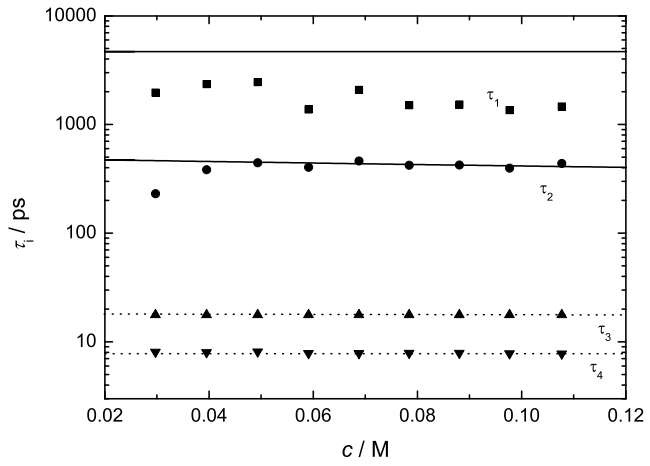

Figure 4.6: Concentration dependence of experimental relaxation times, τ_i of various relaxation modes in NaC12(aq) at 25 °C. Solid lines are the fits with Grosse's theory whereas dotted lines serve as visual aid only.

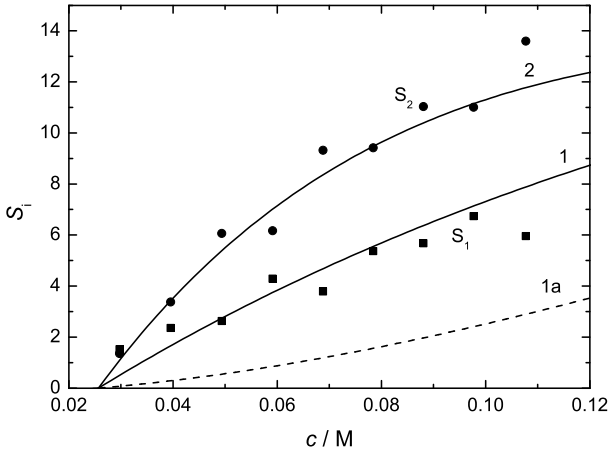

Figure 4.7: Concentration dependence of experimental relaxation amplitudes, S_i of micelle-related relaxation modes in NaC12(aq) at 25 °C. Lines represent the fits with Grosse's model with Debye length calculated according to Eq. 4.2 (curve 1, 2) and Eq. 1.104 (curve 1a for S_1).

As already mentioned the diffusion coefficient of bound Na^+ ions was an adjustable parameter whose adjusted value came out to be $0.65\times\ 10^{-9}\,m^2s^{-1}$, considerably lower than the diffusion coefficient of free Na^+ ions in water at infinite dilution, $1.334\times\ 10^{-9}\,m^2s^{-1}$,[121] which is physically reasonable. It should also be noted that the calculated curve for the dispersion amplitude S_1 of NaC12 system (curve 1a of Figure 4.7) is markedly away from the experimental data points when using the Eq. 1.104. However, excellent agreement is obtained using the Eq. 4.2 for χ^{-1}. The volume fraction of the micelle is related to the V_{mic}, which is the volume occupied by the wet micelles (including the hydration water) and V_{tot}, i.e., the total volume of the solution as

$$\phi_{\mathrm{mic}} = \frac{V_{\mathrm{mic}(c)}}{V_{\mathrm{tot}(c)}} \tag{4.4}$$

In the above equation it is assumed that the volume occupied by the surfactant monomers and their counterions is constant at $c > cmc$ and the possible dissociation of Na^+ ions from the micellar surface is neglected.

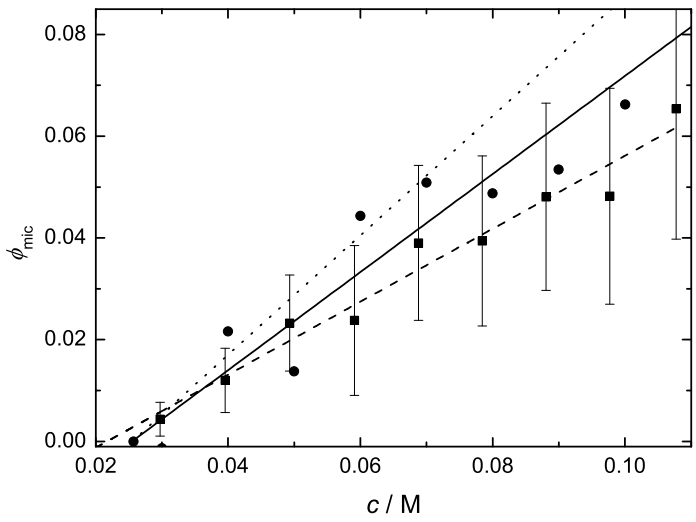

Figure 4.8: Volume fraction, ϕ_{mic} of NaC12 micelles at 25 °C determined from the amount of free water using Eq. 4.5 (●, solid line), from model of Grosse using Eq. 1.106(■, dashed line), and from Eq. 1.101 (dotted line).

In addition to the Eq. 1.106, an alternative approach can also be used to calculate ϕ_{mic} via the relaxation strength of bulk water by first employing Cavell equation (Eq. 1.72), which yielded the apparent bulk water concentration, $c_{\mathrm{w}}^{\mathrm{app,b}}$, so that

$$\phi_{\mathrm{mic}} = \frac{c_{\mathrm{w}}^{\mathrm{app,b}}(\mathrm{cmc}) - c_{\mathrm{w}}^{\mathrm{app,b}}(c)}{c_{\mathrm{w}}(0)} \tag{4.5}$$

Eq. 4.5 yields the volume fraction of the micelles in the solution including all types of hydration water, namely "slow" and "frozen" water, which is not easily accessible from the other experimental methods.[197] As depicted in Figure 4.8, ϕ_{mic} values calculated from Eq. 1.106 are slightly lower than the one obtained from the analysis of solvent relaxation processes via Eq. 4.5. However, the agreement is good between the values obtained via Eq. 4.5 and Eq. 1.101, this supports the acceptance of superposition of four Debye equations (4D) for the presented system.

4.2 DRS of bio-compatible surfactants

4.2.1 Aqueous solutions of choline laurate

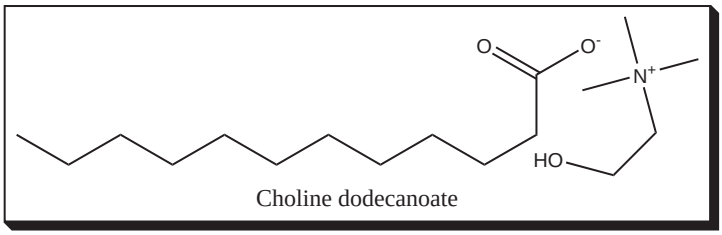

As already mentioned, surfactants having choline as counterions are able to substitute those with tetraalkylammonium (TAA) counterions. The latter are interesting alternatives for the common alkali counterions in conventional soaps due to their remarkably low Krafft points[189] but TAA ions are potentially hazardous, whereas choline is non-toxic and biologically degradable. The present study reports the dielectric relaxation behavior of aqueous solutions of choline dodecanoate at 25 °C and in the frequency range $0.01 \lesssim \nu/\mathrm{GHz} \leq 89$. Low frequency data in the range of $0.01 \lesssim \nu/\mathrm{GHz} \leq 0.2$ was recorded with TDR setup using TX type of cutoff cell. The cell characteristics are provided in Table 2.2 while underlying theory of TDR measurements is already discussed in section 2.2.1. As mentioned in literature TDR has some shortcomings regarding the measurements of low absorbing liquids[201] and electrolyte solutions[202] and is sensitive to the pin-length of the used cutoff cell. Furthermore, imperfections of the feeding line are responsible for the pseudo-reflections which can lead to biased results.[202] Such behavior was observed in the TDR measurements of ChC12(aq) system where the dielectric data in the frequency range $0.1 \lesssim \nu/\mathrm{GHz} \lesssim 0.2$ showed an off set and thus were deleted during the fitting procedure. The data in the frequency range $0.2 \leq \nu/\mathrm{GHz} \leq 20$ was recorded with Agilent E8364B VNA using high tem-

perature probe, A-band interferometer (section 2.2.2 and 2.2.3) was used to record the DR data in the frequency range of $27 \leq \nu/\mathrm{GHz} \leq 40$ while data in the range $60 \leq \nu/\mathrm{GHz} \leq 89$ was recorded using E-band interferometer. For each sample densities and conductivities were experimentally measured and using the conductivity data the DR spectrum of respective sample was then corrected.
As for NaC12(aq) solutions, two regions can be readily identified in the spectra of aqueous solutions of choline laurate, i.e., one below 1 GHz and the other above this frequency, Figure 4.9b. The low frequency mode(s) become more prominent with increasing concentration of solute and this clearly indicates it to be solute related. Due to its location, the higher frequency peak was assigned to the solvent whose position does not vary with c. The recorded DR spectra were further analyzed using different mathematical models. The Grosse model was employed to study micelle-related modes while solvent-related relaxations are used to evaluate hydration numbers for ChC12(aq) micellar system.

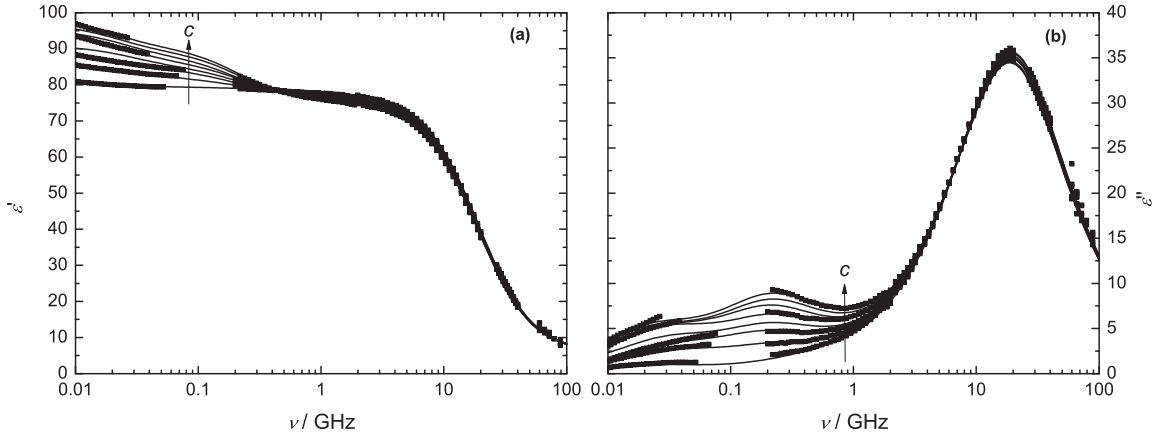

Figure 4.9: Permittivity, $\varepsilon'(\nu)$ (**a**), and dielectric loss, $\varepsilon''(\nu)$ (**b**), spectra for ChC12(aq) at 25 °C and concentrations $c/\mathrm{M} = 0.0292$, 0.0393, 0.0481, 0.0585, 0.0678, 0.0776, 0.0876, and 0.0968 (bottom to top). Symbols show experimental data (for some samples, symbols are omitted for visual clarity) and lines represent the D+D+D+D fit.

4.2.2 Resolution of DR spectra

Spectra of aqueous solutions of choline dodecanoate were best fitted by a superposition of four Debye (D+D+D+D) processes, Figures 4.9 & 4.10. Two low frequency processes, peaking at ∼0.03 GHz and ∼0.2 GHz respectively, are micelle-related. They can be assigned to the fluctuations of the diffuse ion cloud surrounding the micelle and to the tangential motions of bound counterions, respectively.
The relaxation centered at 20 GHz is due to bulk water, whereas the mode peaking at ∼7 GHz is regarded as a "composite" originating from the incidentally overlapping relaxations of "slow" water molecules hydrating the micelles and their counterions and of the choline cations themselves. Table 4.3 summarizes all fitting parameters for ChC12(aq)

Table 4.3: Densities, ρ; Electrical Conductivities, κ; Limiting Permittivities, ε_j; Relaxation Times, τ_j; and Reduced Error Function Values, χ^2_r, for ChC12(aq) at Concentrations, c; and 25 °C[a,b]

c	ρ	κ	ε	τ_1	ε_2	τ_2	ε_3	τ_3	ε_4	τ_4	ε_∞	χ^2_r
0[c]			78.37							8.32	3.48	
0.02915	0.99713	0.138	80.97	7013	79.27	361	77.63	25.9	76.41	8.30F	5.81	0.065
0.03932	0.99706	0.172	85.62	5274	81.66	712	77.56	34.4	76.18	8.30F	5.83	0.109
0.04814	0.99701	0.192	88.35	5378	83.92	799	77.20	27.0	74.96	8.30F	5.79	0.067
0.05853	0.99695	0.221	90.83	5644	84.85	729	76.78	25.1	74.36	8.30F	5.79	0.053
0.06776	0.99688	0.243	94.16	6210	86.06	704	76.41	23.0	73.71	8.30F	5.70	0.042
0.07756	0.99681	0.272	95.22	6526	87.65	747	75.86	23.3	72.82	8.30F	5.72	0.059
0.08757	0.99675	0.299	96.82	7338	88.98	727	75.73	24.9	72.80	8.30F	5.77	0.061
0.09684	0.99669	0.329	98.17	7562	90.04	720	75.50	26.3	72.74	8.30F	5.79	0.080

[a] Parameter values followed by the letter F were held constant during the fitting procedure.
[b] Units: c in M, κ in $\Omega^{-1}\,m^{-1}$; τ_j in 10^{-12} s. [c] Reference 86.

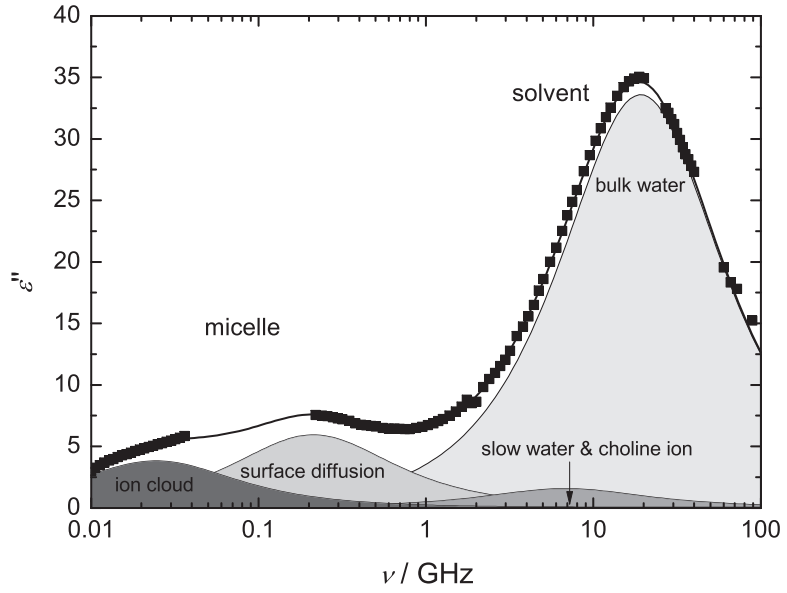

Figure 4.10: Dielectric loss spectrum, $\varepsilon''(\nu)$, of 0.0776 M ChC12(aq) at 25 °C. Symbols represent experimental data, the line represents the D+D+D+D fit, and shaded areas indicate the contributions of the different relaxation modes to the overall spectrum.

system, also given are the experimental values of ρ & κ. The method of Zasetzky and Buchner[105] was also employed to cross check the chosen D+D+D+D model for aqueous choline laurate surfactant system. The method generates four distinguishable peaks, Fig-

ure 4.4, whose relaxation times agree reasonably well with values obtained through MWFIT program[103], except for the peak assigned to be "composite" for which this method gives smaller values. Furthermore, a small, unidentified peak appeared occasionally in the Zasetzky fit at around 200 ps which could also be resolved with our usual fitting routine (MWFIT program[103]). However this model was discarded as the resolved "extra" mode had negligible amplitude (and constant relaxation time of ∼250 ps) throughout the studied concentration range of ChC12 system and no physical justification could be assigned to this mode. Here, it should be noted that in order to get a set of internally consistent and smooth data, τ_4 has to be fixed to the value of 8.30 ps.

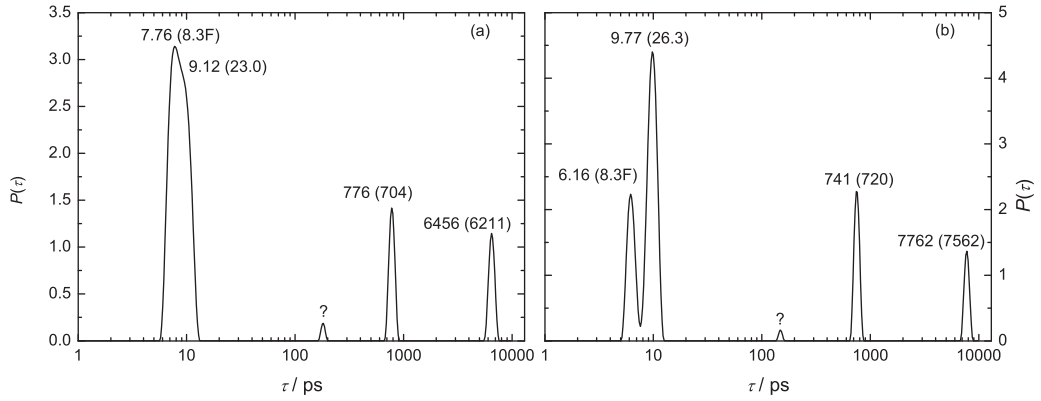

Figure 4.11: Relaxation time distribution function, $P(\tau)$, of ChC12(aq) at 25 °C at concentrations c / M of: **(a)** 0.06776, and **(b)** 0.09684 obtained with the bias-free fitting procedure of Zasetzky and Buchner.[105] Relaxation times for the resolved modes are indicated together with the corresponding values from Table 4.3 (in brackets).

4.2.3 Assignment of micelle-specific modes

As already mentioned, aqueous solutions of ChC12 surfactant can be best described by superposition of four Debye (D+D+D+D) processes, see Figure 4.10. Based on Grosse model the process appearing at ∼0.025 GHz (amplitude, S_1 and relaxation time, τ_1) can be assigned to the fluctuations of the diffuse ion cloud around the micelles and the relaxation mode appearing at ∼0.2 GHz (amplitude, S_2 and relaxation time, τ_2), reflects the interfacial polarization due to presence of bound Ch^+ ions at the surface of ChC12 micelles. As observed for the DR spectra of aqueous solutions of sodium laurate, the static permittivity increases with increasing concentration of ChC12 from a value of 81.0, at 0.03 M to 98.2 at 0.10 M, Table 4.3. Similar to the NaC12 system, dielectric data of aqueous solutions of ChC12 was also put to Grosse analysis. The schematic route of calculations was same as mentioned before in section 4.1.2. Firstly, various micelle related parameters, R_G, λ_s, ϕ_{mic} & χ^{-1} were evaluated from the experimental relaxations times and relaxation amplitudes of micelle-related modes using Eqs. 1.102, 1.105, 1.106, & 1.103, respectively. The standard values for input parameters were used for ε_m and ε_p, see section 4.1.2. Based on the dilute

solutions conductivity data,[203] a value of D=1.118×10^{-9}m^{2}s^{-1} was calculated for the Ch$^+$ ion at infinite dilution, this served as another input parameter for the presented system.

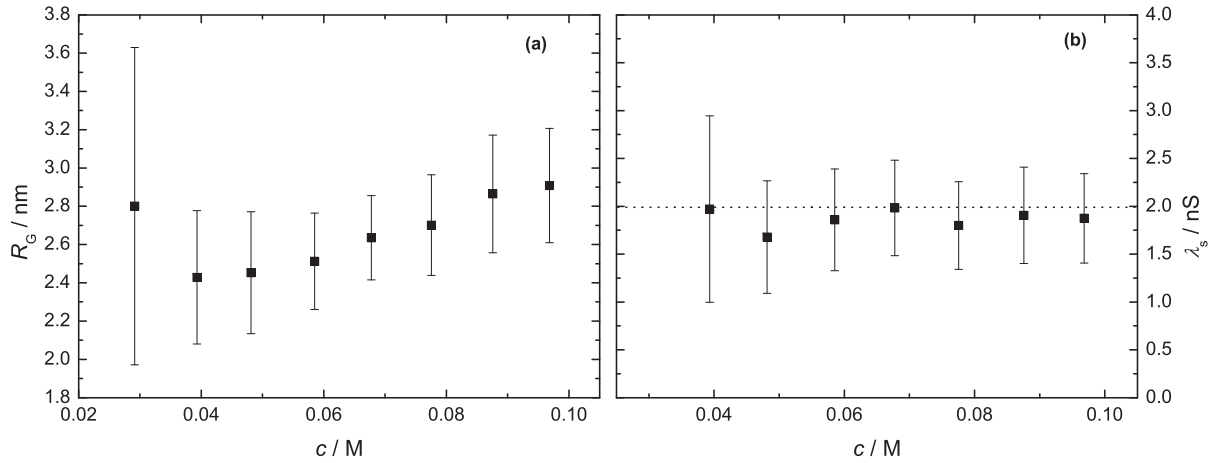

Figure 4.12: Concentration dependence of; Grosse radius, R_G (**a**), and λ_s (**b**), of ChC12(aq) at 25 °C. Dotted line represents λ_s values obtained via Eq. 4.3.

Figure 4.12 represents the variation of obtained R_{G} and λ_{s} upon concentration change. The micellar surface conductance remains virtually invariant of the solute concentration, similar to NaC12 system, so it can be inferred that interactions between carboxylate head groups and counter choline ions are not effected by the concentration, Figure 4.12b. The micellar radius of ChC12 system, however, increases with increasing concentration with the magnitude ranging between 2.4 nm to 2.8 nm, Figure 4.12a. The resulting ϕ_{mic} values are shown as filled squares in Figure 4.15, where an increasing trend was observed with increasing concentration of ChC12. For the obtained χ^{-1}, it was observed that in the studied concentration range, the values could be parameterized as

$$\chi^{-1} = [0.75 + 7.00 \times c] \text{ nm} \tag{4.6}$$

Simultaneous fitting of micelle-related relaxation times and relaxation amplitudes was performed using the adjusted value of R_{G} = 2.70 nm and D_+^s = 1.05×10^{-9}m^{2}s^{-1}, which resulted in excellent agreement between the DRS measured data and one predicted by Grosse theory, Figures 4.13 & 4.14.

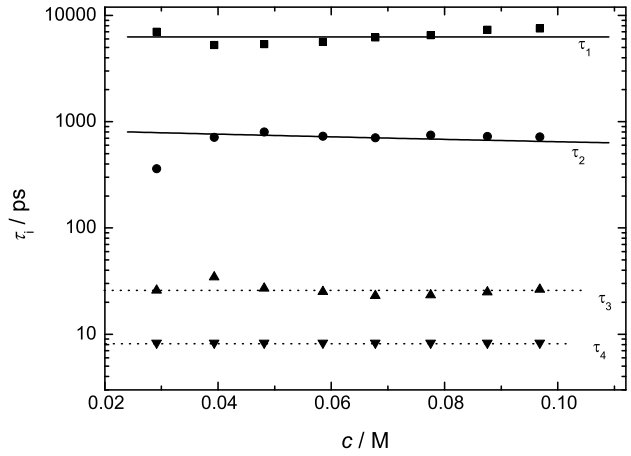

Figure 4.13: Concentration dependence of experimental relaxation times, τ_i of various relaxation modes in ChC12(aq) at 25 °C. Solid lines are the fits with Grosse's theory whereas dotted lines serve as visual aid only.

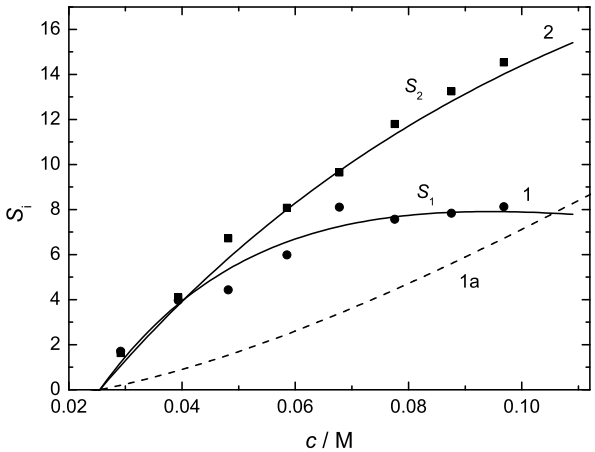

Figure 4.14: Concentration dependence of experimental relaxation amplitudes, S_i of micelle-related relaxation modes in ChC12(aq) at 25 °C. Lines represent the fits with Grosse's model with Debye length calculated according to Eq. 4.6 (curve 1, 2) and Eq. 1.104 (curve 1a for S_1).

It should be noted that, although the obtained R_G proved to be concentration variant, however, keeping in mind the known information that ChCm surfactants form spherical micelles with no sphere-to-rod transition i.e. their size and shape does not vary with concentration[8], R_G was chosen as an adjustable parameter. Micellar aggregation number, N_{ag} of 49 was taken from literature.[14] The degree of counterion attachment, β=0.67, is taken from the literature data of Klein et al.[14] From the adjusted values of R_G and D_+^s, a new set of data was obtained for λ_s and ϕ_{mic} using Eq. 4.3 & Eq. 1.101 and the dotted lines in Figure 4.12b & 4.15 represent the obtained results.
Rest of input parameters were same as described before for NaC12 system. Eq. 4.6 resulted in better fitting of experimental relaxation times and relaxation amplitudes of micelle-related modes of ChC12 system instead of the Eq. 1.104. As shown in Figures 4.13 & 4.14, the micellar parameters, S_1, S_2, τ_1 and τ_2 follow the Grosse's theory (relevent equations are described in section 1.6.3) throughout the studied concentration range.

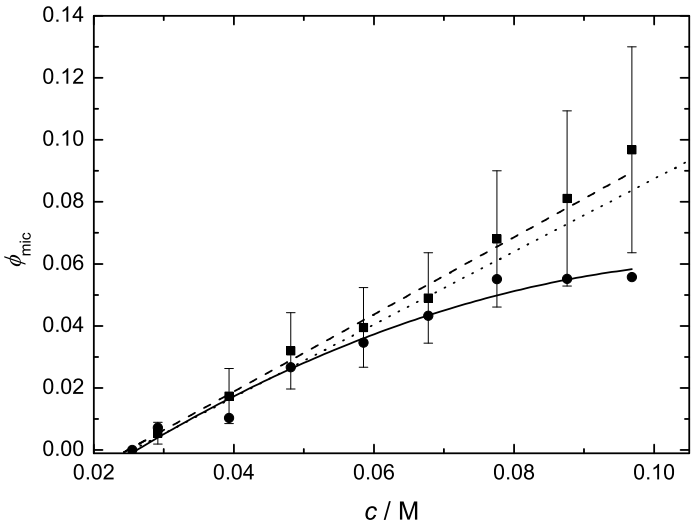

Figure 4.15: Volume fraction, ϕ_{mic} of ChC12 micelles at 25 °C determined from the amount of free water using Eq. 4.5 (●, solid line), from model of Grosse using Eq. 1.106(■, dashed line), and from Eq. 1.101 (dotted line).

The adjusted value of R_G, =2.70 nm, which is within the range of values plotted in Figure 4.12a, is higher than the value of 2.10 nm reported for ChC12 micelle in literature.[194] Since R_G, in addition to the geometric radius of bare micelle, includes the radius of adsorbed counterion as well ($R_G = R_{mic} + R_{Ch^+}$) thus this apparent difference should be corrected for the radius of Ch^+ ion (0.330 nm[204,205]) and also keeping in mind the radius of a water molecule, 0.1425 nm[206], the space between the headgroup and counterion can occupy approximately a single layer of water molecules. So it can be concluded that the choline ions are separated from the micellar surface by an intervening layer of water molecules, Figure 4.27.

Volume fraction of ChC12 was calculated with the help of Eq. 1.106, 1.101 and 4.5, Figure 4.15. Upto 0.05 M concentration ϕ_{mic} obtained from different equations agree well but after this concentration the curves deviate with slightly higher values coming from the Grosse model, Eq. 1.101 & 1.106.

4.2.4 Aqueous solutions of choline dodecylsulfate

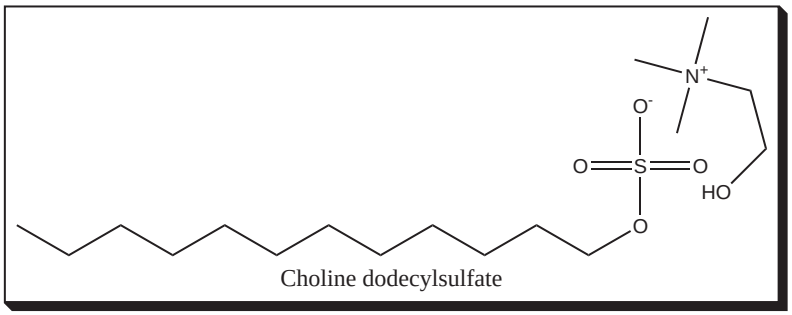

Even though choline carboxylates are known to have low Krafft points and are "eco-friendly", they are associated with problems of alkaline pH and are sensitive to common impurities like sodium chloride.[8] In this regard sodium alkyl sulfates are known to be less salt sensitive and biodegradable.[6,207] Keeping in view these advantages choline alkyl sulfates seem very promising as the acidic nature of sulfate (SO_4^{2-}) group overcomes the problem of high pH. However, regarding the salt sensitivity of these soaps no clear evidence is available.[8] This part of the dissertation deals with the DRS studies of aqueous solutions of choline dodecylsulfate at 25 °C and in the frequency range $0.01 \lesssim \nu/\mathrm{GHz} \leq 89$. DR data in the low frequency range, $0.01 \lesssim \nu/\mathrm{GHz} \leq 0.2$ was recorded with TDR setup using TX type of cutoff cell (for cell specifications see Table 2.2). Similar to the choline laurate system, section 4.2.1, TDR data of concentrated solutions of ChDS in the frequency range $0.06 \lesssim \nu/\mathrm{GHz} \lesssim 0.2$ showed an off set of data points. These were deleted to get smooth fits over the entire studied frequency range. The Agilent E8364B VNA was used to record the data in the frequency range $0.2 \leq \nu/\mathrm{GHz} \leq 20$ with its high temperature probe. The A-band interferometer (section 2.2.2 and 2.2.3) was used to record the DR data in the frequency range of $27 \leq \nu/\mathrm{GHz} \leq 40$ and DR data in the range $60 \leq \nu/\mathrm{GHz} \leq 89$ was recorded using E-band interferometer.

4.2.5 Resolution of DR spectra

The recorded dielectric spectra of aqueous solutions of choline dodecylsulfate (Figures 4.16) appeared similar to those of sodium- and choline laurate solutions. Again a superposition of four Debye (D+D+D+D) processes proved to be the best description to the presented system, Figures 4.16 & 4.17. Modes appearing at ∼0.05 GHz and ∼0.2 GHz were designated to be micelle-specific and were respectively assigned to the fluctuations of the diffuse ion cloud and to the interfacial polarization of bound counterions. The process peaking at ∼7 GHz was assigned to be a "composite" mode i.e. it includes the contributions from "slow" water molecules hydrating the micelles and their counterions and of the choline cations, whereas the highest frequency mode, appearing at 20 GHz is assigned to bulk water. Both "composite" and bulk water mode were quantitatively analyzed to obtain effective hydration numbers for the ChDS micellar system.

Table 4.4 includes values for all fitting parameters and the data of ρ and κ for choline dodecylsulfate system. Similar to the NaC12(aq) and ChC12(aq) systems, a dielectric increment is observed for ChDS(aq) where the static permittivity of the solutions increases from 81.5, at 0.01 M to 100.9 at 0.12 M, Table 4.4, hence formation of more and more micelles results in an increase of the polarity of the system. Furthermore, excellent agreement is obtained for the relaxation times obtained from the D+D+D+D fits and those estimated from the Zasetzky's method[105](Figure 4.18).

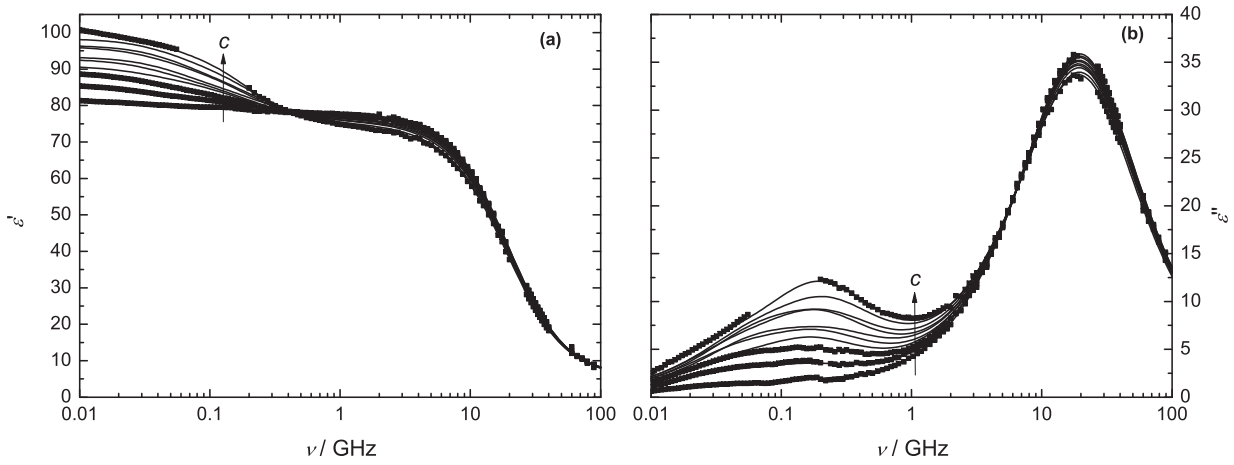

Figure 4.16: Permittivity, $\varepsilon'(\nu)$ (**a**), and dielectric loss, $\varepsilon''(\nu)$ (**b**), spectra for ChDS(aq) at 25 °C and concentrations c/M = 0.01, 0.02, 0.03, 0.04, 0.05, 0.06, 0.07, 0.08, 0.10, and 0.12 (bottom to top). Symbols show experimental data (for some samples, symbols are omitted for visual clarity) and lines represent the D+D+D+D fit.

4.2.6 Assignment of micelle-specific modes

The lowest-frequency modes appearing in DR spectra of all studied solutions of ChDS are related to certain dispersions of ChDS micelles namely, fluctuations of the diffuse ion cloud and tangential polarization of adsorbed counterions on micellar surface. As already described for the micellar systems of sodium laurate and choline laurate, Grosse model was applied to the aqueous solutions of choline dodecylsulfate. Experimental relaxations times and relaxation amplitudes of micelle-related modes, τ_1, τ_2, S_1 & S_2 of ChDS system were analyzed using the corresponding equations for Grosse's model (see section 1.6.3). Using D=1.118×10^{-9}m^{2}s^{-1} for the Ch$^+$ (as used for ChC12 system) and following the procedure described in section 4.1.2, the obtained R_G and λ_s are plotted in Figure 4.19. As depicted in Figure 4.19b, micellar surface conductance remain virtually invariant of the solute concentration which means that interactions between dodecylsulfate headgroups and counter choline ions are not effected by the concentration. Also R_G remains roughly constant at ∼2.2 nm.

Table 4.4: Densities, ρ; Electrical Conductivities, κ; Limiting Permittivities, ε_j; Relaxation Times, τ_j; and Reduced Error Function Values, χ^2_r, for ChDS(aq) at Concentrations, c; and 25 °C[a,b]

c	ρ	κ	ε	τ_1	ε_2	τ_2	ε_3	τ_3	ε_4	τ_4	ε_∞	χ^2_r
0[c]			78.37							8.32	3.48	
0.01	0.99726	0.038	81.50	6363	79.86	898	77.88	25F	76.30	8.05	5.52	0.038
0.02	0.99741	0.058	85.67	4935	82.19	950	77.68	25F	75.05	7.95	5.38	0.062
0.03	0.99757	0.078	88.97	4163	83.75	850	77.09	25F	75.34	8.08	5.49	0.037
0.04	0.99778	0.097	90.87	4581	86.52	925	77.00	25F	73.95	8.00	5.51	0.063
0.05	0.99797	0.118	93.14	4345	87.01	872	76.40	25F	74.20	8.10	5.59	0.062
0.06	0.99816	0.137	93.63	3248	86.10	691	76.16	25F	73.40	8.09	5.66	0.048
0.07	0.99831	0.159	96.18	3619	89.75	824	75.78	25F	73.39	8.15	5.78	0.067
0.08	0.99854	0.179	96.57	2980	89.02	730	75.63	25F	71.54	7.92	5.43	0.059
0.10	0.99891	0.221	98.36	3000	90.71	711	74.97	25F	70.10	7.84	5.38	0.058
0.12	0.99921	0.260	100.93	4715	94.88	797	74.20	25F	70.25	8.04	5.63	0.049

[a] Parameter values followed by the letter F were held constant during the fitting procedure.
[b] Units: c in M, κ in $\Omega^{-1}\,m^{-1}$; τ_j in 10^{-12} s. [c] Reference 86.

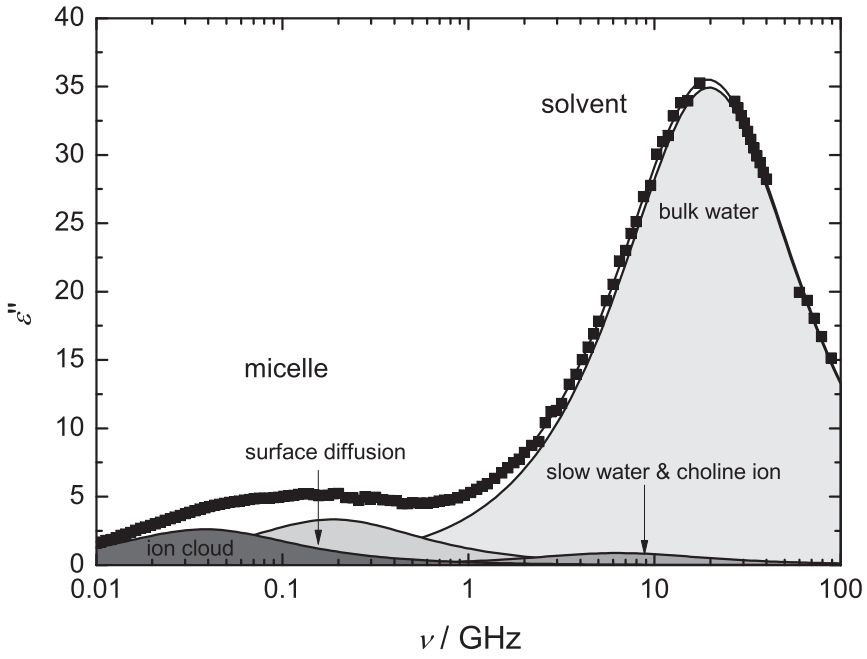

Figure 4.17: Dielectric loss spectrum, $\varepsilon''(\nu)$, of 0.03 M ChDS(aq) at 25 °C. Symbols represent experimental data, the line represents the D+D+D+D fit, and shaded areas indicate the contributions of the different relaxation modes to the overall spectrum.

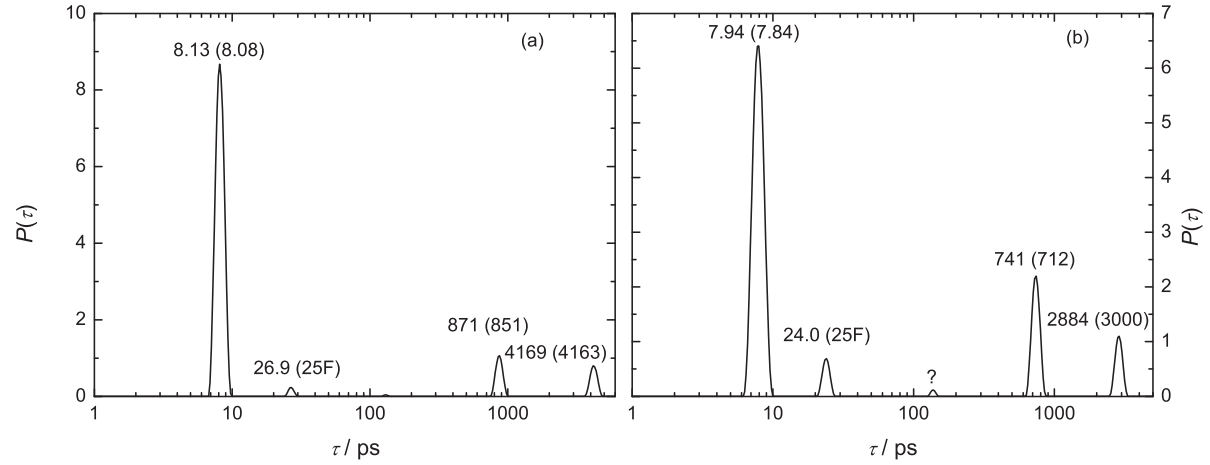

Figure 4.18: Relaxation time distribution function, $P(\tau)$, of ChDS(aq) at 25 °C at concentrations c / M of: **(a)** 0.03, and **(b)** 0.10 obtained with the bias-free fitting procedure of Zasetzky and Buchner.[105] Relaxation times for the resolved modes are indicated together with the corresponding values from Table 4.4 (in brackets).

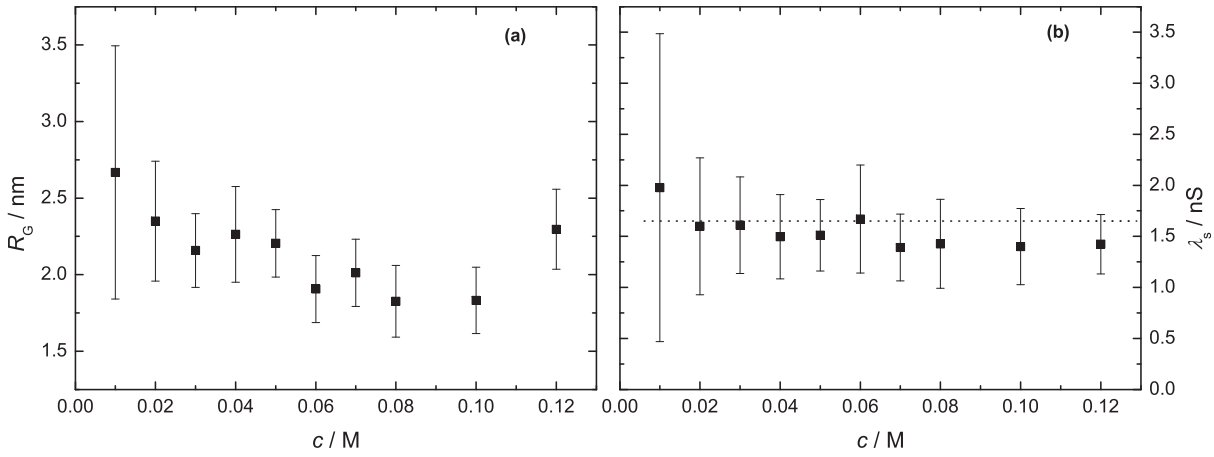

Figure 4.19: Concentration dependence of; Grosse radius, R_G (**a**), and λ_s (**b**), of ChDS(aq) at 25 °C. Dotted line represents λ_s values obtained via Eq. 4.3.

The obtained ϕ_{mic} via Eq. 1.106 is plotted in Figure 4.22, whereas the Debye length of the ChDS micelle obtained through Eq. 1.103, could be presented as

$$\chi^{-1} = [1.01 + 3.24 \times c] \text{ nm} \tag{4.7}$$

Again the micellar parameters S_1, S_2, τ_1 and τ_2 were simultaneously fitted using Eq. 4.3 & 1.101 and the same standard input parameters described in section 4.1.2, Figures 4.20 & 4.21. Micellar aggregation number, N_{ag} of 35 was chosen as a rough estimate for ChDS micelle as to our knowledge no such information is available in literature. However, a lower value of N_{ag} compared to the N_{ag} of ChC12 is used as the aggregation numbers of TAA alkyl

sulfate surfactants are found to be lower and their micellar size is smaller than expected on the basis of their *cmc* and the the degree of counterion dissociation, α[208–212]. The degree of counterion attachment, β=0.75, is taken from the literature.[8] For the analysis, R_G and D_+^s were used as adjustable parameters having adjusted value of 2.3 nm (very close to the averaged value of 2.2 nm, obtained through Eq. 1.102) and $0.75\times10^{-9}m^2s^{-1}$, respectively. Since choline dodecylsulfate belongs to a class of new "green" surfactants, its literature data is scarce. To our knowledge the only data regarding its micellar shape and phase behavior is provided by Klein[8] where a Cryo-TEM micrography of 5 wt% ChDS solution revealed spherical micelles with an approximate radius of 2.00 nm. The adjusted value of R_G =2.30 nm is higher than the reported value of 2.00 nm and this has to be corrected for the radius of Ch^+ ion (0.330 nm[204,205]) as $R_G = R_{mic} + R_{Ch^+}$. Since for ChDS system both geometric and Grosse's predicted radii are in excellent agreement, hence the choline ions possibly adsorb directly on the micellar surface, Figure 4.28. As shown in Figures 4.20 & 4.21 the agreement between experimentally obtained data points and Grosse's predicted values is excellent. The amplitude S_1, however, could be fitted well using Eq. 4.7, whereas Eq. 1.104 failed to reproduce the experimental amplitudes of ion cloud mode (curve 1a of Figure 4.21).

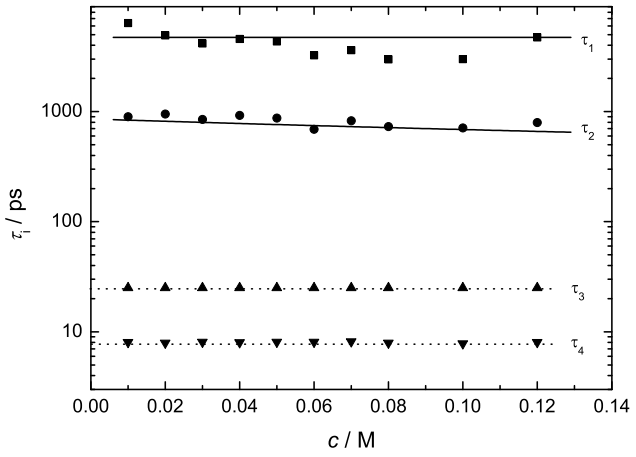

Figure 4.20: Concentration dependence of experimental relaxation times, τ_i of various relaxation modes in ChDS(aq) at 25 °C. Solid lines are the fits with Grosse's theory whereas dotted lines serve as visual aid only.

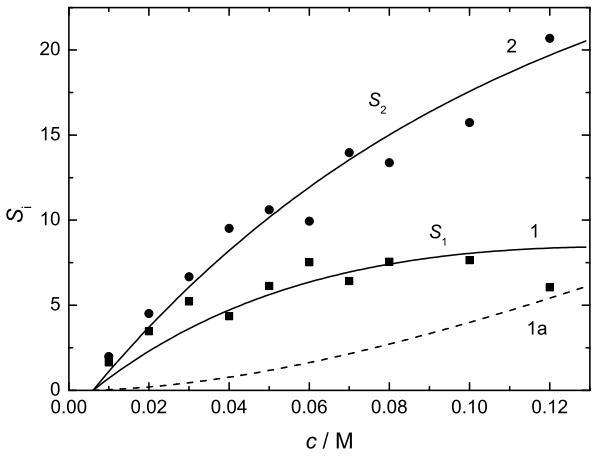

Figure 4.21: Concentration dependence of experimental relaxation amplitudes, S_i of micelle-related relaxation modes in ChDS(aq) at 25 °C. Lines represent the fits with Grosse's model with Debye length calculated according to Eq. 4.7 (curve 1, 2) and Eq. 1.104 (curve 1a for S_1).

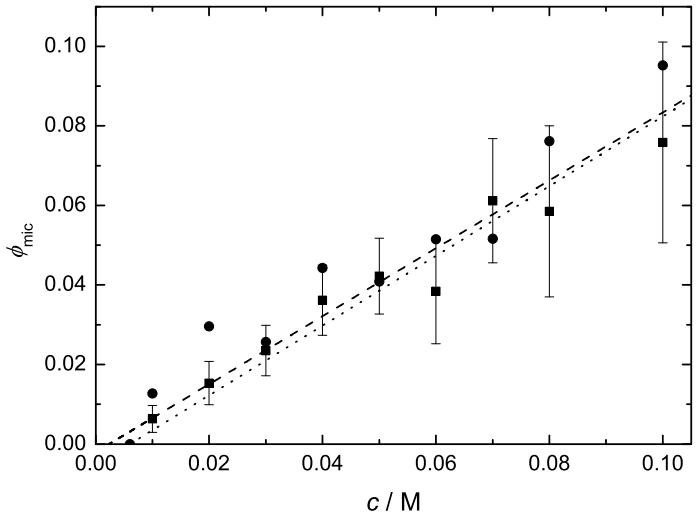

Figure 4.22: Volume fraction, ϕ_{mic} of ChDS micelles at 25 °C determined from the amount of free water using Eq. 4.5 (●, solid line), from model of Grosse using Eq. 1.106(■, dashed line), and from Eq. 1.101 (dotted line).

Figure 4.22 shows ϕ_{mic} obtained from Eq. 1.106, 1.101 and 4.5. Excellent agreement is achieved between the values obtained from different approaches and this strongly supports the selection of D+D+D+D model for ChDS system. Table 4.5 includes adjusted values of Grosse's parameters pertaining to studied systems.

Table 4.5: Adjusted values of R_{G}, literature values of radii, R_{Lit}, adjusted values of D_+^s, and values for the ratio, D_+^s/D, for NaC12(aq), ChC12(aq), ChDS(aq) and SDS(aq) systems.

	R_{G}/ nm	R_{Lit}/ nm	D_+^s/ m^2s^{-1}	D_+^s/ D
NaC12	2.5	2.37-2.58[193]	0.65×10^{-9}	0.49
ChC12	2.7	2.1[194]	1.05×10^{-9}	0.94
ChDS	2.3	2.0[8]	0.75×10^{-9}	0.67
SDS	2.64 (at cmc)[15]	2.23[213]	1.15×10^{-9},[15]	0.86[15]

Based on Collins's concept,[17,18] ions are divided into two classes; "kosmotropes", i.e., small ions with high charge density (hard) and "chaotropes", i.e., big ions with low charge density (soft). Accordingly, sodium can be considered as a "kosmotrope" and choline as "chaotrope". Interestingly, summarizing the results of presented chapter leads to a concrete evidence that Collins's concept is obeyed by the studied micellar solutions. This can be understood by analyzing the R_{G} and R_{Lit} values reported in Table 4.5. It can be concluded that the interaction between $Na^+...RCO_2^-$ in NaC12 micelles and $Ch^+...ROSO_3^-$ in ChDS micelles is strong, hence, counterions are directly attached on the respective headgroups (see Figures 4.26 & 4.28). In case of ChC12 and SDS micelles,[15] however, the interactions between $Ch^+...RCO_2^-$ and $Na^+...ROSO_3^-$ pairs is relatively weak and is water mediated (see Figure 4.27).
Furthermore, as shown in Figures 4.5b, 4.12b & 4.19b, surface conductance of the studied micellar systems varies with the order as $\lambda_s^{\text{NaC12}} \sim \lambda_s^{\text{ChC12}} > \lambda_s^{\text{ChDS}}$. Smaller size of sodium compared to choline ion is responsible for the larger λ_s of NaC12 compared to ChDS micelles whereas weak binding of choline (compared to sodium) to the dodecanoate headgroup leads to $\lambda_s^{\text{NaC12}} \sim \lambda_s^{\text{ChC12}}$. Strong counterion-headgroup binding in NaC12 & ChDS (hard-hard pairing) and weak counterion-headgroup interactions in ChC12 & SDS (soft-hard binding) micelles is also indicated by the ratio D_+^s/D (see Table 4.5) as this ratio value is high for ChC12 compared to NaC12 micelles, similarly, D_+^s/D of SDS[15] is larger than ChDS micelle. Interestingly, all these observations conform to the Figure 4.1.

4.2.7 Solvent relaxations and micellar hydration

As can be seen in Figures 4.3, 4.10 & 4.17 the main contribution to the DR spectra of all studied colloidal systems comes from the water relaxation occurring at ∼20 GHz. As in case of electrolyte solutions, the designation of this mode is quite straight forward and is assigned to the cooperative relaxations of hydrogen bonded network of bulk water molecules, which are actually rotationally mobile water molecules and are unaffected by the solute. The relaxation time of this mode, $\tau_4(=\tau_b)$ decreases slightly with increasing concentration for NaC12(aq) (Table 4.2), for ChC12(aq) solutions its value was fixed to 8.3ps (Table 4.3) which corresponds to the value for pure water, whereas for ChDS(aq) τ_b remained invariant of concentration (Table 4.4).

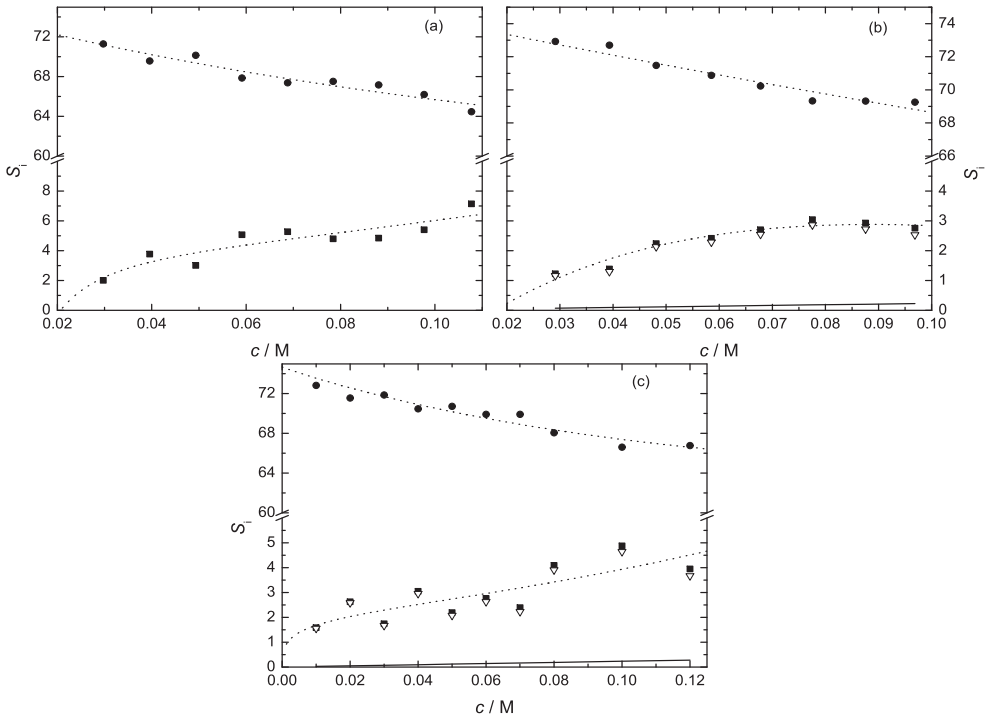

Figure 4.23: Concentration dependence for (**a**) NaC12(aq), (**b**) ChC12(aq) and (**c**) ChDS(aq) at 25 °C of the relaxation amplitudes of: bulk water, S_b (●), the composite mode, $S_s + S_+$ (■), and slow water, S_s (▽). The solid line represents S_+, calculated via Eq. 1.72; the dotted lines are included only as a visual guide.

Another process, which could not be seen in unresolved spectra of all studied surfactant systems, appearing at ∼8 GHz characterized by τ_3 and S_3 was assigned solely to the "slow" water molecules in case of sodium laurate, however for the studied systems containing choline as counterions this mode was designated as to be "composite" and considered as joint venture of "slow" water molecules hydrating the micelles along with their counterions and of the choline cations themselves.
In aqueous solutions of all studied micellar solutions, S_b decreases with increasing concentration of respective solute and this is accompanied by the increasing amplitude of "slow"

water process, S_s in NaC12(aq) and "composite" mode, $S_c = S_s + S_+$ in ChC12(aq) and ChDS(aq) (Figure 4.23).

Cavell equation (Eq. 1.72) was used to relate the amplitudes of various processes to the concentration of species responsible for respective process and by using the solvent normalized Cavell equation, concentration of various types of water like $c_s^{ap,b}$, $c_s^{ap,s}$ and $c_s^{ap,t}$ was calculated by inserting the amplitudes of "bulk" water, S_4, "slow" water, S_3 or total water amplitude, $S_3 + S_4$, respectively and the obtained values were compared to the analytical water concentration, c_s, that was obtained from the density data of solutions. For all studied surfactant systems, it was observed that at $c > 0$, $c_s > c_s^{ap,t}$. This is in accordance to what is already observed for some cationic surfactants (alkyltrimethylammonium halides, C_nTAX),[80] however in contrast to SDS solutions where it was observed that $c_s^{ap,t} = (1.002 \pm 0.002) \times c_s$.[15] Hence in solutions of sodium laurate, choline laurate and choline dodecylsulfate some of the water is irrotationally bound, due to strong solute-solvent interactions and is unable to contribute to the dielectric spectrum. The quantity of such irrotationally bound or "frozen" water molecules was calculated.

Since obtained Z_{ib} values through Eq. 3.12 correspond to total salt unit so in order to assign individual values to headgroups and counterions, these values should be partitioned using the assumption of ionic additivity[214]. Figure 4.24 represents the Z_{ib} values per headgroups for respective micellar system. This means that the effective hydration number of irrotationally bound water molecules is corrected for the Z_{ib} values for counterions as both Na^+,[98] and Ch^+,[215] ions are known to freeze water molecules in there hydration shells. After correcting for $Z_{ib}(Na^+)$, a constant value of Z_{ib} ~5 is obtained per dodecanoate headgroup in sodium laurate micelle. It is interesting to note that in contrast to SDS solutions where no irrotational bounding was observed, Na^+ ions keep their hydration in sodium laurate solutions. This observation receives support from the literature data provided by Gustavsson and Lindman[216] according to which sodium ions retain their primary hydration when incorporated to alkanoate micelles. Despite the fact that $Z_{ib}(\text{-}COO^-, 0)=0$, observed for simple electrolyte solutions[73], there is no reason to expect similar behavior of carboxylate group in surfactant solutions where its connected to long alkyl chain. Moreover, it is not certain that obtained Z_{ib} ~5 obtained per headgroup for sodium laurate system corresponds to headgroup only. Also the literature suggests existence of hydrogen bonding between a water molecule in the hydration shell of sodium and the carboxylate group[217], thus irrotational bounding of water by NaC12 micelles could be classified as hydrophillic and at infinite dilution ($c \to 0$), per NaC12 unit, 8-9 water molecules are frozen in DRS time scale.

In case of choline dodecanoate, as can be seen in Figure 4.24, non-zero values of Z_{ib} are obtained only for last three studied concentrations which range between 1-2 whereas for all lower concentrations negative values are obtained, which is unreasonable. Thus considering the size of error bars $Z_{ib}=0$ could be assigned to per headgroup in choline dodecanoate sytem. Whereas choline retains its hydration water (see chapter 3 for choline hydration) with $Z_{ib}(Ch^+, 0)=5$,[215] so all the irrotational bounding observed in ChC12 system corresponds solely to choline ions. The number of frozen water molecules per dodecylsulfate headgroup vary between 2-5 in ChDS micelles and similar to the ChC12 system, choline as counterion retain its hydration in ChDS micelles with five irrotationally

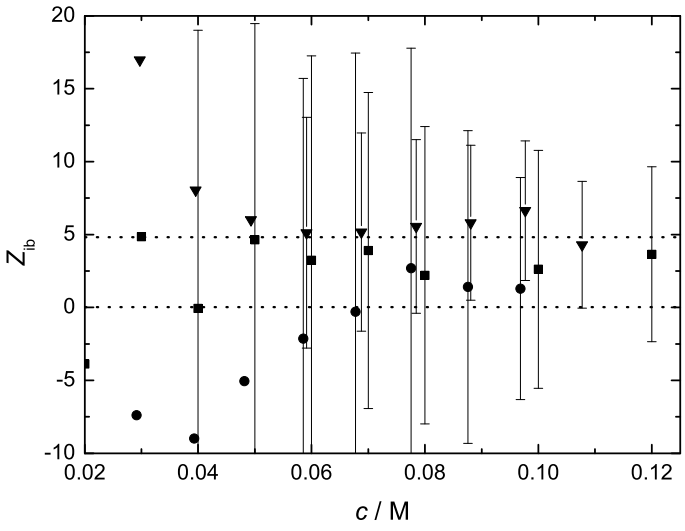

Figure 4.24: Concentration dependence of effective headgroup hydration numbers, Z_{ib}, at 25 °C for NaC12(aq) (▼), ChC12(aq) (●), and ChDS(aq) (■) (error bars[174] are omitted for few initial concentrations for visual clarity). Dotted lines are used only as a visual guide.

bound water molecules, whereas the whole ChDS unit, at infinite dilution is able to freeze approximately 10 water molecules.
Similar to Z_{ib}, a hydration number, Z_s can be defined for "slow" water molecules via Eq. 3.13. Motion of such water molecules is perturbed because of adjacent hydrophobic surface.[12] Sluggish dynamics of water molecules near the hydrophobic surface is explained by screening effect of solute, that actually reduces the access of perturbing fifth water molecule that is required for the rearrangement of hydrogen bond network.[80] Effective number of slow water molecules have been calculated in the presented study for NaC12, ChC12 and ChDS micellar solutions and the values are plotted *versus* concentration in Figure 4.25. The presented data points however, correspond to per headgroup only as the values are already corrected for $Z_{ib}(Ch^+)$.[215] Here it should be noted that DRS studies of aqueous solutions of electrolytes have revealed that Na^+ does not slow down water molecules in its hydration shell.[142,218] At infinite dilution, both dodecanoate and dodecylsulfate headgroups (having choline as counterions) slow down ∼18 water molecules, whereas the number decreases with increasing concentration. This is in close agreement with the DRS result, Z_s=20, for aqueous SDS[15] and higher then the values obtained for C_nTAX micelles[80].

The obtained Z_s values for sodium laurate are rather scattered around a value of 50. It is surprising that despite having same headgroup in choline laurate and sodium laurate, the dodecanoate could slow down more than double the number of water molecules in sodium laurate compared to choline laurate. This observation on the one hand might

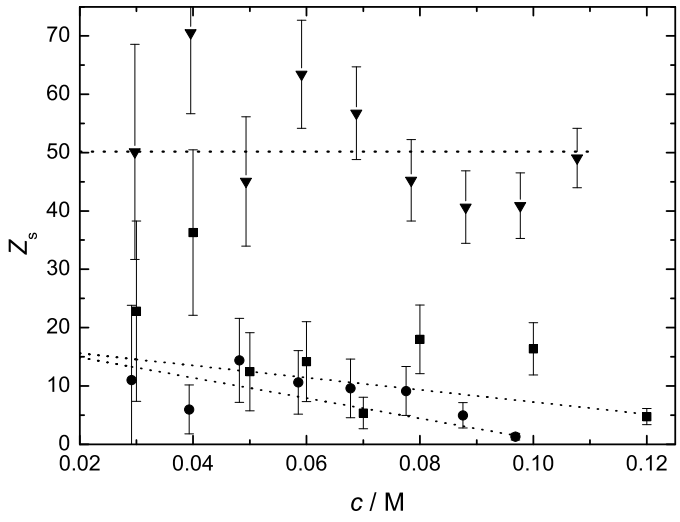

Figure 4.25: Concentration dependence of the slow-water hydration number per headgroup, Z_s, at 25 °C for NaC12(aq) (▼), ChC12(aq) (●), and ChDS(aq) (■).[174] Dotted lines are used only as a visual guide.

reflected only an over estimation of slow-water relaxation amplitude, S_3 in 4D fitting of NaC12(aq) system. If not so, even then, the dynamic roughness of the micellar surface of sodium laurate allows more water-hydrocarbon contact. Furthermore, small size of sodium compared to choline also increases the possibility of water penetration into sodium laurate micelle, hence out of these large number of slow water molecules some are possibly held only by penetration effects and rest due to interactions of charged headgroups and their associated counterions with water, Figure 4.26. Although the obtained hydration numbers are sensitive to the choice of used values for aggregation number and micellar radius, even then the surface of sodium laurate micelle is only partly covered by the hydration water.
Similarly, more extensive hydration of NaC12 compared to SDS micelles could be explained on the basis of relative sizes of carboxylate and sulfate headgroups as already revealed by the NMR studies on sodium dodecylsulfate and sodium dodecanoate where it was observed that compared to sulfates there is more space available for water molecules to penetrate between the headgroups of alkanoate micelles[219]. This difference of hydration between sulfate and carboxylate head groups was however not observed for ChC12 and ChDS micelles and this may corresponds to the bulky size of choline ion which can possibly cover the surface of both types of micelles equally well (Figures 4.27 & 4.28), also the lower aggregation number and smaller size of ChDS micelle compared to ChC12 micelle also compensates for the the larger size of sulfate compared to carboxylate when it comes to the surface covering efficiency of choline ion in these systems.
It should be noted that Z_s(-COO^-, 0)$\sim$ 5.2 and is concentration invariant[73], also keeping in mind a constant $\sim$ 5 frozen water molecules in NaC12, the question that whether these

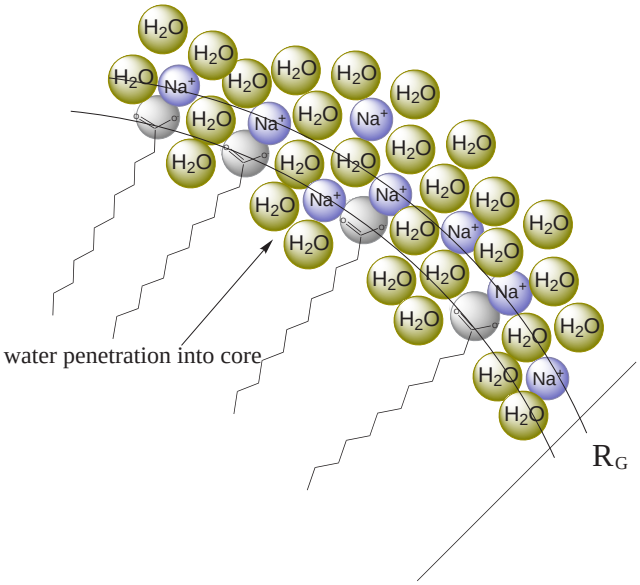

Figure 4.26: A portion of hydrated NaC12 micelle.

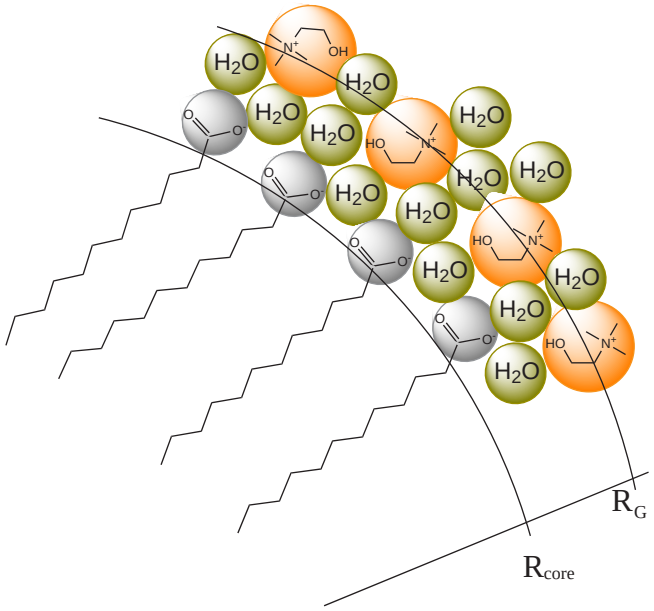

Figure 4.27: A portion of hydrated ChC12 micelle.

water molecules appear as frozen or slow is not clear. However incapability of carboxylate group to freeze water molecules in ChC12 system at the one hand supports the assumption that Z_{s}(-COO$^-$, 0) becomes part of hydrophobically slowed water and Z_{ib}(NaC12) is due to extensive hydration of sodium ions only, while at the other hand this might only depict that shielding of carboxylate group by bulky choline group is more pronounced then by

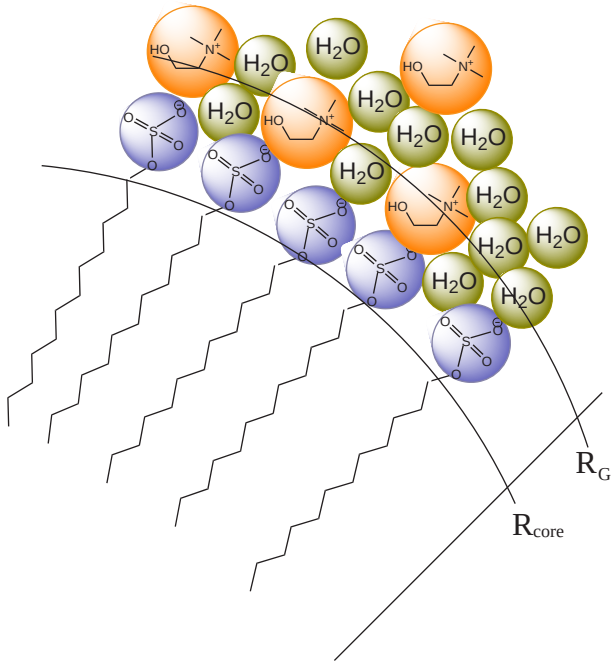

Figure 4.28: A portion of hydrated ChDS micelle.

small sodium ions.

4.2.8 Effect of added salt on dielectric properties of choline dodecylsulfate

In order to have qualitative information about the effect of added salt on the dielectric properties of micellar systems, three different concentrations of each; common alkali salt, NaCl and ChCl were prepared in 0.03 M ChDS(aq) solutions. Since the DR behavior and hydration of ChDS(aq) is already discussed (section 4.2.4), so stress will be given only on the changes that occur in the dielectric spectra of 0.03 M ChDS(aq) solutions containing the added electrolyte. The obtained spectra are displayed in Figure 4.30. As mentioned before (section 4.2.4) the low frequency data resulted in off sets of data points in the region where TDR and "high temperature" probe data joins, hence, in this frequency range few data points had to be removed in order to avoid biasing of results in terms of number of modes and values of obtained dielectric parameters. For both types of systems i.e. solutions of NaCl and ChCl in 0.03 M ChDS(aq), different mathematical models were tested and similar to the aqueous solutions of ChDS the spectra were best described by a superposition of four Debye (D+D+D+D) processes, see Figure 4.31 for resolved modes and Table 4.6 for the fitting parameters. This is logical as added sodium is unable to produce any separate DR signal while the relaxation of added choline ions again seems to remain submerged with solvent relaxation peak. Compared to the solution of 0.03 M ChDS(aq), the static permittivities of the solutions containing NaCl and ChCl are higher which indicates

increased polarity of the salt added solutions. The relaxation times of ion-cloud relaxation mode (τ_1) increased considerably in both types of solution (Table 4.6) which makes sense as the nature and size of ion cloud may vary with the addition of solute. This was also manifested by the change of peak position of ion-cloud relaxation mode to slightly lower frequencies in solutions containing NaCl and ChCl (see Figures 4.17 & 4.31). Furthermore, relaxation time (τ_2) and peak position of surface diffusion mode, remained nearly constant for the ChDS solutions added with ChCl. In case of NaCl however, both varied which indicated the effect of "changed" ion cloud on the surface diffusion of choline ions in ChDS micelles. Nevertheless, the solvent-related region apparently seemed unaffected by the solute addition. In this regard, comparison of the relaxation amplitude of "composite mode" in 0.03 M ChDS(aq) and ChCl added solutions of ChDS showed that this amplitude increased a bit which is explainable as the relaxation of choline ion is considered as a part of this mode and increased concentration of choline ion was responsible for this increased amplitude. For ChDS solutions containing NaCl, however, the difference in amplitude of this mode was observed to be negligible (see Figure 4.29).
As described earlier, choline carboxylates are sensitive to the presence of common impurities like NaCl, whereas due to increased binding efficiency of "soft" choline ion and "soft" sulfate group, choline dodecylsulfate was expected to be free of this problem[8] but this unfortunately, could not be proven until yet. The presented part of the study, in principle, is able to give a rough estimate about the salt sensitivity of ChDS surfactant. On the one hand the fitting model and the resulting parameters provided in Table 4.6, when compared to the values for 0.03 M ChDS(aq) and to the Table 1 of available literature data of SDS system[15] did not give any indication of the replacement of “soft” choline ion by “hard” sodium ion from soft sulfate group, while on the other hand the parameters given in Table 4.6 seemed self consistent and did not reflect any sudden change in the physicochemical properties of the studied systems. Hence, it can be concluded that although the dielectric properties of ChDS micelles could be modified with the addition of NaCl but no new types of micelles are formed. However, it should be kept in mind that although the inferred results seemed appealing but the rigorous testing of theses conclusions demands for a more detailed study, by using number of different concentrations of NaCl added solutions of ChDS, study of their hydration pattern and also analysis of the data using Grosse's theory and the resulting parameters could then help to build any concrete evidence for the salt sensitivity of choline dodecylsulfate surfactant. Furthermore, in order to increase the accuracy of the measurements and to avoid biasing of the results, there is a high need of better quality low-frequency data.

Table 4.6: Limiting Permittivities, ε_j; Relaxation Times, τ_j; and Reduced Error Function Values, χ^2_r, for 0.03 M ChDS(aq) at different concentrations, c of NaCl and ChCl at 25 °C[a,b]

c	ε	τ_1	ε_2	τ_2	ε_3	τ_3	ε_4	τ_4	ε_∞	χ^2_r
0[c]	78.37							8.32	3.48	
0.03 M ChDS[d]	88.97	4163.2	83.75	850.6	77.09	25F	75.34	8.08	5.49	0.037
				NaCl						
0.01553	90.99	8089.3	82.14	736.6	76.53	28.8	74.27	7.85	5.54	0.076
0.03481	91.28	9862.6	80.48	479.3	76.10	21.0	73.15	7.86	5.57	0.078
0.05562	91.46	9989.8	80.43	477.7	76.11	21.4	73.14	7.85	5.58	0.078
				ChCl						
0.01562	90.59	8162.4	81.36	659.8	76.55	18.5	73.25	8.00F	5.56	0.079
0.03475	88.34	8899.5	79.78	534.0	76.18	18.3	73.16	8.06	5.62	0.082
0.05564	90.70	8986.1	83.85	878.4	76.68	54.7	75.72	8.05	5.69	0.077

[a] Parameter values followed by the letter F were held constant during the fitting procedure. [b] Units: c in M and τ_j in 10^{-12} s. [c] Reference 86. [d] Parameter values taken from Table 4.4.

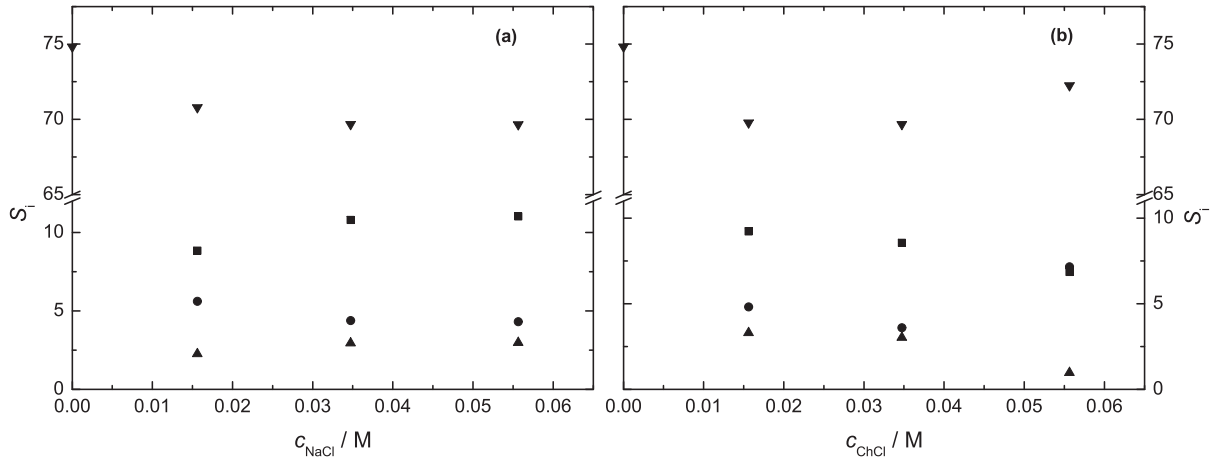

Figure 4.29: Concentration dependence for (**a**) different solutions of NaCl in 0.03 M ChDS and (**b**) different solutions of ChCl in 0.03 M ChDS at 25 °C of the relaxation amplitudes of: bulk water, S_b (▼), the "composite" mode, $S_s + S_+$ (▲), and micelle-related relaxation modes, S_1 (■), and S_2 (●).

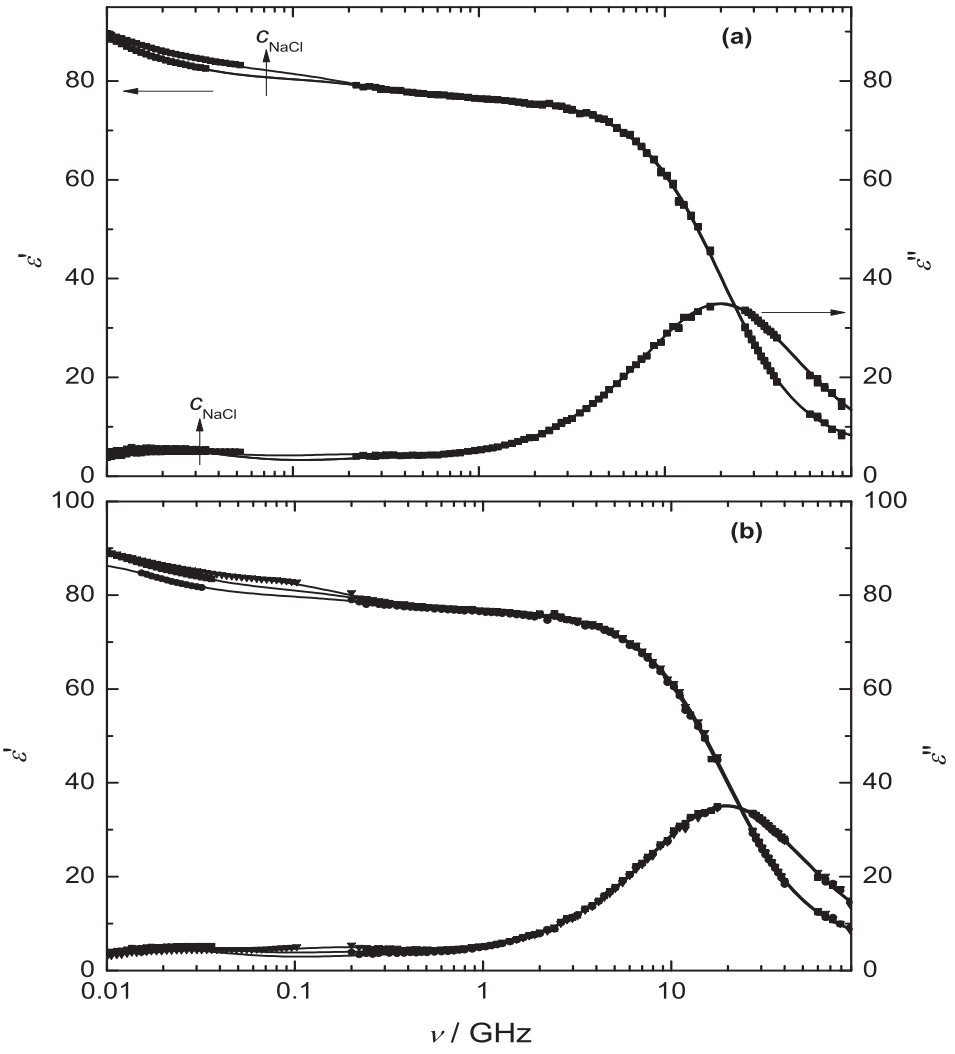

Figure 4.30: Spectra of Permittivity, $\varepsilon'(\nu)$, and dielectric loss, $\varepsilon''(\nu)$, for 0.01553, 0.03481 and 0.05562 M NaCl in 0.03 M ChDS (**a**) 0.01562 (■), 0.03475 (●) and 0.05564 M ChCl (▼) in 0.03 M ChDS (**b**) at 25 °C. Symbols show experimental data and lines represent the D+D+D+D fit.

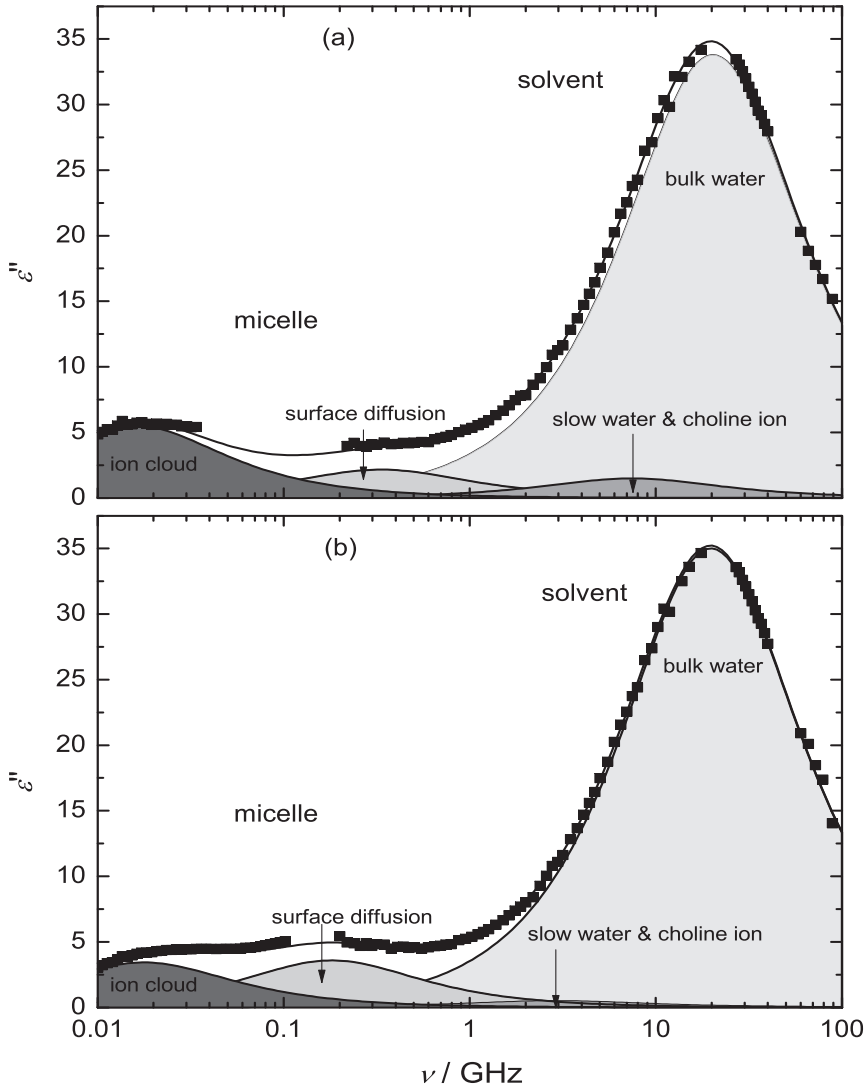

Figure 4.31: Dielectric loss spectrum, $\varepsilon''(\nu)$, of **(a)** 0.05562 M NaCl in 0.03 M ChDS and **(b)** 0.05564 M ChCl in 0.03 M ChDS at 25 °C. Symbols represent experimental data, the line represents the D+D+D+D fit, and shaded areas indicate the contributions of the different relaxation modes to the overall spectrum.

Summary and conclusions

The present thesis includes systematic broadband DRS study of choline-containing electrolytes and surfactants. Supplementary data for the physical properties of these systems is also provided. For electrolyte solutions special emphasis is given to the study of ion pairing and ion hydration whereas micellar solutions are characterized on the basis of their hydration behavior and headgroup-counterion binding. In this regard carboxylate ($-CO_2^-$) and sulfate ($-OSO_3^-$) as headgroups, while Na^+ and Ch^+ as counterions were chosen. Moreover, salt sensitivity of choline dodecylsulfate was also studied qualitatively. In addition to the choline-based systems, aqueous solutions of NH_4Cl(aq) and sodium dodecanoate (NaC12(aq)) were chosen as reference systems for the comparison purpose, hence, were studied in detail.

Choline-based electrolytes

Electrical conductivities (at 25 °C) and densities (in the range, 0-45 °C) of aqueous solutions of choline chloride (ChCl), chlorocholine chloride (Cl-ChCl) and NH_4Cl are reported. The dynamic viscosities (in the range, 0-45 °C) are also provided for ChCl(aq) and Cl-ChCl(aq). The obtained data were compared with the available literature values for the studied systems. Conductivities are well fitted by the Casteel-Amis equation, Eq. 3.1, whereas low-order polynomials (Eq. 3.2) were used to fit $\rho(m)$ and $\eta(m)$. Apparent molar volumes calculated from ρ (only for ChCl(aq) and Cl-ChCl(aq)) are well described by the Redlich-Meyer approach, Eq. 3.4. The obtained sensitivity parameter, h, suggest at best weak ion pairing for ChCl(aq) and Cl-ChCl(aq), whereas the Walden product at 25 °C points at significant ion-ion interactions and/or changes in ion hydration with rising concentration. The small but notable difference in the h values of ChCl(aq) and Cl-ChCl(aq), as well as the different concentration dependence of the activation energy of viscous flow might indicate that solvation effects predominate.
DRS data of all the studied electrolyte solutions did exhibit a small amplitude low frequency process (occurring at <1 GHz), which is fairly assigned to the ion-pairs and/or ion-cloud relaxation in each of these electrolyte solutions. Ion-pair association constants are determined for the studied systems assuming that this lowest frequency process is solely due to presence of ion-pairs in these systems, reasonable values are obtained for each of the studied systems which in practise could serve only as an upper limit for the possible association in the studied systems.
Two types of hydration are observed in aqueous solutions of ChCl and Cl-ChCl as the numbers obtained for strongly bound, Z_{ib}, and moderately bound water molecules, Z_{s}, are

non-zero for them. However, for aqueous solutions of NH_4Cl no irrotational bounding of water molecules has been observed. For all three studied electrolyte systems Z_s decreases strongly with increasing concentration of respective salt which indicates presence of labile hydration spheres, which is consistent with the Walden product results of ChCl and Cl-ChCl at 25 °C. Also the relaxation time of bulk water mode, τ_b remains fairly constant for ChCl(aq) and decreases for Cl-ChCl(aq) and NH_4Cl(aq) which shows that bulk water dynamics is not affected by the ChCl(aq) while Cl-Ch^+ and NH_4^+ ions affect the water molecules beyond their primary hydration shells.

Choline-based surfactants

The DR spectra of post-micellar concentrations of sodium dodecanoate (NaC12(aq)), choline dodecanoate (ChC12(aq)) and choline dodecylsulfate (ChDS(aq)) over the frequency range $0.01 \lesssim \nu/\mathrm{GHz} \leq 89$ were recorded. Two types of micelle-related modes could be resolved for each of the studied surfactant systems. The lowest-frequency mode was assigned to the radial charge fluctuations of the diffuse ion cloud whereas next to this appeared a relaxation, due to interfacial polarization of adsorbed counterions at the micellar surface. The dielectric properties of the studied colloidal systems were modeled with the theory of Grosse and micelle-related parameters such as the radius (R_G), surface conductance (λ_s), volume fraction (ϕ_{mic}) and Debye length (χ^{-1}) were obtained through that analysis.

Physico-chemical parameters obtained for all studied surfactant solutions were compared with the available literature data. Based on the difference between R_G and R_{Lit} values, it was observed that headgroup-counterion binding is strong between Na^+...–CO_2^- and Ch^+...–OSO_3^- in NaC12(aq) and ChDS(aq) micelles, respectively. However, the binding is weak for Ch^+...–CO_2^- and Na^+...–OSO_3^- pairs in ChC12(aq) and SDS(aq) micelles, respectively and is water mediated. This observation lead to the conclusion that for the presented surfactants, Collins's law is obeyed.

Hydration studies of the presented micellar solutions did reveal that in ChC12(aq) system no irrotational bounding is observed for the carboxylate headgroup, whereas in NaC12(aq) and ChDS(aq) micelles, per headgroup, Z_{ib} ∼5 and ∼2-5 are obtained, respectively. Also it was observed that choline retains its individual hydration water, $Z_{ib}(Ch^+, 0)$=5, in ChC12(aq) and ChDS(aq) systems. After correcting for $Z_s(Ch^+, 0)$=18, the effective slow-water hydration number per headgroup were found to be ∼18 for both ChC12(aq) and ChDS(aq) systems, this number decreases sharply with rising concentration of respective solute. The obtained Z_s values for sodium laurate were rather scattered around a value of 50. This might be, at the one hand, due to an over estimation of slow-water relaxation amplitude in 4D fitting of NaC12(aq) system. On the other hand the 'literature indicated' extensive hydration and surface roughness of sodium in NaC12(aq) micelle as well as the smaller size of Na^+ compared to Ch^+ ion was used to argue for more hydration in NaC12(aq) micelles compared to choline-containing micelles.

A rough estimate of salt sensitivity of ChDS was established by qualitatively analyzing the spectra of 0.03 M ChDS(aq) with added NaCl and ChCl. The comparison of obtained DR data with DR parameters of 0.03 M ChDS(aq) and SDS(aq) did not give a clear hint for

the replacement of "soft" choline ion by "hard" sodium ion from soft sulfate group, which conforms to the Collins's concept. However, the dielectric properties of ChDS(aq) micelles were found to be modified with the addition of NaCl or ChCl. As a future prospect, better quality low-frequency data, which requires improved instrumentation, as well as systematically detailed DRS studies are needed to get more rigorous results of this issue.

Bibliography

[1] Lum, K.; Chandler, D.; Weeks, J. D. *J. Phys. Chem. B* **1999**, *103*, 4570.

[2] Food and Nutrition Board, Institute of Medicine, *Dietary Reference Intakes for Thiamin, Riboflavin, Niacin, Vitamin B6, Folate, Vitamin B12, Pantothenic Acid, Biotin, and Choline*, National Academic Press, Washington DC, 1998.

[3] Howe, J. C.; Williams, J. R.; Holden, J. M. *USDA Database for the Choline Content of Common Foods*; National Academic Press: http://www.nal.usda.gov/fnic/foodcomp/Data/Choline/Choline.html, 2004.

[4] Zeisel, S. H.; Blusztajn, J. K. *Ann. Rev. Nutr.* **1994**, *14*, 269.

[5] Lindman, B. *Handbook of Applied Surface and Colloid Chemistry*; ed. Holmberg, K.; John Wiley & Sons Ltd: Chichester, 2002.

[6] Schmalsteig, A.; Wasov, G. W. *Handbook of Applied Surface and Colloid Chemistry*; ed. Holmberg, K.; John Wiley & Sons Ltd: England, 2002; Vol. 1.

[7] Kunz, W.; Kellermeier, R.; Klein, R.; Maurer, E.; Tourad, D. *Biologically Acceptable Choline Compounds and their Use as Tensides*, EP 2010-152626 (University of Regensburg, Germany), 2010.

[8] Klein, R. Ph.D. Thesis, Regensburg, 2011.

[9] Abbott, A. P.; Barron, J. C.; Ryder, K. S.; Wilson, D. *Chem. Eur. J.* **2007**, *13*, 6495.

[10] Buchner, R.; Hefter, G. *Phys. Chem. Chem. Phys.* **2009**, *11*, 8954.

[11] Buchner, R. *Pure Appl. Chem.* **2008**, *80*, 1239.

[12] Buchner, R.; Hölzl, C.; Stauber, J.; Barthel, J. *Phys. Chem. Chem. Phys.* **2002**, *4*, 2169.

[13] Mcbain, J. W.; Lee, W. W. *Oil Soap* **1943**, *20*, 17.

[14] Klein, R.; Tourad, D.; Kunz, W. *Green Chem.* **2008**, *10*, 433.

[15] Fernandez, P.; Schrödle, S.; Buchner, R.; Kunz, W. *Chem. Phys. Chem.* **2003**, *4*, 1065.

[16] Hofmeister, F. *Arch. Exp. Path. Pharm.* **1887**, *24*, 247.

[17] Collins, K. D.; Neilson, G. W.; Enderby, J. E. *Biophys. Chem.* **2007**, *128*, 95.

[18] Collins, K. D. *Biophys. Chem.* **2006**, *119*, 271.

[19] Maxwell, J. C. *A Treatise on Electricity and Magnetism*; Claredon Press: Oxford, 1881.

[20] Greschner, G. S. *Maxwellgleichungen*; Hüthig: Basel, 1981.

[21] Böttcher, C. F. J.; Bordewijk, P. *Theory of Electric Polarization*; Elsevier: Amsterdam, 1978; Vol. 1 and 2.

[22] Falkenhagen, H. *Theorie der Elektrolyte*; Hirzel: Leipzig, 1971.

[23] Kremer, F.; Schönhals, A. *Broadband Dielectric Spectroscopy*; Springer-Verlag: Germany, 2003.

[24] Barthel, J.; Buchner, R. *Chem. Soc. Rev.* **1992**, *21*, 263.

[25] Barthel, J.; Buchner, R.; Steger, H. *Wiss. Zeitschr. THLM* **1989**, *31*, 409.

[26] Cole, R. H. *Ann. Rev. Phys. Chem.* **1977**, *28*, 283.

[27] Debye, P. *Polar Molecules*; Dover Publ.: New York, 1930.

[28] Pellat, H. *Ann. Chim. Phys.* **1899**, *18*, 150.

[29] Cole, K. S.; Cole, R. H. *J. Chem. Phys.* **1941**, *9*, 341.

[30] Cole, K. S.; Cole, R. H. *J. Chem. Phys.* **1942**, *10*, 98.

[31] Davidson, D. W.; Cole, R. H. *J. Chem. Phys.* **1950**, *18*, 1417.

[32] Davidson, D. W.; Cole, R. H. *J. Chem. Phys.* **1951**, *19*, 1484.

[33] Havriliak, S.; Negami, S. *J. Polym. Sci., Part C* **1966**, *14*, 99.

[34] Chalmers, J. M.; Griffiths, P. R. *Handbook of Vibrational Spectroscopy*; Wiley–VCH: Weinheim, 2001.

[35] Onsager, L. *J. Am. Chem. Soc.* **1936**, *58*, 1486.

[36] Kirkwood, J. G. *J. Chem. Phys.* **1939**, *7*, 911.

[37] Fröhlich, H. *Theory of Dielectrics*, 2nd ed.; Oxford University Press: Oxford, 1965.

[38] Cavell, E. A. S.; Knight, P. C.; Sheikh, M. A. *Trans. Faraday Soc.* **1971**, *67*, 2225.

[39] Scholte, T. G. *Physica* **1949**, *15*, 437.

[40] Barthel, J.; Hetzenauer, H.; Buchner, R. *Ber. Bunsen–Ges. Phys. Chem.* **1992**, *96*, 1424.

[41] Powles, J. G. *J. Chem. Phys.* **1953**, *21*, 633.

[42] Glarum, S. H. *J. Chem. Phys.* **1960**, *33*, 639.

[43] Madden, P.; Kivelson, D. *Adv. Chem. Phys.* **1984**, *56*, 467.

[44] Kivelson, D.; Madden, P. *Annu. Rev. Phys. Chem.* **1980**, *31*, 523.

[45] Dote, J. C.; Kivelson, D.; Schwartz, R. N. *J. Phys. Chem.* **1981**, *85*, 2169.

[46] Perrin, F. *J. Phys. Radium* **1934**, *5*, 497.

[47] Dote, J. C.; Kivelson, D. *J. Phys. Chem.* **1983**, *87*, 3889.

[48] Barthel, J.; Kleebauer, M.; Buchner, R. *J. Solution Chem.* **1995**, *24*, 1.

[49] Buchner, R.; Chen, T.; Hefter, G. *J. Phys. Chem. B* **2004**, *108*, 2365.

[50] Winkler, K.; Lindner, J.; Börsing, H.; Vöhringer, P. *J. Chem. Phys.* **2000**, *113*, 4674.

[51] Eisenberg, D.; Kauzmann, W. *The structure and Properties of Water*; Clarendon: London, 1969.

[52] Rossky, P. J.; Karplus, M. *J. Am. Chem. Soc.* **1979**, *101*, 1913.

[53] Woutersen, S.; Emmerichs, U.; Bakker, H. J. *Science* **1997**, *278*, 658.

[54] Abragam, A. *The Principles of Nuclear Magnetism*; Clarendon: Oxford, UK, 1961.

[55] Teixeira, J.; Bellissent-Funel, M. C.; Chen, S. H.; Dianoux, A. J. *Phys. Rev. A* **1985**, *31*, 1913.

[56] Barthel, J.; Bachhuber, K.; Buchner, R.; Hetzenauer, H. *Chem. Phys. Lett.* **1990**, *165*, 369.

[57] Lawrence, C. P.; Skinner, J. L. *J. Chem. Phys.* **2003**, *118*, 264.

[58] Silvestrelli, P. L. *J. Phys. Chem. B* **2009**, *113*, 10728.

[59] Laage, D.; Stirnemann, G.; Sterpone, F.; Rey, J. T., R. Hynes *Annu. Rev. Phys. Chem.* **2011**, *62*, 395.

[60] Ivanov, E. N. *Soviet Phys. JETP* **1964**, *18*, 1041.

[61] Laage, D.; Hynes, J. T. *J. Phys. Chem. B* **2008**, *112*, 14230.

[62] Moore, W. J.; Hummel, D. O. *Physikalische Chemie*; de Gruyter: Berlin, 1986.

[63] Glasstone, S.; Laidler, K. J.; Eyring, H. *The Theory of Rate Processes*; McGraw Hill: New York, 1977.

[64] Buchner, R.; Barthel, J.; Stauber, J. *Chem. Phys. Lett.* **1999**, *306*, 57.

[65] Marcus, Y.; Hefter, G. *Chem. Rev.* **2006**, *106*, 4585.

[66] Buchner, R.; Samani, F.; May, P. M.; Sturm, P.; Hefter, G. *Chem. Phys. Chem.* **2003**, *4*, 373.

[67] Eigen, M.; Tamm, K. *Z. Electrochem.* **1962**, *66*, 93 & 107.

[68] Hefter, G. *Pure Appl. Chem.* **2006**, *98*, 1571.

[69] Rudolph, W. W.; Irmer, G.; Hefter, G. T. *Phys. Chem. Chem. Phys.* **2003**, *5*, 5253.

[70] Robinson, R. A.; Stokes, R. H. *Electrolyte Solutions*, 2nd ed.; Butterworths: London, 1970.

[71] Debye, P.; Falkenhagen, H. *Phys. Z.* **1928**, *29*, 121.

[72] Koryta, J.; Dvořák, J.; Kavan, L. *Principles of Electrochemistry*, 2nd ed.; John Wiley Sons: Chichester, 1993.

[73] Rahman, H. M. A.; Hefter, G.; Buchner, R. *J. Phys. Chem. B* **2012**, *116*, 314.

[74] Fedotova, M. V.; Kruchinin, S. E.; Rahman, H. M. A.; Buchner, R. *J. Mol. Liq.* **2011**, *159*, 9.

[75] Wachter, W.; Fernandez, S.; Buchner, R.; Hefter, G. *J. Phys. Chem. B* **2007**, *111*, 9010.

[76] Yamaguchi, T.; Matsuoka, T.; Koda, S. *J. Chem. Phys.* **2009**, *130*, 094506.

[77] Yamaguchi, T.; Matsuoka, T.; Koda, S. *J. Chem. Phys.* **2007**, *127*, 234501.

[78] Eiberweiser, A.; Buchner, R. *J. Mol. Liq.* **2012**, doi:10.1016/j.molliq.2012.03.025.

[79] Grosse, C. *J. Phys. Chem.* **1988**, *92*, 3905.

[80] Buchner, R.; Baar, C.; Fernandez, P.; Schrödle, S.; Kunz, W. *J. Mol. Liq.* **2005**, *118*, 179.

[81] Göttmann, O.; Kaatze, U.; Petong, P. *Meas. Sci. Technol.* **1996**, *7*, 525.

[82] Buchner, R.; Barthel, J. *Ber. Bunsen–Ges. Phys. Chem.* **1997**, *101*, 1509.

[83] Cole, R. H. *J. Phys. Chem.* **1975**, *79*, 1469.

[84] Cole, R. H.; Mashimo, S.; Winsor, P. *J. Phys. Chem.* **1980**, *84*, 786.

[85] Hölzl, C. Ph.D. Thesis, Regensburg, 1998.

[86] Schrödle, S. Ph.D. Thesis, Regensburg, 2005.

[87] Barthel, J.; Buchner, R.; Eberspächer, P. N.; Münsterer, J., M. nad Stauber; Wurm, B. *J. Mol. Liq.* **1998**, *78*, 83.

[88] Grant, E. H.; Sheppard, R. J.; South, G. P. *Dielectric Behaviour of Biological Molecules in Solution*; Oxford University Press: Oxford, 1978.

[89] Kaatze, U.; Giese, K. *J. Phys. E: Sci. Instrum.* **1980**, *13*, 133.

[90] Birch, J. R.; O'Neil, G. P.; Yarwood, J.; Bennouna, M. *J. Phys. E: Sci. Instrum.* **1982**, *15*, 684.

[91] Wan Abdullah, A. K.; Parker, T. J. *Infrared. Phys.* **1989**, *29*, 799.

[92] Barthel, J.; Bachhuber, K.; Buchner, R.; Hetzenauer, H.; Kleebauer, M. *Ber. Bunsen–Ges. Phys. Chem.* **1991**, *95*, 853.

[93] Hunger, J. Ph.D. Thesis, Regensburg, 2010.

[94] Levine, H.; Papas, C. H. *J. Appl. Phys.* **1951**, *22*, 29.

[95] Blackham, D. V.; Pollard, R. D. *IEEE Trans. Instr. Meas.* **1997**, *46*, 1093.

[96] Wölbl, J. Ph.D. Thesis, Regensburg, 1982.

[97] Schrödle, S.; Hefter, G.; Kunz, W.; Buchner, R. *Langmuir* **2006**, *22*, 924.

[98] Buchner, R.; Hefter, G.; May, P. M. *J. Phys. Chem. A* **1999**, *103*, 1.

[99] Feldman, Y.; Polygalov, E.; Ermolina, I.; Polevaya, Y.; Tsentsiper, B. *Meas. Sci. Technol.* **2001**, *12*, 1355.

[100] Bordi, F.; Cametti, C.; Gili, T. *Bioelectrochemistry* **2001**, *54*, 53.

[101] Hunger, J.; Stoppa, A.; Hefter, G.; Buchner, R. *J. Phys. Chem. B* **2008**, *112*, 12913.

[102] Gregory, A. P.; Clarke, R. N. *Meas. Sci. Technol.* **2007**, *18*, 1372.

[103] Bevington, P. R. *Data Reduction and Error Analysis for the Physical Sciencies*; McGraw–Hill: New York, 1969.

[104] Steger, H. Ph.D. Thesis, Regensburg, 1988.

[105] Zasetsky, A. Y.; Buchner, R. *J. Phys.: Condens. Matter* **2011**, *23*, 025903.

[106] Tikhonov, A. *Dokl. Acad. Nauk SSSR* **1963**, *151*, 501.

[107] Kratky, O.; Leopold, H.; Stabinger, H. *Z. Angew. Phys.* **1969**, *27*, 273.

[108] Lide, D. R., Ed. *CRC Handbook of Chemistry and Physics*, 85th ed.; CRC Press: Boca Raton, USA, 2004.

[109] Barthel, J.; Wachter, R.; Gores, H. J. In *Modern Aspects of Electrochemistry*; Conway, B. E., Bockris, J. O., Eds.; Plenum: New York, 1979; Vol. 13; pp 1–79.

[110] Barthel, J.; Graml, H.; Neueder, R.; Turq, P.; Bernard, O. *Curr. Top. Solution Chem.* **1994**, *1*, 223.

[111] Stoppa, A.; Hunger, J.; Buchner, R. *J. Chem. Eng. Data* **2009**, *54*, 472.

[112] Barthel, J.; Feuerlein, F.; Neueder, R.; Wachter, R. *J. Solution Chem.* **1980**, *9*, 209.

[113] Hoover, T. B. *J. Phys. Chem.* **1964**, *68*, 876.

[114] Shaukat, S.; Buchner, R. *J. Chem. Eng. Data* **2011**, *56*, 4944.

[115] Stewart, J. J. P. MOPAC2009, Stewart Computational Chemistry, Colorado Springs, CO, USA.

[116] Stewart, J. J. P. *J. Mol. Modeling* **2007**, *13*, 1173.

[117] Baker, J. *J. Com. Chem.* **1986**, *7*, 385.

[118] Bondi, A. *J. Phys. Chem.* **1964**, *68*, 441.

[119] Senda, N. Winmostar, version 3.78f. http://winmostar.com.

[120] Marcus, Y., Ed. *Ion Solvation*; Wiley: Chichester, UK, 1985.

[121] Bockris, J. O.; Reddy, A. K. N. *Modern Electrochemistry*; 2nd ed., Plenum: New York, 1998; Vol. 1.

[122] Smith, W. H. *Chem. Eng. News* **1991**, *69*, 31.

[123] Perrin, C. L.; Gipe, R. K. *J. Am. Chem. Soc.* **1984**, *96*, 5631.

[124] Perrin, C. L.; Gipe, R. K. *J. Am. Chem. Soc.* **1986**, *108*, 1088.

[125] Sharygin, A. V.; Wood, R. H. *J. Chem. Thermodyn.* **1996**, *28*, 851.

[126] Rooney, S. A. *Environmental Health Perspectives* **1984**, *55*, 205.

[127] Klein, R.; Tourad, D.; Kunz, W. *Green Chem.* **2008**, *10*, 433.

[128] Klein, R.; Kellermeier, M.; Drechsler, M.; Tourad, D.; Kunz, W. *Colloids and surfaces A: Physicochem. Eng. Aspects* **2009**, *338*, 129.

[129] Liao, J.-H.; Wu, P.-C.; Bai, Y.-H. *Inorg. Chem. Commun.* **2005**, *8*, 390.

[130] Tolbert, N. E. *J. Biol. Chem.* **1960**, *235*, 475.

[131] Westhof, E. E. *Water and Biological Macromolecules*; Macmillan: London, 1993.

[132] Bellissent-Funel, M.-C. E. *Hydration Processes in Biology*; IOS Press: Amsterdam, 1999.

[133] Billeter, M. *Prog. Nucl. Mag. Res. Spectrosc.* **1995**, *27*, 635.

[134] Wohlfarth, C. *Enthalpy Data of Polymer-Solvent Systems*; CRC Press: Boca Raton, 2006.

[135] Graziano, G. *Can. J. Chem.* **2001**, *79*, 1310.

[136] Wyttenbach, T.; Bowers, M. *Chem. Phys. Lett.* **2009**, *480*, 1.

[137] Buchner, R.; Barthel, J. *Ann. Rep. Prog. Chem. Sect. C* **2001**, *97*, 349.

[138] Buchner, R. *Dielectric Spectroscopy of Solutions, in: J. Samios und V.A. Durov (Eds.), Novel Approaches to the Structure and Dynamics of Liquids: Experiments, Theories and Simulations*, nato asi ser. ii ed.; Kluwer: Dordrecht, 2004; Vol. 133; p p. 265.

[139] Belleau, B. *Ann. N. Y. Acad. Sci.* **1967**, *144*, 705.

[140] Hefter, G.; Buchner, R. *Dielectric spectroscopy: a new old tool for studying ions in solution. In : 235th National Meeting of the American Chemical Society*; American Chemical Society: 6 - 10 April, New Orleans, 2008.

[141] Casteel, J. F.; Amis, A. S. *J. Chem. Eng. Data* **1972**, *17*, 55.

[142] Buchner, R.; Capewell, S. G.; Hefter, G.; May, P. M. *J. Phys. Chem. B* **1999**, *103*, 1185.

[143] Fleming, R. *J. Chem. Soc. A* **1960**, 4914.

[144] Wishaw, B. F.; Stokes, R. H. *J. Am. Chem. Soc.* **1954**, *76*, 2065.

[145] McCleskey, R. B. *J. Chem. Eng. Data* **2011**, *56*, 317.

[146] Spieweck, F.; H., B. *Technisches Messen* **1992**, *59*, 285.

[147] Millero, F. J.; Hansen, W. D. *J. Phys. Chem.* **1968**, *72*, 1758.

[148] Motin, M. A. *J. Chem. Eng. Data* **2004**, *49*, 94.

[149] Pearce, J. N.; Pumplin, G. G. *J. Am. Chem. Soc.* **1937**, *59*, 1221.

[150] Albright, J. G.; Mitchell, J. P.; Miller, D. G. *J. Chem. Eng. Data* **1994**, *39*, 195.

[151] kaminsky, M. *Z. Phys. Chem. N. F.* **1955**, *5*, 154.

[152] Rashkovskaya, E. A.; Chernen'kaya, E. I. *J. Appl. Chem. USSR* **1967**, *40*, 301.

[153] Desnoyers, J. E.; Arel, M. *Can. J. Chem.* **1967**, *45*, 359.

[154] Redlich, o.; Meyer, D. M. *Chem. Rev.* **1964**, *64*, 221.

[155] Millero, F. J. *Chem. Rev.* **1971**, *71*, 147.

[156] Archer, D. G.; Wang, P. *J. Phys. Chem. Ref. Data* **1990**, *19*, 371.

[157] Klofutar, C.; Horvat, J.; Rudan-Tasič, D. *Acta Chim. Slov.* **2006**, *53*, 274.

[158] Hepler, L. G. *Can. J. Chem.* **1969**, *47*, 4613.

[159] Millero, F. J. *J. Phys. Chem.* **1970**, *74*, 356.

[160] Bešter-Rogač, M.; Neueder, R.; Barthel, J. *J. Solution Chem.* **1999**, *28*, 1071.

[161] Wachter, W.; Buchner, R.; Hefter, G. *J. Phys. Chem. B* **2006**, *110*, 5147.

[162] Tromans, A.; May, P. M.; Hefter, G.; Sato, T.; Buchner, R. *J. Phys. Chem. B* **2004**, *108*, 13789.

[163] Rønne, C.; Thrane, L.; Åstrand, P.-O.; Wallqvist, A.; Mikkelsen, K. V.; Keiding, S. R. *J. Chem. Phys.* **1997**, *107*, 5319.

[164] Morrow, T. I.; Maginn, E. *Fluid Phase Equilib.* **2004**, *217*, 97.

[165] Marlow, G. E.; Pettitt, B. *Biopolymers* **2003**, *68*, 192.

[166] Lee, H.; Wilmshurst, J. K. *Aust. J. Chem.* **1964**, *17*, 943.

[167] Impey, R. W.; Madden, P. A.; Mcdonald, I. R. *J. Phys. Chem.* **1993**, *87*, 5071.

[168] Korson., L.; Drost-Hansen., W.; Millero, F. J. *J. Phys. Chem.* **1969**, *73*, 34.

[169] Alavi, D. S.; Hartman, R. S.; Waldeck, D. H. *J. Chem. Phys.* **1991**, *94*, 4509.

[170] Hubbard, J. B.; Onsasager, L. *J. Chem. Phys.* **1977**, *67*, 4850.

[171] Hubbard, J. B. *J. Chem. Phys.* **1978**, *68*, 1649.

[172] Hubbard, J. B.; Colonomos, P.; Wolynes, P. G. *J. Chem. Phys.* **1979**, *71*, 2652.

[173] Mancinelli, R.; Botti, A.; Bruni, F.; Ricci, M. A.; Soper, A. K. *Phys. Chem. Chem. Phys.* **2007**, *9*, 2959.

[174] Error bars for Z_{ib} were calculated from the standard deviations of fits of the polynomial $S_{\mathrm{b}}(c) = S_{\mathrm{b}}(0) - a_1 c + a_2 c^{3/2}$ with $S_{\mathrm{b}}(0)$ fixed to the corresponding value of pure water taken from ref. 86, for Z_{s}, the standard deviations were obtained via the fits of the polynomial $S_{\mathrm{s}}(c) = a_1 c + a_2 c^{3/2}$.

[175] Fleming, R. *J. Chem. Soc. A* **1966**, 946.

[176] Shao, Q.; He, Y.; White, A. D.; Jiang, S. *J. Phys. Chem. B* **2010**, *114*, 16625.

[177] Szász, G. I.; Heinzinger, K. *Z. Naturforsch.* **1979**, *34a*, 840.

[178] Bohm, H. J.; McDonald, I. R. *Mol. Phys.* **1984**, *80*, 887.

[179] Dang, L. X. *Chem. Phys. Lett.* **1993**, *213*, 541.

[180] Harmon, K.; Akin, A. C.; Avci, G. F.; Nowas, L. S. *J. Mol. Struct.* **1991**, *244*, 223.

[181] Intharathep, P.; Tongraar, A.; Sagarik, K. *J. Comput. Chem.* **2005**, *26*, 1329.

[182] Walrafen, G. E.; Fisher, M. R.; Hokmabadi, M. S.; Yang, W. H. *J. Chem. Phys.* **1986**, *85*, 6970.

[183] Tanford, C. *The Hydrophobic Effect-Formation of Micelles and Biological Membraness*; Wiley: New York, 1980.

[184] Laughlin, R. G. *The Aqueous Phase Behavior of Surfactants*; Academic Press: San Diego, 1994.

[185] Madelmont, C.; Perron, R. *Colloid Polym. Sci.* **1976**, *254*, 581.

[186] Lin, B.; McCormick, A. V.; Davis, H. T.; Strey, R. *J. Colloid Interface Sci.* **2005**, *291*, 543.

[187] Preston, W. C. *J. Phys. Chem.* **1948**, *52*, 84.

[188] Shinoda, K.; Kunieda, H. *J. Phys. Chem.* **1976**, *80*, 2468.

[189] Jansson, M.; Jönsson, A.; Li, P.; Stilbs, P. *Colloids Surfs.* **1991**, *59*, 387.

[190] Zana, R. *Langmuir* **2004**, *20*, 5666.

[191] Vlachy, N.; Jagoda-Cwiklik, B.; Vácha, R.; Tourad, D.; Jungwirth, P.; Kunz, W. *Adv. Colloid Interface Sci.* **2009**, *146*, 42.

[192] Zhao, G.; Zhu, B. *Princip. Surf. Action (Chin.)* **2003**, 242.

[193] Caponetti, E.; Martino, D. C.; Floriano, M. A.; Triolo, R. *Langmuir* **1993**, *9*, 1193.

[194] Klein, R. Diploma Thesis, Regensburg, 2006.

[195] Quina, F. H.; Nassar, P. M.; Bonilha, J. B. S.; Bales, B. L. *J. Phys. Chem.* **1995**, *99*, 17028.

[196] Sasaki, T.; Hattori, M.; Sasaki, J.; Nukina, K. *Bull. Chem. Soc. Jpn.* **1975**, *48*, 1397.

[197] Baar, C.; Buchner, R.; Kunz, W. *J. Phys. Chem. B* **2001**, *105*, 2906.

[198] Pauly, H.; Schwan, H. P. *Z. Naturforsch. B* **1959**, *14*, 125.

[199] R-Pulido, A.; Casado, A.; M-Úbeda, M.; Junquera, E.; Aicart, E. *Langmuir* **2010**, *26*, 9378.

[200] King, D. T.; Warren, D. B.; Pouton, C. W.; Chalmers, D. K. *Langmuir* **2011**, *27*, 11381.

[201] Bertolini, D.; Cassettari, M.; Salvetti, G.; Tombari, E.; Veronesi, S. *Rev. Sci. Instrum.* **1990**, *61*, 450.

[202] Hunger, J. Diploma Thesis, Regensburg, 2006.

[203] Spivey, H. O.; Snell, F. M. *J. Phys. Chem.* **1964**, *68*, 2126.

[204] Levitt, D. G.; Decker, E. R. *Biophys. J.* **1988**, *53*, 33.

[205] Abbott, A. P.; Boothby, D.; Capper, G.; Davies, D. L.; Rasheed, R. K. *J. Am. Chem. Soc.* **2004**, *126*, 9142.

[206] Gibbs, J. H.; Cohen, C.; Fleming III, P. H. i. *The Physical Chemistry of Aqueous Systems*, ed. kay, r. l. ed.; Plenum: New York, 1973.

[207] Stache, H. W. *Surfactant Science Series-Anionic Surfactants*; Marcel Dekker: New York, 1996.

[208] Zana, R.; Benrrau, M.; Bales, B. L. *J. Phys. Chem. B* **2004**, *108*, 18195.

[209] Benrrau, M.; Bales, B. L.; Zana, R. *J. Phys. Chem. B* **2003**, *107*, 13432.

[210] Bales, B. L.; Tiguida, K.; Zana, R. *J. Phys. Chem. B* **2004**, *108*, 14948.

[211] Paul, A.; Griffiths, P. C.; Pettersson, E.; Stilbs, P.; Bales, B. L.; Zana, R.; Heenan, R. K. *J. Phys. Chem. B* **2005**, *109*, 15775.

[212] Tcacenco, C. M.; Zana, R.; Bales, B. L. *J. Phys. Chem. B* **2005**, *109*, 15997.

[213] Itri, R.; Amaral, L. Q. *J. Phys. Chem.* **1991**, *95*, 423.

[214] Although additivity rule is applicable only at infinite dilution but due to the approximate nature of these calculations and consistent with previous experience,[10,11,98] it is applied to finite concentrations as well.

[215] Shaukat, S. and Buchner, R. *Unpublished results*.

[216] Gustavsson, H.; Lindman, B. *J. Am. Chem. Soc.* **1978**, *100*, 4647.

[217] Gustavsson, H.; Lindman, B. *J. Am. Chem. Soc.* **1975**, *97*, 3923.

[218] Wachter, W.; Kunz, W.; Buchner, R.; Hefter, G. *J. Phys. Chem. A* **2005**, *109*, 8675.

[219] Halle, B.; Caristrom, G. *J. Phys. Chem.* **1981**, *85*, 2142.

Regensburg, den 30.10.2012

Saadia Shaukat